A Novel Approach to Detecting *Listeria monocytogenes*:

Creating Species-Specific Ribonuclease (RNase)-Cleaved Fluorescent Substrate (RFS) by *In Vitro* Selection

By

Pushpinder Kanda, B.Sc.

A Thesis Submitted to the School of Graduate Studies in Partial Fulfillment of the Requirements for the Degree Master of Science

McMaster University

MASTER OF SCIENCE (2013)
(Biochemistry & Biomedical Sciences)

McMaster University
Hamilton, Ontario

TITLE:	A Novel Approach to Detecting *Listeria monocytogenes*: Creating Species-Specific Ribonuclease (RNase)-Cleaved Fluorescent Substrate (RFS) by *In Vitro* Selection.
AUTHOR:	Pushpinder Singh Kanda, B.Sc. (McMaster University)
SUPERVISOR:	Professor Yingfu Li
NUMBER OF PAGES:	124

ABSTRACT

The food-borne pathogen, *Listeria monocytogenes*, is a global health concern as it has been responsible for multiple food contamination outbreaks over the past century. Current detection methods like the enzyme-linked immunoassays (ELISA), and polymerase chain reaction (PCR) take over 24 h to attain results, are costly, require specialized equipment and trained personnel. In this study we investigated the use of functional nucleic acid (FNA) to develop a rapid and cost-effective detection method for *L. monocytogenes*. We carried out in *vitro* selection in order to isolate a fluorescently labeled DNA-RNA hybrid strand that can be bound and cleaved by specific endoribonucleases (RNase) from *L. monocytogenes*. We termed these DNA-RNA hybrid strands RNase-cleaved fluorescent substrate (RFS). Since no past studies have isolated RNases from *L. monocytogenes*, we first identified the genes based on sequence similarities with well characterized RNases. We purified and characterized RNase HII, RNase III and RNase G. Since this study focused primarily on developing RFS for RNase HII, we performed an in depth *in vitro* biochemical analysis to characterize this enzyme. We found that RNase HII from *L. monocytogenes* plays an important role in DNA replication and repair. Furthermore, we obtained six sequence classes by *in vitro* selection which could interact with RNase HII. The key nucleotide regions involved with RNase HII interactions were identified. In the final study, we showed the sequences isolated by *in vitro* selection could also be used as a tool to study ribonuclease function and identify new interaction between enzyme and substrate.

ACKNOWLEDGEMENTS

I would like to extend my gratitude to Dr. Yingfu Li for his strong guidance and support through the past three years of my Masters education. I would also like to show my appreciation for Dr. Alba Guarne and Dr. Lori Burrows for their insightful advice and suggestions in helping improve my project and strengthen my skills as a researcher.

I would also like to thank the past and present members of the Li Lab for their encouragement and friendship throughout the past three years. Furthermore, I would like to say thanks the Biochemistry department for their assistance along the way.

Last, but not least, I would like to extend my sincere gratitude to my family and friends for always believing in me and cheering me along the way.

TABLE OF CONTENTS

LIST OF ABBREVATION

CD	**circular dichroism**
CFU	**colony forming units**
CS	**counter selection**
DNA	**deoxyribonucleotide**
dPAG	**denaturing polyacrylamide gel**
DTT	**Dithiothreitol**
dsDNA/RNA	**double stranded DNA or RNA**
EDTA	**ethylenediaminetetra-acidic acid**
ELISA	**enzyme-linked immune assays**
FAM	**6-carboxyfluorescein**
F	**fluorophore**
IMS	**immunomagnetic separation**
Lm	***Listeria monocytogenes***
nt	**nucleotides**
PAGE	**polyacrylamide gel electrophoresis**
PCR	**polymerase chain reaction**
Q	**quencher**
rA	**riboadenosine**
RNA	**ribonucleotide**
RNase	**ribonuclease**
SELEX	**Systematic Evolution of Ligands by Exponential Enrichment**
ssDNA/RNA	**single stranded DNA or RNA**
Taq	***Thermus aquaticus***
Wt	**wild type**
ΔN	**N-terminus deletion**

CHAPTER 1: General Introduction to Current Pathogen Detection Methods

1.1 Food-Borne Pathogens

Food-borne illnesses pose a serious threat to public health and safety; hence, methods to detect pathogens are of great importance. Pathogens involved with food-borne illnesses include *Escherichia coli*, *Campylobacter*, *Salmonella typhimurium*, *Staphylococcus aureus*, *Vibrio cholerae* and *Listeria monocytogenes*.[1] Pathogens such as *E. coli* O157:H7 have caused incidents like the 1997 Hudson ground-beef recalls that caused illnesses in over 9000 cases, of which 313 died.[2] Since the consumption of few pathogen cells pose a threat to an individual's health, legislations implementing a zero tolerance policy necessitate that food industries use detection methods which must be sensitive enough to detect at least 100 cells or less per gram or mL of sample.[3, 4] As a result, great research efforts have been implemented towards the development of sensitive pathogen detection methods. In fact, the food industry alone accounts for nearly 40% of all research dedicated towards food pathogen analysis.[5] Conventional methods used to identify pathogens use laborious culturing techniques which take 4-5 days to produce results and are not adequate to monitor the safety of our food on a timely basis.[5, 6] As a result, novel rapid methods have been developed that significantly reduced the time needed to detect pathogens. The advent of methods like the enzyme-linked immune assays (ELISA) in 1971 revolutionized the speed of food pathogen analysis and dominated the market ever since.[5, 7] However, food companies and health sectors need to evaluate alternative techniques that have emerged over the past two decades with the potential of greater sensitivity, simplicity, efficiency and cost effectiveness.

1.2 Introduction to Current Pathogen Detection Methods

1.2.1 Conventional Assays

Great care must be taken to prepare samples prior to detection to obtain reliable and reproducible results. The goal of sample enrichment is to increase pathogen quantity to a specific threshold for detection, as well as to concentrate and separate pathogens from food matrices and competing background flora that can interfere with the detection assays in the latter steps.[8, 9] Target organisms are enumerated by submerging homogenized samples into a selective-enrichment medium for a period of 24 hours. Selective agents in the culture, the nutrient composition of the medium, the growth temperature and the aerobic/anaerobic conditions are optimized to enumerate pathogens and suppress the growth of background flora.[8, 10]

The conventional method, which consists of multiple selective-enrichment steps, agar plating, and biochemical assays, can be used to confirm the presence or absence of the pathogen. Presumptive positive colonies are identified phenotypically on agar plates that often contain chromogenic agents that give colonies a specified colour for easy identification.[6, 11] Suspect colonies are subjected to a battery of biochemical assays to confirm the identity of the organism down to the genus or species level depending on the test kit used. For example, *Listeria monocytogenes* can be distinguished from other *Listeria* species by assessing hemolytic reactions and the metabolism of various carbon sources (D-xylose, L-rhamnose, etc).[12] These biochemical test kits have become miniaturized and automated requiring only a small volume of bacterial suspensions; however, most tests require 18-24 hours of incubation to obtain results.

Unfortunately, monitoring food quality at the industrial scale by conventional methods is not feasible due to the cost associated with the maintenance of specialized facilities, trained personnel and the time lost from withholding products from the market. Although the preferences for rapid-detection methods are taking precedence over conventional assays, they cannot replace the traditional methods as they remain the gold standard to confirm the true identity of bacteria isolates.

1.3 Introduction to Immunoassays

1.3.1 Enzyme-Linked Immune Assay

The specificity of antibody for its antigen has been exploited since early 1920s for identifying and serotyping bacteria.[13] However, early advancements in the immunoassay field occurred after the development of chemically modified antibodies with fluorescent molecules. In 1942 Coons *et al.* demonstrated that fluorescently (fluorescein-4-isocyanate) labelled antibodies could be used to detect bacteria within tissue cultures.[6] However it was not until the development of ELISA that the detection of various food-borne pathogens or their toxins became rapid, sensitive and commercially feasible.

The prevalent format of ELISA that is commercially available is the two-site ELISA also called the sandwich-ELISA (Figure 1.1). The typical sensitivity of ELISA for whole-cell detection is limited to 10^4-10^6 colony-forming units (CFU)/mL which is not adequate to detect the infectious dose of many pathogens (100 cells or less).[6, 8, 13, 14] Furthermore, even with full automation of ELISA test results are obtained after 24-30 hours, largely due to necessary

enrichment steps. In fact, enrichment is necessary to enumerate and isolate the target organism before performing any immunoassays. This is due to the propensity of antibodies to bind non-specific compounds present within the foods or to antigens from closely related competing flora.[13, 15] Furthermore, antigens that are masked by various food components can reduce the overall sensitivity of the assays. Strategies such as the use of fluorescent or chemiluminescent signal instead of colour production by enzymatic reactions have been used to achieve a higher sensitivity than traditional ELISA.[14, 16] Furthermore a process known as immunomagnetic separation (IMS) has revolutionized the way in which many biological materials can be concentrated and separated away from complex matrices. Originally designed to isolate blood cells, it was quickly adapted for pathogen isolation from foods in the early 1990s.[9] The process involves the use of antibody-coated magnetic particles to capture the antigens in enriched cultures which are then easily separated from the solution by applying an external magnetic field.

1.3.2 Surface Plamon Resonance Using Antibodies

Surface plasmon resonance (SPR) has become an attractive immuno-optical biosensing method due to its extreme sensitivity, compatibility with complex fluid matrices, detecting target in real time, no need for specific labels to identify the presence of the target, and the ease by which the sensor can be functionalized with antibodies.[17-19] The principle behind detection relies on the small changes in the refractive index that occur near the gold-metal surface coated with antibodies when an analyte is captured (Figure 1.1). The detection of specific *Salmonella enterica* serovars spiked milk product was demonstrated using a combination of polyclonal and

monoclonal antibodies resulting in a detection limit of 2.5×10^5 *S. Typhimurium* cells/mL.[20] Others have also shown lower detection limits of 10^3 to 10^4 CFU/mL with *E. coli* cells. The SPR detection method can also be arranged into an array-based system in which multiple targets can be captured and detected at once in real time. This array-based SPR format was demonstrated for the detection of *Mycobacterium tuberculosis* using patient serum samples.[21] The main disadvantages of SPR include the large size of the equipment (although portable SPR devices are becoming available such as the Texas Instrument's Spreeta SPR system), high costs and the need for highly trained personnel.

1.3.3 Electrochemical Immunoassays

Electrochemical biosensing is an alternative method for detecting pathogens in which the analyte recognition event is translated into an electrical signal.[1, 22, 23] Antibody-based electrochemical biosensors (also called immunosensors) are amongst the most popular.[22] An amperometric based immunosensor is the most common form of an electrochemical sensing.[24] This method detects an increase in current between two electrodes upon the formation of a sandwich-antibody-antigen complex, similar to ELISA, followed by the production of electrochemically active compound by an enzyme (the enzyme is often conjugated to the secondary antibody; Figure 1.1). These active compounds can then transfer electrons at the electrode to alter the current which can be used to measure the amount of target captured. This method detects different food-borne pathogens with detection limits that can range from 10^1 to 10^4 CFU/mL.[1] One limitation of this method is that electrochemically active compounds can

interfere with the assay and generate false currents. Background signal can be improved with the use of specific membranes or filters which can limit, based on size or charge, only specific analytes to access the electrode.

Other electrochemical sensors including potentiometric, conductometric and impedimetric devices have also been used to detect foodborne pathogens and are discussed in more detail in select reviews.[1, 22, 25, 26] Of the three, impedance spectroscopy (EIS) has gained a wide range of application in foodborne pathogen detection, especially since it can be customized as a label-free method.[25, 27] It is based on measuring the changes within the electrical impedance brought upon by the formation of antibody-antigen complexes on the electrode. Nandakumar *et al.* has shown the detection of *S. typhimurium* with a lower detection limit of 500 CFU/mL within 6 min.[28] One of the great advantages of such electrical biosensors is the acquisition of a fully automated system using computers thus, eliminating human intervention for intermediate steps in the process. Although immunosensors can prove to be a highly sensitive method, detection of pathogens within a complex food matrix require the need of an overnight enrichment step and an IMS process to enhance the sensitivity and performance of the sensor.

1.3.4 Latex Agglutination Assay

The latex agglutination assay is a cheaper and simper alternative to ELISA as it does not require multiple steps, or an expensive spectrophotometer device to assess results.[13, 29] Antibody coated coloured latex particles, also called sensitized latex, agglutinate or cluster in the presence of antigen (Figure 1.1). Visible sediments are formed almost immediately upon mixing and

confirm the presence of antigen. Although the detection is quick and simple, the low sensitivity (detection range of 10^6-10^7 CFU/mL) and non-specific agglutination triggered by food components mandate the use of enriched culture samples. The various commercially available immunoassays are listed in Table 1.1.[30-33]

1.3.5 Lateral Flow Immunoassay

Lateral flow immunoassays (LFIA), often commercialized in a form of a small test strip, are simple to use and one of the few technologies which can claim to be used outside of a laboratory setting.[32, 34, 35] A sample applied to the absorption pad migrates down the test strip *via* capillary action and the target can be captured by antibodies (Figure 1.1). The first interaction involves the binding of the antibodies specific to the target. This primary antibody is often conjugated to a coloured particle such as gold nanoparticles or latex beads. This complex is then captured by a secondary anti-target antibody that has been immobilized on the test strip membrane in a line format. The capture of the target is evident by the presence of a coloured line. A control test line, composed of immobilized antibodies that target the primary antibody, is used to indicate if the test was performed correctly. Although the test strips are simple to use and does not require the end user to purchase additional equipment for detection, the test are limited to small volumes and samples containing small number of cells must be enriched before use. Furthermore, samples that are not fluids must be enriched and purified since solid food matrix can clog membrane pores and destroy the test strips. Hence, commercially available kits are supplemented with enrichment media.

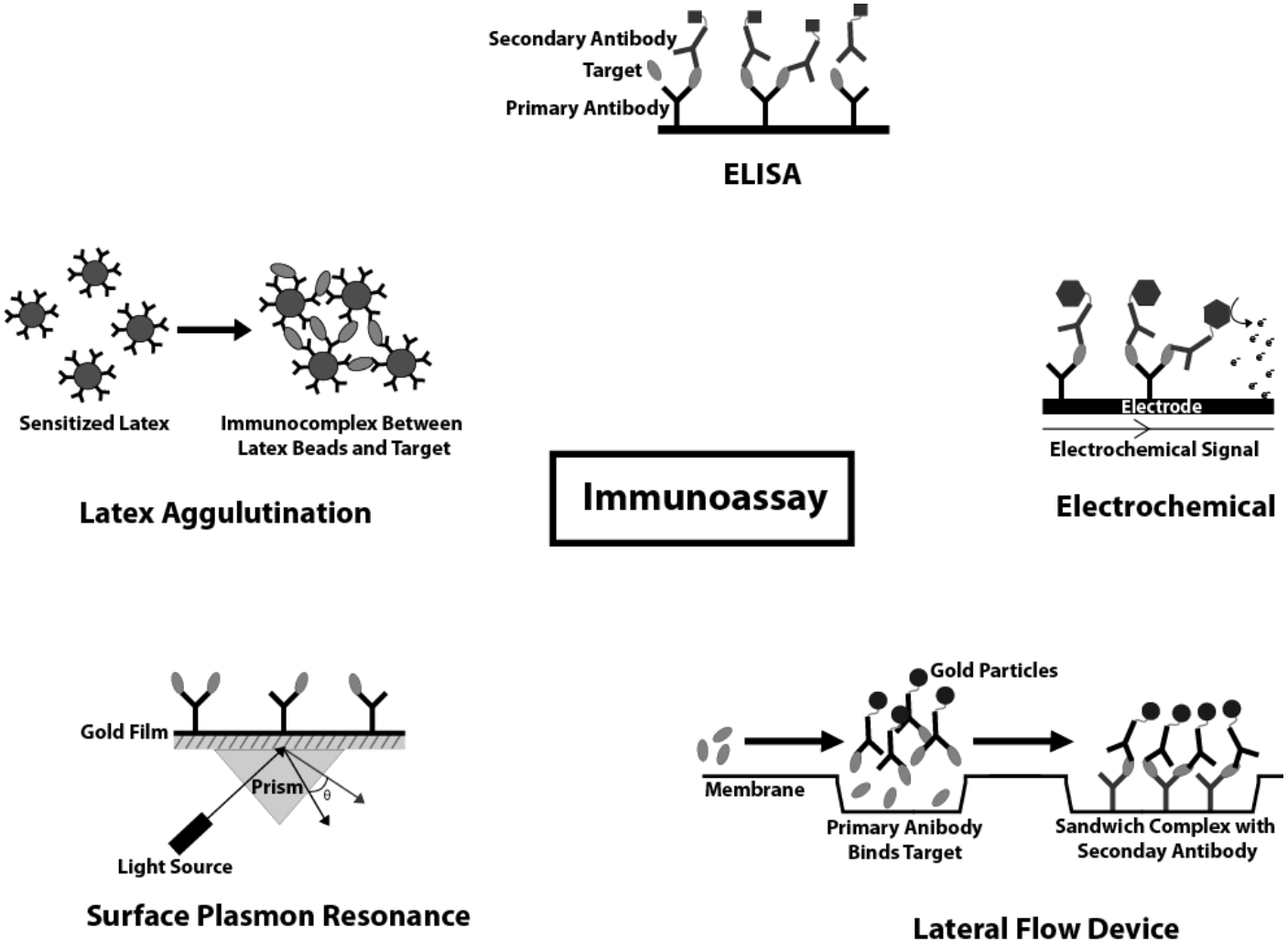

Figure 1.1. Immunoassays. *Enzyme-Linked Immunosorbant Assay (ELISA)*: The immobilized antibodies are conjugated to a solid support and are used to capture the antigen. A secondary antibody that recognizes a different epitope on the same antigen is added to produce a colourimetric signal for detection. The secondary antibody is chemically linked to either alkaline phosphatase or horseradish peroxidase which catalyze chromophoric substrates to form coloured products. *Latex Agglutination (LA) Assay*: Coloured latex particles coated with antibodies (sensitized latex) form large visible sediments in the presence of antigen as a result of an immunocomplex network between sensitized latex and the antigens. *Amperometric Electrochemical Assay*: Primary antibodies are captured onto an electrode. The secondary antibody is tagged with enzyme which produce electrochemically active compound. Electrons (e^-) from the electrochemically active compounds are transferred to the electrode which is measured as an increase in the current. *Surface Plasmon Resonance (SPR)*: Gold film is coated with an antibody which captures an antigen. The capture of the antigen causes the change in the refractive index which causes the incident polarized light to be reflected at a different angel. *Lateral Flow Device*: The antigen flows across the membrane into the first region where it is bound by the primary antibody. The primary antibody is tagged with gold-nanoparticle. The primary antibody-antigen complex is captured by the immobilized secondary antibody. The sandwich complex is visualized as a blue colour due to the presence of gold particles.

1.4 Introduction to Nucleic Acid-Based Assays

1.4.1 DNA Hybridization Probes

A single gene or a cluster of genes in a pathogen can code for virulence factors which cause pathogenesis thus, if the gene is detected so is the pathogen. This simple principle has been used to design nucleic acid probes that can be used to promptly detect pathogens with high specificity and sensitivity. Although commercial assays relying on antibodies for pathogen detection have dominated the market, the DNA-based methods have made impressive progress over the last two decades.[36] The ease with which DNA can be chemically modified with various molecules such as fluorophores, the control over the precise location of chemical modifications, the simplicity of manipulating the sequence of DNA, and the ability to have large scale synthesis at relatively low cost has made DNA-based technologies an attractive diagnostic tool. Some current commercially available DNA-based assays for pathogen detection are listed in Table 1.1.

DNA probes were the first nucleic acid-based assay used for pathogen detection within foods in the early 1980s.[13, 37] Synthesized DNA oligonucleotides (probes) form Watson-Crick base-pairs which allow specific hybridization with complementary DNA or RNA strands from the pathogen. Probes have been designed to target specific virulence genes such as SLT I and SLT II toxins produced by *E. coli* O157:H7; however, most commercially available kits target specific regions of the 16S ribosomal RNA (rRNA) due to its high copy number (10^3-10^4 copies/cell).[13, 38, 39] The GENE-TRAK (or GENE Quence) system (Neogen) and Accuprobe (Gen-Probe) are two main commercially available kits targeting 16S rRNA (Table 1.1).

Table 1.1. Commercially available pathogen detection assays. (LA) Latex agglutination. (LF), Lateral flow device.

Organism	Trade Name	Manufacturer	Assay Format
E. coli O157:H7	VIA-TECRA	3M TECRA	ELISA
	Assurance GDS	BioControl	ELISA
	Dupont lateral flow system	Dupont Qualicon	LF
	RapidChek	Strategic Dignostics Inc.	LF
	GeneDisc	Pall GeneDisc Technologies	PCR
	BAX	Dupont Qualicon	PCR
	E.coli O157:H7 LT	BioFire Diagnostics Inc.	PCR
	foodproof	BIOTECON Diagnostics	PCR
Listeria	VIA-TECRA	3M TECRA	ELISA
	Assurance EIA	BioControl	ELISA
	Listeria Latex	Microgen	LA
	Oxoid Rapid Test	ThermoScientific	LA
	RapidChek	Strategic Dignostics Inc.	LF
	GENE-TRAK	Neogen	DNA-probe
	Accuprobe	GEN-PROBE	DNA-probe
	iQ-Check	Bio-Rad	PCR
	BAX	Dupont Qualicon	PCR
	foodproof	BIOTECON Diagnostics	PCR
Salmonella	VIA-TECRA	3M TECRA	ELISA
	Assurance EIA	BioControl	ELISA
	Oxoid Rapid Test	ThermoScientific	LA
	GENE-TRAK	Neogen	DNA-probe
	BAX	Dupont Qualicon	PCR
	foodproof	BIOTECON Diagnostics	PCR
Staphylococcus aureus	VIA-TECRA	3M TECRA	ELISA
	Staphyloslide	Remel	LA
	Dry Spot	ThermoScientific	LA
	Accuprobe	GEN-PROBE	DNA-probe
	GENE-TRAK	Neogen	DNA-probe
	BAX	Dupont Qualicon	PCR

The GENE-TRAK assays are composed of two key oligonucleotides, the capture probe which hybridizes to the target rRNA and contains a poly-deoxyadenosine tail and the detection probe which binds to an adjacent region of the target rRNA and is chemically linked to horseradish peroxidase (HRP).[30] The rRNA extracted from the cell is mixed with the two DNA probes and forms a complex that is captured onto a dipstick or micro-well plates coated with poly-deoxythymidine nucleotides. Any unbound material is washed and the addition of enzyme substrates produces a blue colour (450 nm) which is analyzed spectrophotometrically. The assays take 100-150 min however due to the low detection range of 10^5-10^6 cells/mL, overnight enrichment cultures are necessary. In the Accuprobe system, a single DNA probe conjugated with a chemiluminescent label, acridium ester, is hybridized with the target rRNA to protect the acridium ester from alkaline hydrolysis (chemically treated products are nonchemiluminescent).[30] The protected labels emit photons which are analyzed using a luminometer. Studies show that GENE-TRAK and Accuprobe perform nearly identically (detection limit of 10^6 CFU/mL) in detecting *Listeria monocytogenes* and *Campylobacter*.[40, 41] Yet, fast turnover of results and fewer steps involved in the Accuprobe assays make it easier for analyzing large quantities of sample.

1.4.2 Polymerase Chain Reaction

The development of polymerase chain reaction by Mullis in 1983, the use of heat-stable *Thermus aquaticus (Taq*) polymerase to generate amplicons, and the invention of the thermocycler have provided scientists a powerful tool for genetic studies.[36] The early PCR studies

assessed the presence or absence of genetic mutations or alleles to study inherent metabolic disorders such as sickle cell anemia.[42] Soon after, PCR rapidly expanded for the analysis of infectious agents, given that the presence of a gene in the sample indicated the presence of the pathogen. This method is sensitive and rapid due to the exponential amplification of DNA that can be achieved within a few minutes. However, the sensitivity and specificity depends on the unique primer sequence, the process of extracting target genes, the conditions used for thermal-cycle amplification, and the methods used to detect amplicons.[8] The typical detection range of the PCR methods is 10^3-10^4 CFU/mL and varies based on the procedure used to isolate, grow, and lyse the cells.[36] Furthermore, PCR is susceptible to non-specific amplification leading to false positive results which are more likely in the presence of background flora.[8, 36] As a result, sample enrichment and IMS steps are necessary before performing PCR.

1.4.3 Real Time PCR (RT-RCR)

Early PCR assays using ethidium-stained agarose gels to analyse results were labour intensive, inefficient in analyzing large quantity of samples and required additional equipment.[36] Advances in PCR technology stemmed from the development of thermocyclers with a built-in fluorimeter that could analyze the production of fluorescent amplicons in real time. Fluorescent dyes like SYBR green which becomes incorporated into the newly synthesized double stranded DNA during thermal amplification, as seen in Figure 1.2, replaced ethidium bromide and provided a 1000-fold increase in sensitivity.[43] Moreover, the fluorescent signal allowed accurate quantification of the bacterial load due to the inverse relationship between the amount of initial

target gene and the number of cycles required to observe fluorescence.[36, 44] As a result, fewer cells present within the sample would require more PCR cycles to observe equal fluorescence compared to a sample with a greater cell load. Although RT-PCR is a faster detection process relative to the older gel based detection method, due to the enrichment process the overall time to obtain results is extended to 24-48 h.

A disadvantage of SYBR green dye is it can be incorporated into non-specific amplicons resulting in false positive results. Consequently, DNA probes internally labelled with fluorescent molecules replaced the free dye.[45] The TaqMan DNA probe contains a 5'-end fluorescent label and a 3'-end quencher. During the annealing step, the probe hybridizes to the target at a region different from the primers, and the quencher absorbs the emitted energy resulting in no fluorescence.[45] In the elongation step, the 5' to 3' exonuclease activity of the *Taq* polymerase separates the quencher from the fluorophore resulting in an enhancement in fluorescence (Figure 1.2). Thus, fluorescence is observed only when the TaqMan probe binds the appropriate amplicon.

Similarly, molecular beacons avoid false positive signals by binding internally to the target amplicon. The beacons are hairpin structures containing a 5'- and 3'-end fluorophore and quencher that are in close proximity and a loop region with a complementary sequence to the target DNA.[46] The quencher is separated from the fluorophore when the hairpin unfolds to anneal to the target sequence (Figure 1.2).

1.4.4 Nucleic Acid Lateral Flow

The nucleic acid lateral flow (NALF) device is similar to the LFIA in which capillary action carries the target to a capture zone in which coloured particles make a visible line. However, the difference is that NALF uses nucleic acid capture probes, instead of antibodies, to capture nucleic acid targets. The capture probes can be functionalized on the test strip membrane in multiple ways including streptavidin layered membranes bound to biotinylated capture probes; absorption of BSA-oligonucleotide conjugated capture probe on the membrane; capture probe absorbed directly onto the membrane.[47-50] Amplicons generated by PCR or RT-PCR can be applied to an absorption pad which then migrates down the test strip to hybridize with the capture probe and a secondary signalling oligonucleotide conjugated to a gold nanoparticle (Figure 1.2). The device offers a quick and easy interpretation of PCR results, and has also been developed as a multiplex-lateral flow device which is capable of binding to multiple amplicon targets.[48] However, multiple steps including enrichment process, cell lysis, RNA or genomic DNA extraction and PCR are required prior to using NALF.

1.4.5 Electrochemical DNA Hybridization Assay

Similar to the immunosensors, electrochemical sensing has also been adopted for rapid and sensitive detection of target DNA or RNA strands. Most of the current methods employ a PCR amplification step to improve detection sensitivity. Once the amplicon is hybridized to a capture probe located on the electrode, it can be detected by either using electrochemically active

organic dyes which can intercalate within dsDNA, cationic metal complex that can bind DNA *via* electrostatic interaction, or generate redox active compounds by an enzymatic process.[51]

The redox dye, Methylene blue (MB), has been used in many electrochemical DNA assays and the work by Li *et al.* (2006) represents an excellent example of the use of MB for DNA detection. In their work, the probe DNA conjugated to a gold electrode formed a stem-loop structure and was also chemically linked to MB. The stem-loop structure maintained the MB in close proximity to the electrode, generating a small current. Upon hybridization of the probe with the target amplicon, the stem-loop structure is opened up and the MB is further from the electrode, effectively reducing the current (Figure 1.2). This method could detect 500 fg of DNA (equivalent of ~ 90 cells).[52]

Steps such as culturing, lysis of cells and PCR amplification increase the time and cost required to perform electrochemical DNA hybridization assays. Few groups have provided methods to improve the assay and the one discussed here is the work done by Lam *et al.* (2012). Their work demonstrated a PCR-free method to detect bacteria with a detection limit of 10^3 CFU/mL.[53] Although lower detection limits can be achieved by other DNA hybridization methods, this method incorporates the use of a small electronic device that integrates a cell lysis chamber to provide rapid results in 30 minutes.[54] Cells were injected into the lysis chamber where an applied voltage was used to lyse them. An air injection moved the lysed sample onto the chip where the target RNA hybridized with its complimentary peptide nucleic acid (PNA) strand. A cationic metal electroactive compound $Ru(NH_3)_6^{3+}$ paired with $Fe(CN)_6^{-3}$ was used to create a

current. The current was generated only if the negatively charged RNA was captured on to the chip by PNA (neutral charge) and attracts Ru(III) electrostatically.

Enzymes have also been used to create electrochemical signals in DNA hybridization assays. This method is attractive as the cyclic nature of an enzymatic reaction allows for signal amplification, hence improving the sensitivity of the assay. Alkaline phosphatase (AP) is one of the most commonly used enzymes which convert electro-inactive α-naphthyl phosphate to an electroactive α-naphthol. A sandwich-based assay was demonstrated by Farabullini *et al.* (2007) in which the amplicons hybridized with the capture probes (conjugated onto an electrode) and a biotinylated signalling probe.[55] The streptavidin–AP was coupled to the biotinylated hybrids to generate a signal and a detection limit of low nanomolar levels was achieved. Other enzymes like horseradish peroxidase, and glucose-6-phosphate dehydrogenase have also been employed in similar sandwich assay format.[56-58]

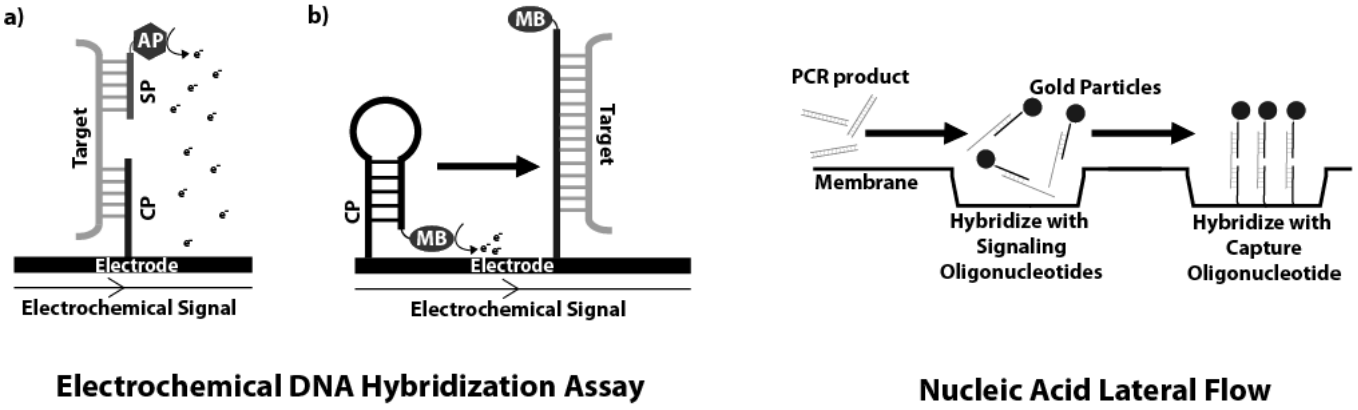

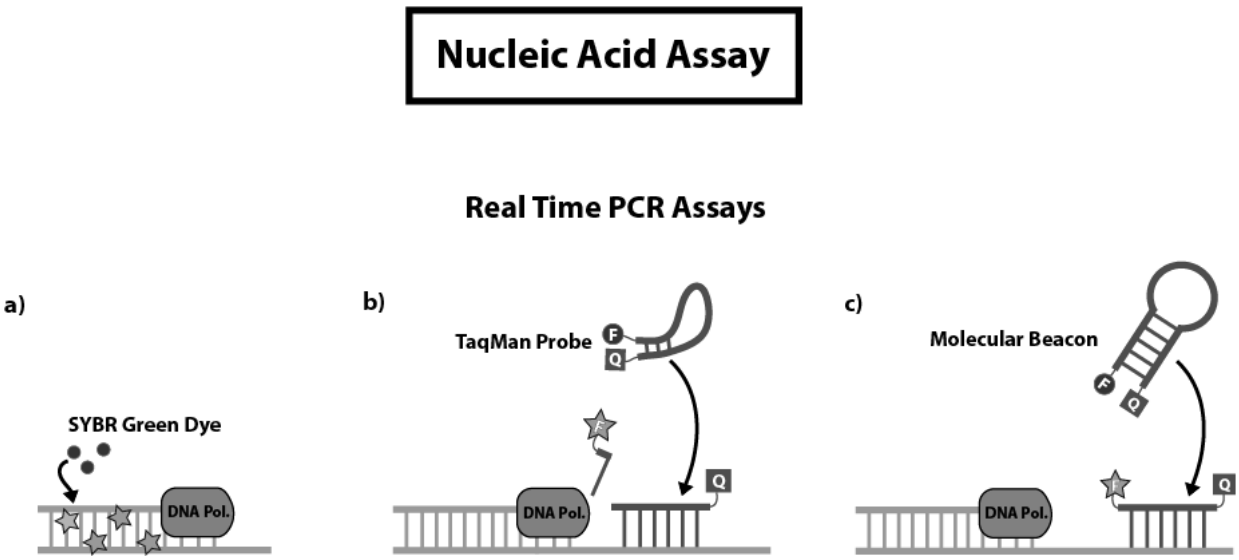

Figure 1.2. Nucleic Acid Assays. *Real Time PCR Assay*: a) The fluorescence emitted by SYBR green dye is enhanced several fold when it binds to double-stranded DNA after each round of PCR. b) The TaqMan probe contains covalently linked fluorophore (F) and quencher (Q) labels that are in very close vicinity. Following the hybridizing to the target DNA template, the 5'- to 3'- exonuclease activity of *Taq* DNA polymerase (Pol.) releases the fluorophore label resulting in enhanced fluorescent emission. c) Molecular beacon forms a hairpin structure that positions the fluorophore and quencher close together. An enhanced fluorescent signal output is observed during the annealing step, due to the hybridization of the probe to the target DNA sequence which causes the fluorophore and quencher pair to become distant. *Electrochemical DNA Hybridization Assay*: a) The capture probe (CP) is conjugated to an electrode. The target amplicon hybridizes with the capture probe and the signaling probe (SP). The signaling probe is bound with alkaline phosphatase (AP) which produces electrochemically active compounds that transfer electrons to the electrode. b) The stem-loop structure of the capture probe positions the methylene blue (MB) near the electrode. Close proximity of MB to the electrode allows for electron transfer and production of electrical current. The target hybridizes to the capture probe causing the MB to be distant from the electrons so that no electrons are transferred. *Nucleic Acid Lateral Flow* Assay: The target amplicons flow across the membrane into the first regions where it hybridizes to signaling oligonucleotides. The signaling oligonucleotides are tagged with gold-nanoparticles. This complex then hybridizes with capture oligonucleotides which is visualized as a blue colour due to the presence of gold particles.

1.5 Introduction to DNA based Biosensors

1.5.1 Biosensors

Bacterial detection technologies are progressing towards biosensors that have been manufactured for portability, full automation (elimination or reduction of sample preparation steps), and efficiency for quick results with great sensitivity.[5] A biosensor is a device that integrates a biological element such as enzymes, antibodies, receptors or DNA with transducer elements for the analysis of the signal produced upon the presence of specific analytes.[59] Biological elements provide target specific recognition whereas optical or electrochemical transducers respond to the signals that are generated by photon emission, colour change or electrochemical current, etc. This section will specifically focus on biosensors that use DNA or RNA aptamers as the molecular recognition element. It is important to note that no single method used to detect the bacteria can achieve the idealized characteristics of a biosensor as mentioned above. For example, rapid detection systems may sacrifice sensitivity to achieve their results.

1.5.2 Introduction to Aptamers

Aptamers are short single stranded DNA (ssDNA) or RNA molecules which have high affinity and specificity towards a target molecule.[60, 61] In 1990s, Ellington & Szostak created the first RNA aptamer that bound to specific organic dyes such as Cibracon Blue 3GA and Reactive green 19.[62] They also created a DNA aptamer which could bind organic dyes. Since then, aptamers have been created to bind various small molecules such as nucleotides (ATP), amino

acids (L-arginine), antibiotics (neomycin), theophylline, and larger biomolecules such as proteins (thrombin).[8] Aptamers are created by a technique called selective evolution of ligands by exponential enrichment (SELEX).[8, 60, 63] Briefly, the strategy involves a pool of 10^{15} DNA or RNA molecules containing randomized sequences which are subjected to multiple rounds of selective pressures. Only the sequences which are capable of binding to the target will be isolated and amplified using PCR.[8, 64] Aptamers provide several advantages which include high affinity and specificity towards a wide range of targets and functionality at a wide range of salt concentrations, pH and temperatures. They can also be chemically modified (e.g. fluorophores) at precise locations and can be immobilized on various surfaces (e.g. gold electrodes) without affecting their overall binding affinity. The ability to engineer an aptamer to bind essentially any target of interest holds great potential for developing pathogen biosensors.

Whole-cell based SELEX strategies can be adopted to develop aptamers that bind specific bacterial strains by recognizing cell-specific surface markers, or secreted metabolites.[8, 64] Early attempts to detect pathogens include the development of DNA aptamers that are capable of recognizing and binding to Sterne strain *Bacillus anthracis* spores using an aptamer-magnetic beads-electrochemiluminescence (ELC) sandwich assay.[65] Aptamers that can bind to *Campylobacter jejuni* or *Mycobacterium tuberculosis* have also been created using whole-cell SELEX strategies; however, cross-reactivity of these aptamers with other bacterial organisms raises a concern.[64]

1.5.3 Aptasensors

Aptamers can form complex tertiary structures and often undergo distinct conformational changes in the presence of a target. These properties have been exploited to devise strategies for creating wide range of conformational-dependent aptamer-based biosensors, or aptasensors, many of which depend on fluorescence or an electronic signal readout.[60, 61, 64, 66, 67]

The fluorescence resonance energy transfer (FRET)-based aptasensors change the fluorescent signal output by altering the distance between the covalently attached fluorophore and quencher molecule. Liu *et al.* (2009) demonstrated a "signal-off" strategy in which a thrombin binding aptamer labeled with a 5'-fluorophore and 3'-quencher initially adopts a relaxed conformation (on-state) in the absence of a target (Figure 1.3a).[68] In the on-state, a large fluorescent emission is observed as the two ends of the aptamer are distant and freely moving. The off-state existed when the aptamer adopting a ridged G-quartet or hairpin-like structure in the presence of lead (Pb^{2+}) and mercury (Hg^{2+}) ions, respectively. This structural change brought the two ends of the aptamer in close proximity thereby reducing the fluorescent emission. The group achieved a detection limit of Pb^{2+} and Hg^{2+} ions in the low nanomolar range and even validated the practicality of the method by measuring the target in soil and pond samples.

In a typical "signal-on" method the aptamer conjugated to a fluorophore at one end is initially quenched by quencher in the absence of a target (Figure 1.3b). One way to bring the quencher in proximity to the fluorophore is by hybridizing a quencher-modified complementary

strand to the aptamer. The fluorescence is enhanced when the aptamer dissociates from the complementary strand brought upon by structural change when bound to its target.[69, 70]

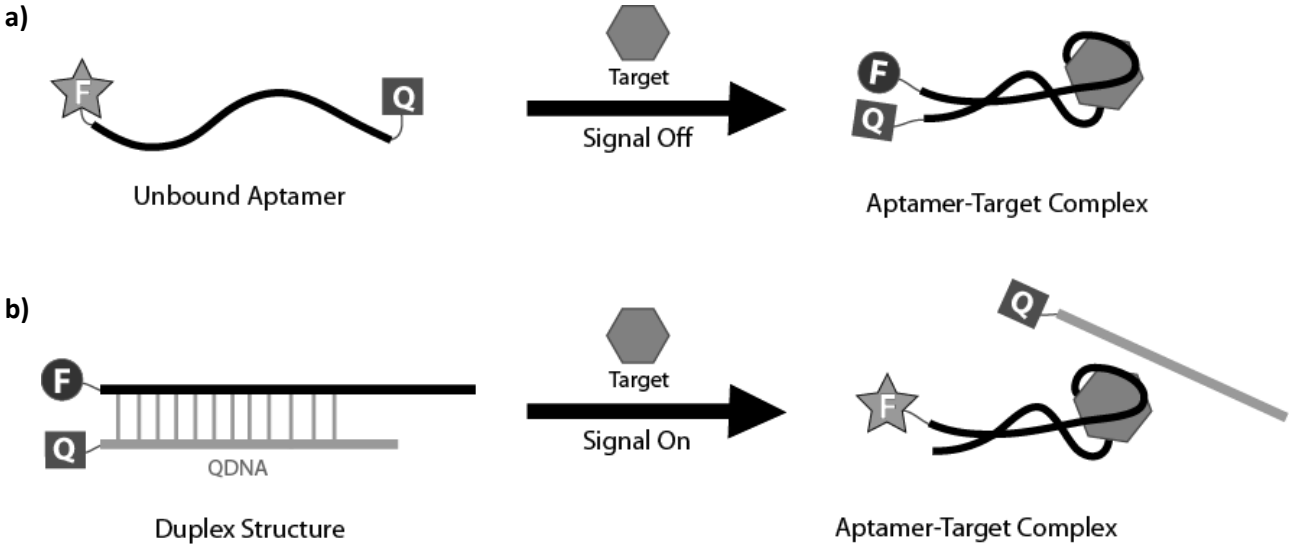

Figure 1.3. Aptasensors. a) "*Signal-off*" *Aptasenors*: In the absence of a target, the fluorescence emission is visualized since the fluorophore (F) distantly placed from the quencher (Q) on the aptamer. Structural change brought upon by target binding positions the quencher near the fluorophore which reduces the fluorescent emission. b) "*Signal-on*" *Aptasensor*: The aptamer modified with fluorophore is hybridized to a quencher modified DNA (QDNA). In the absence of target, the quencher is within close proximity of the fluorophore. The QDNA is displaced due to the structural change of the aptamer brought upon by target binding.

Several electrochemical aptasensors rely on the changes in the three-dimensional structure of aptamers to control the proximity of the electrode to the redox-active compound tethered to the aptamer.[60, 71-73] Radi *et al.* (2006) conjugated bifunctionilized thrombin aptamer to a gold electrode by a thiol group at one end and ferrocene redox label at the opposite end. In the absence of potassium ion (K^+) target, the flexible, free moving aptamer kept the ferrocene distant from the electrode surface thereby preventing electron flow.[73] The K^+ ion bound aptamer adopted a ridged G-quartet structure which brought ferrocene close to the electrode surface to allow electron transfer.

Examples of aptamers in the literature which have been developed to target disease causing bacterium or their toxins are listed in Table 1.2.[64] However, the use of these aptamers as recognition elements in aptasensors for pathogens detection, particularly in foods or water, is limited. Zelada-Guillén *et al.* (2009) devised a label-free electronic potentiometric sensor to selectively detect 1 CFU/mL of *S. Typhi* (ST).[74] They covalently immobilizing a high-affinity RNA aptamer which binds to type IVB pili of ST to the surface of single-walled carbon nanotubes (SWCNTs). The changes in the potential at the working electrode was measured upon ST cells binding. Zelada-Guillén also investigated the ability of their potentiometric aptasensor to detect pathogenic bacteria in real samples requiring minimum sample preparation steps. They were able to specifically measure *E. coli* CECT 675 (a nonpathogenic substitute for *E. coli* O157:H7) spiked in milk and apple juice with a detection limit of 6 CFU/mL and 26 CFU/mL, respectively.[75] The detection was nearly in real time as the spiked samples were used directly for detection without further culturing steps. However, a filtration and wash step was required to remove charged ions present in the sample matrix which could potentially interfere with the assay. Furthermore, in Zelada-Guillén's more recent work, they applied the same method to detect *Staphylococcus aureus* in pig skin with a detection limit of 8×10^2 CFU/mL.[76]

Table 1.2. Aptamers developed for pathogen detection and therapeutics. This table was adopted from Chavolla *et al.* (2009).

Target	Function	Target Identification
Whole-cell Targets		
B. anthracts Sterne strain spores	Detection	Non-identified
B. thuringiensis spores	Detection	Non-identified
E. coli DH5α	Detection	Non-identified
M. tuberculosis	Anti-mycobacterial agent	Membrane Protein
T. brucet	Anti-parasitic drug	Parasite flagellar protein
T. cruzi	Invasion inhibitor agent	Parasite receptors for the host cell matrix molecules laminin, fibronecitin, thrombospondin and heparin sulfate.
Human Influenza A virus (H3N2)	Influenza A virus genotyping and inhibitor agent	Haemagglutinin (HA1 peptide chain)
S. aureus[77]	Detection	Non-identified
L. acidophilus[78]	Detection	Non-identified
S. typhimurium[79]	Detection	Non-identified
Non whole-cell targets		
F. tularensis bacterial protein cell lysate	Detection	Non-identified
Rous Sarcoma virus (RSV) particles	Virus inhibitor agent	Non-identified
Vaccinia virus particles	Infection inhibitor agent	Non-identified
Microbial and viral protein/toxin target	**Function**	
Cholera whole toxin	Detection	
E. coli release factor 1	Non-sense suppression based technology	
Mycobacterium avium subsp. *paratuberculosis* recombinant MAP0105c gene product	Detection	
S. enterica serovar Typhi IVP pili protein	Cell invasion inhibitor agent	
Shiga toxin	Detection	
Staphylococcal enterotoxin B	Detection	
Hepatitis C virus (HCV) NS3 protease	Anti-HCV agent	
HCV NS3 helicase	Therapeutics and Dignostic	
HCV NS5B RNA poltmerase	Polymerase inhibitor	
Herpes Simplex Virus 1 gD protein[80]	Virus inhibitor agent	
HIV-1 TAT protein	Transcription inhibitor	
HIV-1 reverse transcriptase	Reverse transcription inhibition	
HIV-1 R5 SU glycoprotein	Antiviral	
Influenza A virus	Antiviral	
SARS coronavirus NTPase/Helicase	Anti-SCV agents	
Rift Valley fever virus (RVFV) Nucleocapsid (N) protein[81]	Detection	

1.5.4 RNA-Cleaving Fluorescent DNAzyme

RNA or DNA nucleic acid enzymes, termed ribozymes or deoxyribozymes (DNAzymes) respectively, can catalyze reactions much like protein enzymes.[8] Early deoxyribozymes isolated by SELEX catalyzed the cleavage of riboadenosine embedded within a DNA sequence and current deoxyribozymes can perform DNA or RNA ligation, phosporylation, deglycosylation and more.[61, 82] The catalysis by the aptazyme is allosterically modulated by conformational changes brought upon by the binding of a target to the aptamer. Sensitive DNAzyme biosensors used to detect environmentally hazardous metal ions such as lead or uranium have been developed and validate the potential of catalytic nucleic acids as tools for biosensors.[61] However, only recently has there been any progress in using DNAzymes in the application of detecting pathogenic bacteria. Ali *et al.* (2011) performed SELEX in order to isolate an RNA cleaving aptazyme which was catalytically activated only in presence of a target secreted specifically by *E. coli* K12.[83] The aptazyme cleaved a single riboadenosine (R) embedded within a short DNA strand (Figure 1.4). The deoxyribonucleoties flanking R were modified with a fluorophore and a quencher, and in the presence of cleavage, an intense fluorescent signal was observed either by a fluorimeter or a portable UV box. This aptazyme was aptly called RNA-cleaving fluorescent DNAzyme (RFD). This method provides an easy approach to detect pathogens using an intense fluorescent signal and eliminates many laborious steps involved in other methods like ELISA. Although aptamer or aptazymes are excellent candidates for the analysis of foodborne pathogens, much progress is still required to understand and improve the process of SELEX using crude cellular targets.

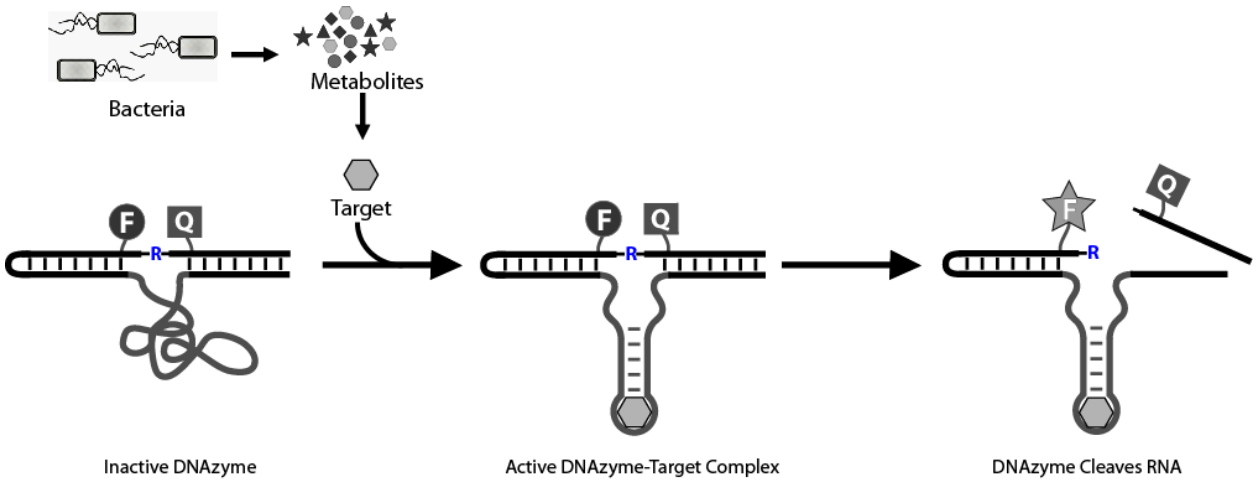

Figure 1.4. RNA-cleaving fluroscent DNAzyme (RFD). The single ribonucleotide (R) is situated between deoxyribonucleotides modified with a fluorophore (F) as the quencher (Q). The bacteria secretes many metabolites some of which are specific to the organism. The target binds to the RFD thereby activating the DNAzyme. The active DNAzyme cleaves the single ribonulceotide, which releases the fragment containing the quencher. The removal of the quencher allows the fluorophore to emit strong fluorescence.

1.6 Conclusion

The field of rapid-pathogen detection has advanced greatly over the past two decades, introducing techniques like the real-time PCR, and electrochemical or optical biosensors. Although these methods are classified as 'rapid sensors' the term is misleading because there is still the need for time-consuming enrichment cultures and multi-step process in detection. Thus, the next milestone for researchers will be to develop methods that are compatible with the complex matrices of food. Given the physical limitation of antibodies- and PCR-based methods, aptamers hold great promise in achieving such goals. The ability to perform SELEX in almost any given matrix, it might be possible to create aptamers compatible with various complex matrices.

Hence, it becomes very important to improve on the process of SELEX, namely trying to develop more efficient methods of high-throughput aptamer screening. Although the progress of aptamer-based technology towards commercialization has been slow, current examples for their use as biological elements for electronic or optical biosensors show their potential to achieve sensitive and specific pathogen detection.

1.7 References

1. Velusamy, V., Arshak, K., Korostynska, O., Oliwa, K. & Adley, C. An overview of foodborne pathogen detection: In the perspective of biosensors. *Biotechnology Advances* **28**, 232-254 (2010).
2. U.S. Department of Agriculture (USDA). Hudson foods recalls beef burgers nationwide for *E.coli* O157:H7. **0272.92** (1997).
3. Literature review of common food safety problems and applicable controls (2004). Available from: http://www.fda.gov/Food/FoodSafety/FoodborneIllness/default.htm.
4. Environmental assessment: Factors potentially contributing to the contamination of fresh whole cantaloupe implicated in a multi-state outbreak of listeriosis (2011). Available from: http://www.fda.gov/Food/FoodSafety/FoodborneIllness/ucm276247.htm.
5. Lazcka, O., Del-Campo, F. J. & Munoz, F. X. Pathogen detection: A perspective of traditional methods and biosensors. *Biosens. Bioelectron.* **22**, 1205-1217 (2007).
6. Feng, P. & Swaminathan, B. Rapid detection of food-borne pathogenic bacteria. *Annu. Rev. Microbiol.* **48**, 401-426 (1994).
7. Lequin, R. M. Enzyme Immunoassay (EIA)/Enzyme-Linked Immunosorbent Assay (ELISA). *Clin. Chem.* **51**, 2415-2418 (2005).
8. Turner, A., Elwary, S. & Zourob, M. *Principles of bacterial detection: biosensors, recognition receptors and microsystems* (Springer science, New York, USA, 2008).
9. Stevens, K. A. & Jaykus, L. A. Bacterial seperation and concentration from complex sample matrices: A review. *Crit. Rev. Microbiol.* **30**, 7-24 (2004).
10. (FDA) bacteriological analytical manual: Food sampling and preparation of sample homogenate (2003). Available from: http://www.fda.gov/Food/ScienceResearch/LaboratoryMethods/BacteriologicalAnalyticalManualBAM/ucm063335.htm.
11. Willis, C., Baalham, T., Greenwood, M. G. & Presland, F. Evaluation of a new chromogenic agar for the detection of Listeria in food. *J. App. Microbiol.* **101**, 711-717 (2006).

12. Bille, J. *et al.* API *Listeria*, a new and promising one-day system to identify *Listeria* isolates. *Appt. Environ. Microbiol.* **58**, 1857-1860 (1992).
13. Feng, P. Impact of molecular biology on the detection of foodborne pathogens. *Mol. Biotechnol.* **7**, 267-278 (1997).
14. Banada, P. P. & Bhunia, A. K. *Principles of bacterial detection: biosensors, recognition receptors and microsystems* (eds Zourob, M., Elwary, S. & Turner, A.) (Springer Science, New York, USA, 2008).
15. Notermans, S. & Wernars, K. Immunological methods for detection of foodborne pathogens and their toxins. *Int. J. Food Microbiol.* **12**, 91-102 (1991).
16. Peruski, A. H. & Peruski, L. F. Immunological methods for detection and identification of infections disease and biological warfare agents. *Clin. Diagn. Lab. Immunol.* **10**, 506-513 (2003).
17. Taylor, A.D., Yu, Q., Chen, S., Homola, J., and Jiang, S. Comparison of E. coli O157:H7 preparation methods used for detection with surface plasmon resonance sensor. *Sens. Actuators B. Chem.* **107**, 202-208 (2005).
18. Baccar, H., Mejri, M.B., Hafaiedh, I., Ktari, T., Aouni, M., and Abdelghani, A. Surface plasmon resonance immunosensor for bacteria detection. *Talanta* **82**, 810-814 (2010).
19. Deisingh, A. K. & Thompson, M. Biosensors for the detection of bacteria. *Can. J. Microbiol.* **50**, 69-77 (2004).
20. Barlen, B., Mazumdar, S.D., Lezrich, O., Kampfer, P., and Keusgen, M. Detection of *Salmonella* by surface plasmon resonance. *Sensors* **7**, 1427-1446 (2007).
21. Hsieh, S.C., Chang, C.C., Lu, C.C., Wei, C.F., Lin, C.S., Lai, H.C., and Lin C.W. Rapid identification of *Mycobacterium tuberculosis* infection by a new array format-based surface plasmon resonance method. *Nanoscale Res. Lett.* **7**, 1-6 (2012).
22. Ronkainen, N. J., Halsall, H. B. & Heineman, W. R. Electrochemical biosensors. *Chem. Soc. Rev.* **39**, 1747-1763 (2010).
23. Palchetti, I., and Mascini, M. Electroanalytical biosensors and their potential for food pathogen and toxin detection. *Anal. Bioanal. Chem.* **391**, 455-471 (2008).
24. Lin, H.Y., Chen, S.H., Chuang, Y.C., Lu, Y.C., Shen, T.Y., Chang, A.C., and Lin, S.C. Disposable amperometric immunosensing strips fabricated by Au nanoparticles-modified screen-printed carbon electrodes for the detection of foodborne pathogen *Escherichia coli* O157:H7. *Biosens. Bioelectron.* **23**, 1832-1837 (2008).
25. Yang, L., and Bashir, R. Electrical/electrochemical impedance for rapid detection of foodborne pathogenic bacteria. *Biotechnol. Adv.* **26**, 135-150 (2008).
26. Grieshaber, D., MacKenzie, R., Voros, J., and Reimhult E. Electrochemical biosensors- Sensor principles and architectures. *Sensors* **8**, 1400-1458 (2008).
27. Tully, E., Higson, P.S., and Kennedy, O.R. The development of a 'labeless' immunosensor for the detection of *Listeria monocytogenes* cell surface protein, Internalin B. *Biosens. Bioelectron.* **23**, 906-912 (2008).

28. Nandakumar, V. A low-cost electrochemical biosensor for rapid bacterial detection. *IEEE Sens. J.* **11**, 210-216 (2011).
29. Ortega-Vinuesa, J. L. & Bastos-Gonzalez, D. A review of factors affecting the performances of latex agglutination tests. *J. Biomater. Sci. Polymer Edn.* **12**, 379-408 (2001).
30. Raugel, P. J. in *Rapid food analysis and hygiene monitoring: kits, instruments and systems* (Springer Science, Germany, 1999).
31. Bacteriological analytical manual. appendix 1: Rapid methods for detecting foodborne pathogens (2001). Available from: http://www.fda.gov/food/scienceresearch/laboratorymethods/bacteriologicalanalyticalmanualbam/ucm109652.htm.
32. Posthuman-Trumpie, G. A. & Korf, J. Lateral flow (immono) assay: its strengths, weaknesses, opportunities and threats. A literature survey. *Anal. Bioanal. Chem.* **393**, 569-582 (2009).
33. Performance tested methods, validated methods (2012). Available from: http://www.aoac.org/testkits/testedmethods.html#antibiotics.
34. Blazkova, M., Koets, M. & Rauch, P. Development of a nucleic acid lateral flow immunoassay for simultaneous detection of *Listeria* spp. and *Listeria monocytogenes*. *Eur. Food Res. Technol.* **229**, 867-874 (2009).
35. Krska, R. & Molinelli, A. Rapid test strips for analysis of mycotoxins in food and feed. *Anal. Bioanal. Chem.* **393**, 67-71 (2009).
36. Maurer, J. J. Rapid detection and limitation of molecular techniques. *Annu. Rev. Food Sci. Technol.* **2**, 259-279 (2011).
37. Hill, W. E. DNA hybridization method for detecting entrotoxigenic *Escherichia coli* in human isolates and its possible application to food samples. *J. Food Safety* **3**, 233-247 (1981).
38. Eom, S. H. *et al.* Multiple detection of food-borne pathogenic bacteria using a novel 16S rDNA-based oligonucleotide signature chip. *Biosens. Bioelectron.***22**, 845-853 (2007).
39. Muthukumar, A., Zitterkopf, N. L. & Payne, D. Molecular tools for detection and characteization of bacterial infections: A review. *Labmedicine* **39**, 430-436 (2008).
40. Patel P.D. in *Rapid analysis techniques in food microbiology* (Springer Science, London, England, 1994).
41. Ninet, B., Bannerman, E. & Bille, J. Assessment of the accuprobe *Listeria monocytogenes* culture identification reagent kit for rapid colony confirmation and its application in various enrichment broths. *Appt. Environ. Microbiol.* **58**, 4055-4059 (1992).
42. Saiki, R. K., Scharf, S., Faloona, F., Mullis, K. B. & Horn, G. T. Enzymatic amplification of B-globin genomic sequences and restriction site analysis for diagnosis of sickle cell anemia. *Science* **230**, 1350-1354 (1985).
43. Schneeberger, C., Speiser, P., Kury, F. & Zellinger, R. Quantitative detection of reverse transcriptase-PCR products by means of a novel and sensitive DNA stain. *PCR Methods Appl.* **4**, 234-238 (1995).

44. Richards, G. P., Watson, M. A. & Kingsley, D. H. A SYBRE green, real-time RT-PCR method to detect and quantitate Norwalk virus in stools. *J. Virol. Methods* **116**, 63-70 (2004).
45. Viedma, G. Rapid detection of resistance in *Mycobacterium tuberculosis*: review discussing molecular approaches. *Clin. Microbiol. Infect.* **9**, 349-359 (2003).
46. Tyagi, S. & Kramer, F. R. Molecular beacons: probes that fluoresce upon hybridization. *Nat. Biotechnol.* **14**, 303-308 (1996).
47. Lie, P., Liu, J., Fang, Z., Dun, B. & Zeng, L. A lateral flow biosensor for detection of nucleic acids with high sensitivity and selectivity. *Chem. Commun.* **48**, 236-238 (2012).
48. Carter, D. & Cary, B. R. Lateral flow microarrays: a novel platform for rapid nucleic acid detection based on miniaturized lateral flow chromatography. *Nucleic Acids Res.* **35**, 1-11 (2007).
49. Glynou, K., Loannou, P. C., Christopoulos, K. T. & Syriopoulou, V. Oligonucleotide-functionalized gold nanoparticles as probes in a dry-reagent strip biosensor for DNA analysis by hybridization. *Anal. Chem.* **75**, 4155-4160 (2003).
50. Aveyard, J., Mehrabi, M., Cossins, A., Braven, H. & Wilson, R. One step visual detection of PCR products with gold nanoparticles and a nucleic acid lateral flow (NALF) device. *Chem. Commun.* 4251-4253 (2007).
51. Pedrero, M., Campuzano, S. & Pingarron, M. J. Electrochemical genosensors based on PCR strategies for microorganisms detection and quantification. *Anal. Methods* **3**, 780-789 (2011).
52. Lai, Y. R., Lagally, T.E., Lee, H.S., Soh, H.T., Plaxco, W.K., and Heeger, J.A. Rapid, sequence-specific detection of unpurified PCR amplicons via a resuable, electrochemical sensor. *Proc. Natl. Acad. Sci.* **103**, 4017-4021 (2006).
53. Lam, B., Fang, Z., Sargent, H. E. & Kelley, O. S. Polymerase chain reaction-free, sample-to-answer bacterial detection in 30 minutes with integrated cell lysis. *Anal. Chem.* **84**, 21-25 (2012).
54. Yean, Y. C. *et al.* Enzyme-linked amperometric electrochemical genosensor assay for the detection of PCR amplicons on a streptavidin-treated screen-printed carbon electrode. *Anal. Chem.* **80**, 2774-2779 (2008).
55. Farabullini, F., Lucarelli, F., Palchetti, I., Marrazza, G. & Mascini, M. Disposable electrochemical genosensor for the simultaneous analysis of different bacterial food contaminants. *Biosens. Bioelectron.* **22**, 1544-1549 (2007).
56. Tang, L. *et al.* Sensitive detection of lip genes by electrochemical DNA sensor and its application in polymerase chain reaction amplicons from *Phanerochaete chrysosporium*. *Biosens. Bioelectron.* **24**, 1474-1479 (2009).
57. Djellouli, N., Dequaire, R. M., Limoges, B., Druet, M. & Brossier, P. Evaluation of the analytical performances of avidin-modified carbon sensors based on a mediated horseradish peroxidase enzyme label and their application to the amperometric detection of nucleic acids. *Biosens. Bioelectron.* **22**, 2906-2913 (2007).

58. Suye, S. *et al.* Amperometric DNA sensor using gold electrode modified with polymerized mediator by layer-by-layer adsorption. *Microelectronic Engineering* **81**, 441-447 (2005).
59. Lei, Y., Chen, W. & Mulchandani, A. Microbial biosensors. *Analytica Chimica Acta.* **568**, 200-210 (2006).
60. Mok, W. & Li, Y. Recent progress in nucleic acid aptamer-based biosensors and bioassays. *Sensors* **8**, 7050-7084 (2008).
61. Liu, J., Cao, Z. & Lu, Y. Functional Nucleic Acid Sensors. *Chem. Rev.* **109**, 1948-1988 (2009).
62. Ellington, A. D. & Szostak, J. W. In vitro selection of RNA molecules that bind specific ligands. *Nature* **346**, 818-822 (1990).
63. Tuerk, C. & Gold, L. Systematic evolution of ligands by exponential enrichment: RNA ligands to bacteriophage T4 DNA polymerase. *Science* **249**, 505-510 (1990).
64. Chavolla, E. & Alocilja, E. C. Aptasensors for detection for microbial and viral pathogens. *Biosens. Bioelectron.* **24**, 3175-3182 (2009).
65. Bruno, J. G. & Kiel, J. L. In vitro selection of DNA aptamers to anthrax spores with electrochemiluminescence detection. *Biosens.Bioelectron.* **14**, 457-464 (1999).
66. Hianik, T. & Wang, J. Electrochemical Aptasensors – Recent Achievements and Perspectives. *Electroanalysis* **21**, 1223-1235 (2009).
67. Song, S., Wang, L., Li, J., Zhao, J. & Fan, C. Aptamer-based biosensors. *Trends Anal. Chem.* **27**, 108-117 (2008).
68. Liu, C.W., Huang, C.C., and Tsung, H. Highly selective DNA-based sensor for lead (II) and mercury (II) ions. *Anal. Chem.* **81**, 2383-2387 (2009).
69. Nutiu, R., and Li, Y. In vitro selection of structure-switching signaling aptamers. *Angew. Chem. Int. Ed.* **44**, 1061-1065 (2005).
70. Nutiu, R., and Li, Y. Structure-switching signaling aptamers. *J. Am. Chem. Soc.* **125**, 4771-4778 (2003).
71. Cheng, A.K.H., Ge, B., and Yu, H.Z. Aptamer-based biosensors for label-free voltammetric detection of lysozyme. *Anal. Chem.* **79**, 5158-5164 (2007).
72. Lu, Y., Li, X., Zhang, L., Yu, P., Su, L., and Mao, L. Aptamer-based electrochemical sensors with aptamer-complementary DNA oligonucleotides as probe. *Anal. Chem.* **80**, 1883-1890 (2008).
73. Radi, E.A., and O'Sullivan, K.C. Aptamer conformational switch as sensitive electrochemical biosensor for potassium ion recognition. *Chem. Commun.* 3432-3434 (2006).
74. Zelada-Guillen, G.A., Riu, J., Duzgun, A., and Rius F.X. Immediate detection of living bacteria at ultralow concentration using carbon nanotube based potentiometric aptasensor. *Angew. Chem. Int. Ed.* **48**, 7334-7337 (2009).
75. Zelada-Guillen, G.A., Bhosale, S.V., Riu, J., and Rius, F.X. Real-time potentiometric detection of bacteria in complex samples. *Anal. Chem.* **82**, 9254-9260 (2010).

76. Zelada-Guillen, G.A., Sebastian-Avila, J.L., Blondeau, P., Riu, J., and Rius, F.X. Label-free detection of *staphylococcus aureus* in skin using real-time potentiometric biosensors based on carbon nanotubes and aptamers. *Biosens. Bioelectron.* **31**, 226-232 (2012).
77. Cao, X., Li, S., Chen, L., Ding, H., Xu, H., Huang, Y., Li, J., Liu, N., Cao, W., Zhu, Y., Shen, B., and Shao, N. Combining use of a panel of ssDNA aptamer in detection of *Staphylococcus aureus*. *Nucleic Acids Res.* **37**, 4621-4628 (2009).
78. Hamula, C.L.A., Zhang, H., Guan, L.L., Li, X.F., and Le, X.C. Selection of aptamers against live bacteria. *Anal. Chem.* **80**, 7812-7819 (2008).
79. Dwivedi, H.P., Smiley, R.D., and Jaykus, L.A. Selection of DNA aptamers for capture and detection of *Salmonella typhimurium* using a whole-cell SELEX approach in conjunction with cell sorting. *Appl. Microbiol. Biotechnol.* **97**, 3677-3686 (2013).
80. Gopinath, S.C.B., Hayashi, K., and Kumar, K.R.P. Aptamer that binds to the gD protein of the Herpes Simplex virus 1 and efficently inhibits viral entry. *J. virol.* **86**, 6732-6744 (2012).
81. Ellenbecker, M., Sears, L., Li, P., Lanchy, J.M., and Lodmell, J.S. Characterization of RNA aptamers directed against the nucleocapsid protein of Rift Valley fever virus. *Antiviral Res.* **93**, 330-339 (2012).
82. Breaker, R. R. & Joyce, G. F. A DNA enzyme that cleaves RNA. *Chem. Biol.* **1**, 223-229 (1994).
83. Ali, M. M., Sergio D. A., Lazim H., & Li, Y. Fluorogenic DNAzyme probes as bacterial indicators. *Angewandte Chemie*. (2011).
84. Pretzev, A. V. & Nicholson, A. W. Characterization of RNA sequence determinants and anti-determinants of processing reactivity for a minimal substrate of *Escherichia coli* ribonuclease III. *Nucleic Acids Res.* **34**, 3708-3721 (2006).

CHAPTER 2: Materials and Methods

2.1 Construction of Plasmid and Cell Cloning

The *L. monocytogenes* 4b (strain CLIP80459) genes *rnc* (Lm-RNase III), *rng* (Lm-RNase G), *rnhb* (Lm-RNase HII) and the N-terminus deleted (ΔN)-*rnhb* (ΔN Lm-RNase HII) were amplified by PCR and ligated into either pET 15b vector (Novagen) using the XhoI-Bpu1102 restriction sites. The primer sequences used for PCR are listed in Table 2.1 and the restriction sites are underlined. Restriction enzymes were bought either from Thermo Scientific or New England Biolabs (NEB).

Table 2.1

Gene	Primers	Constructed Plamid
rnc	1) TATTAT**CTCGAG**ATGAATCAATGGGAAGAGTTACAAGAA 2) ATTATT **GCTCAGC**TTATCTGTGTGTTAGTTGGTTTATAGC	pET-15b-Lm-*rnc*
rng	1) TATTAT**CTCGAG**ATGAAAAAGCTAGTAGTAAGTGC 2) ATTATT **GCTCAGC**TTAGTTTTCCACCCGGC	pET-15b-Lm-*rng*
rnhb	1) TATTAT**CTCGAG**ATGAGCGATTCCATATCCGTTA 2) ATTATT **GCTCAGC**TTATTTTAAACTATCAAAATGCAAC	pET-15b-Lm-*rnhb*
(ΔN)-*rnhb*	1) TATTAT**CTCGAG**ATGAAACAATATGAAACAG 2) ATTATT **GCTCAGC**TTATTTTAAACTATCAAAATGCAAC	pET-15b-Lm-(ΔN)*rnhb*
rnhb	1) TATTAT**GAATTC**ACTTTAAGAAGGAGATATACCATGG 2) ATTATT**TCTAGA**AGTTATTGCTCAGCGGTGG	pBAD wt Lm-*rnhb*
(ΔN)-*rnhb*	1) TATTAT**GAATTC**ACTTTAAGAAGGAGATATACCATGG 2) ATTATT **AAGCTT**AGTTATTGCTCAGCGGTGG	pBAD (ΔN) Lm-*rnhb*

The plasmids are referred to as pET 15b-Lm-*gene name*. The constructed plasmids were transformed either into *E. coli* strain BL21 (DE3) or pRARE2 using standard heat-shock method. All cell strains were kindly donated by Dr. Alba Guarné.

The wildtype (wt) *rnhb* and (ΔN)-*rnhb* genes were inserted into the pBAD 30 plasmid using EcoRI-XbaI and EcoRI-HindIII restriction sites, respectively. The pET 15b-Lm-*rnhb* or

pET 15b-Lm-(ΔN) *rnhb* plasmid served as the template for PCR and the primers are listed in Table 2.1.

2.2 Protein Solubility and Expression Assay

A 20 mL cell culture containing antibiotics ampicillin (Sigma Aldrich) was grown to an OD_{600} of ~0.7. Only for cells containing pET 15b-Lm-*rnhb* an additional antibiotic was added, (chloramphenicol). A 600 µl of culture was collected into an Eppendorf tubes (1.5 mL) and spun down (16000× g for 13 minutes); this sample severed as a control for celles not induced with Isopropyl β-D-1-thiogalactopyranoside (-IPTG). The remainder of the culture was split into two 15 mL flacon tubes (6 mL each) and induced with 0.5 mM IPTG (Sigma Aldrich). Induced samples were cultured at 37°C for 3 hr and 25°C for 5 hr. A 350 µl sample was collected from each induced sample and spun down (16000× g for 3 minutes) and only the cell pellet was kept; the sample was termed the +IPTG. The remainder of the culture was spun down at 16000× g for 20 min and resuspended in 200 µl of 20 mM Tris (pH 8.0) and 1.4 mM β-mercaptoethanol. Lysozyme was added with a final concentration of 1mg/mL and incubated on ice for 30 min. Sodium Chloride (NaCl) was added with a final concentration of 0.5 M, followed by the addition of 0.05% Lauryldimethylamine-N-Oxide (LDAO, Sigma Aldrich) and incubated on ice for 30 min. The lysed samples were spun (16000x g for 20 min) and 20 µl of the supernatant was mixed and boiled with 1× Sodium dodecyl sulfate (SDS)-loading buffer for 10 min; this sample was termed the +IPTG (soluble). All other samples (50 µl of -IPTG and +IPTG) were boiled for 10 min with 1× SDS-loading buffer. The samples were loaded onto and resolved by 15% SDS-

Polyacrylamide gel electrophoresis (PAGE). The expression of the enzymes and the experimental conditions are found in Figure 2.1a, b and c. Nearly equal expression of Lm-RNase III was observed in all growth conditions, and the enzyme was largely present in the soluble fraction as visualized by sodium dodecyl sulfate polyacrylamide gel electrophoresis (SDS-PAGE) (Figure 2.1a). Greater expression for Lm-RNase G was achieved when cells were grown at 25°C for 5 hr compared to 37°C for 3 hr (Figure 2.1b). Compared to Lm-RNase III and G, the expression of RNase HII in all growth conditions was poor and, the enzyme was largely insoluble as revealed by 15% SDS-PAGE (data not shown). The poor expression may be due to the presence of multiple rare codons within the gene sequence of RNase HII (*rnhb*). The *E. coli BL21 (DE3) pRARE 2* strain was used to improve the protein yield.

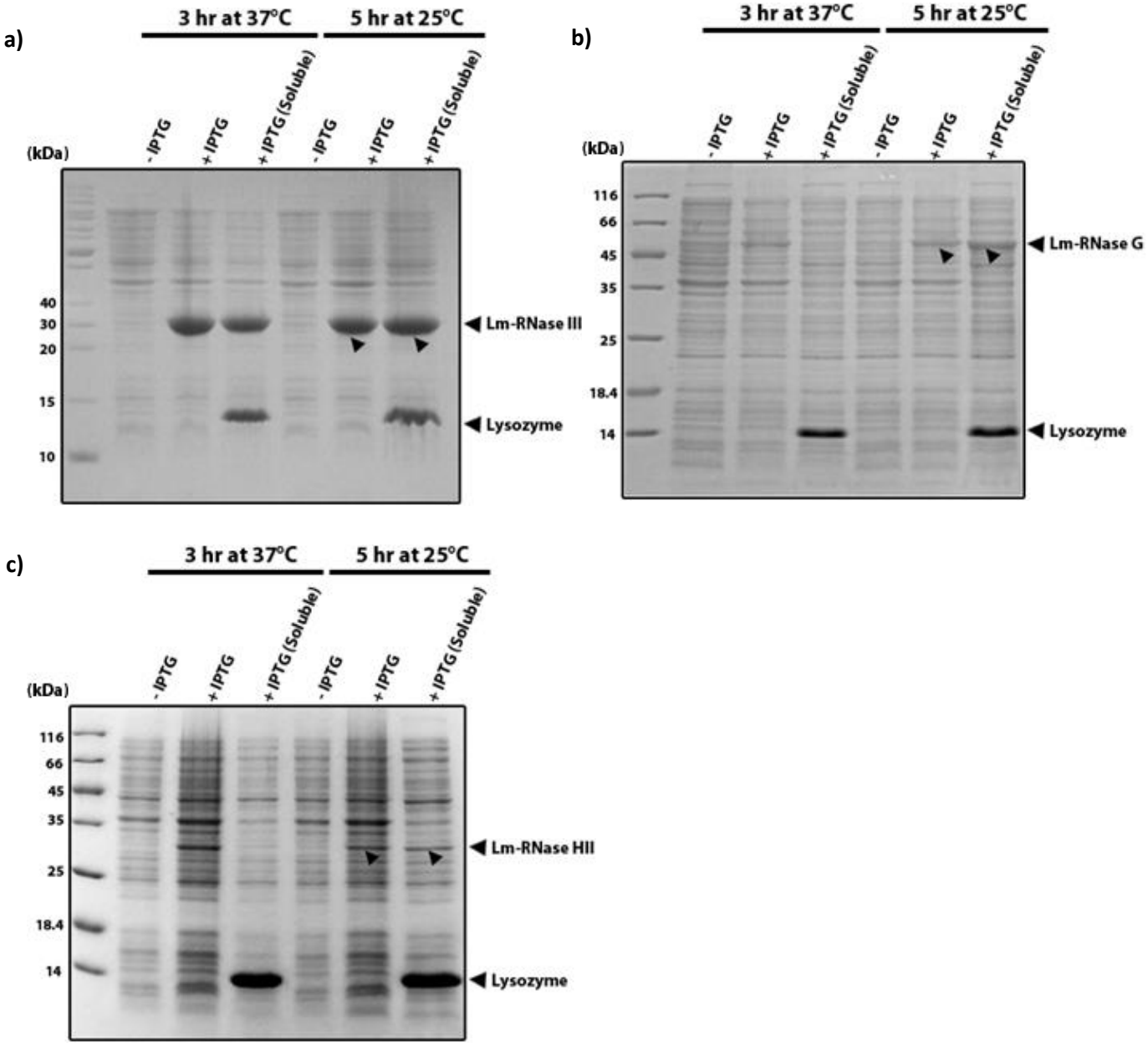

Figure 2.1. Protein expression and solubility assay for Lm-RNase III, G and HII. Cells were induced and grown at various conditions, as indicated above. RNase III (a) and G (b) were expressed in *E. coli BL21 (DE3)* and RNase HII (c) expressed in *E. coli BL21 (DE3) pRARE 2.* Cells that were not induced served as a control (-IPTG). Both the soluble component of the cell lysate and the cell pellet (insoluble component) were loaded onto 15% SDS-PAGE gel. The insoluble component is labeled as +IPTG and the soluble component as +IPTG (soluble). Smaller arrows highlight the presence of RNase following induction. A 28 kDa band representing Lm-RNase III is present in both +IPTG and +IPTG (soluble) at all growth conditions. Lm-RNase G (~53 kDa) expressed at both growth conditions but a greater portion of the enzyme was soluble in solution when grown at 25°C for 5 hr. Lm-RNase HII (~32 kDa) expressed at both growth conditions but a greater portion of the enzyme was soluble when grown at 25°C for 5 hr.

2.3 Protein Purification and Storage

A 1 L cell culture was grown at 37°C to an OD_{600} of ~0.7 followed by IPTG induction. Induced cells were and grown for 3 hr at 37°C for RNase III, 5 hr at 25°C for RNase G and RNase HII. Cell debris was pelleted after sonication and the supernatant was collected. The crude cell lysate was loaded onto a 5 mL General Electric (GE) Healthcare Ni^{2+} column using the Peristaltic (P)-1 pump (GE Healthcare). Fast protein liquid chromatography (FPLC) (Amersham Biosciences AKTA) was used to elute the bound protein with stepwise gradient of imidazole. The protein was eluted at 240 mM imidazole (Figure 2.2a, 2.3a, and 2.4a). Fractions containing protein were pooled and loaded onto an ion exchange column, Mono Q (GE Healthcare) (Figure 2.2b, 2.3b, and 2.4b). For RNase III and G, the Mono Q column was equilibrated with 20 mM Tris pH 8, 5 mM DTT, 5% glycerol, 0.1 M NaCl followed by a gradient elution from 0.1 M to 0.5 M NaCl. For RNase HII, the Mono Q column was equilibrated with 20 mM Tris pH 8, 5 mM DTT, 5% glycerol, 0.05 M NaCl followed by a gradient elution from 0.05 M to 0.5 M NaCl. The fractions collected during the MonoQ purification contained only a single molecular weight band, ~28kDa, 53kDa and 32kDa corresponding to Lm-RNase III, G and HII, respectively. During the Mono Q column purification of Lm-RNase III, the enzyme eluted at low and high salt concentrations as evident by the multiple peaks seen on the column elution graph (Figure 2.2b). However, all the fractions corresponding to the different peaks contained Lm-RNase III. Multiple peaks were observed as the protein formed distinct populations that differ in surface charge due to aggregation or different degrees of folding in the presence of the elution buffer.

The fractions eluted from Mono Q column were pooled and the buffer was exchanged for 20 mM Tris-HCl (pH 8), 0.15 M NaCl, 1 mM EDTA, 5 mM DTT, 5% glycerol (sizing column buffer) by using a 10,000K or 30,000K MWCO PES VIVASPIN 2 spin-columns (Sartorius Stedim Biotech). The protein sample was then loaded onto a superdex S200 sizing column (GE Healthcare) using the FPLC (Figure 2.2c, 2.3c, and 2.4c). The column was equilibrated with sizing column buffer at 4°C.

The hexa histidine-tag at the N-terminus of the protein was removed by thrombin (Sigma-Aldrich). The protein was first diluted to 0.5 mg/mL in a low salt buffer containing 20 mM Tris pH 8, 5 mM DTT, 5% glycerol, 150 mM NaCl, and 5 mM $CaCl_2$. It was then incubated with thrombin for 1 h at room temperature. A series of dilution of thrombin were used to determine the optimal concentration of thrombin needed for hexa histidine-tag removal. The digested hexa histidine-tag was separated from the protein by using Mono Q column.

RNase III was stored in 12 mM Tris (pH 8.0), 300 mM NaCl, 3 mM DTT, 30% glycerol at -80°C at a final concentration of ~2.8 mg/mL or 50 μM. Concentration was measured by Bradford assay (Bio-Rad) using the protocol provided by the manufacture. Lm-RNase G was stored in 12 mM Tris (pH 8.0), 200 mM NaCl, 3 mM DTT, and 30% glycerol at -80°C with a final concentration of ~2 mg/mL or 18 μM. Lm-RNase HII was stored in 12 mM Tris (pH 8.0), 150 mM NaCl, 3 mM DTT, 30% glycerol at -80°C with a final concentration of ~1.3 mg/mL or 40 μM.

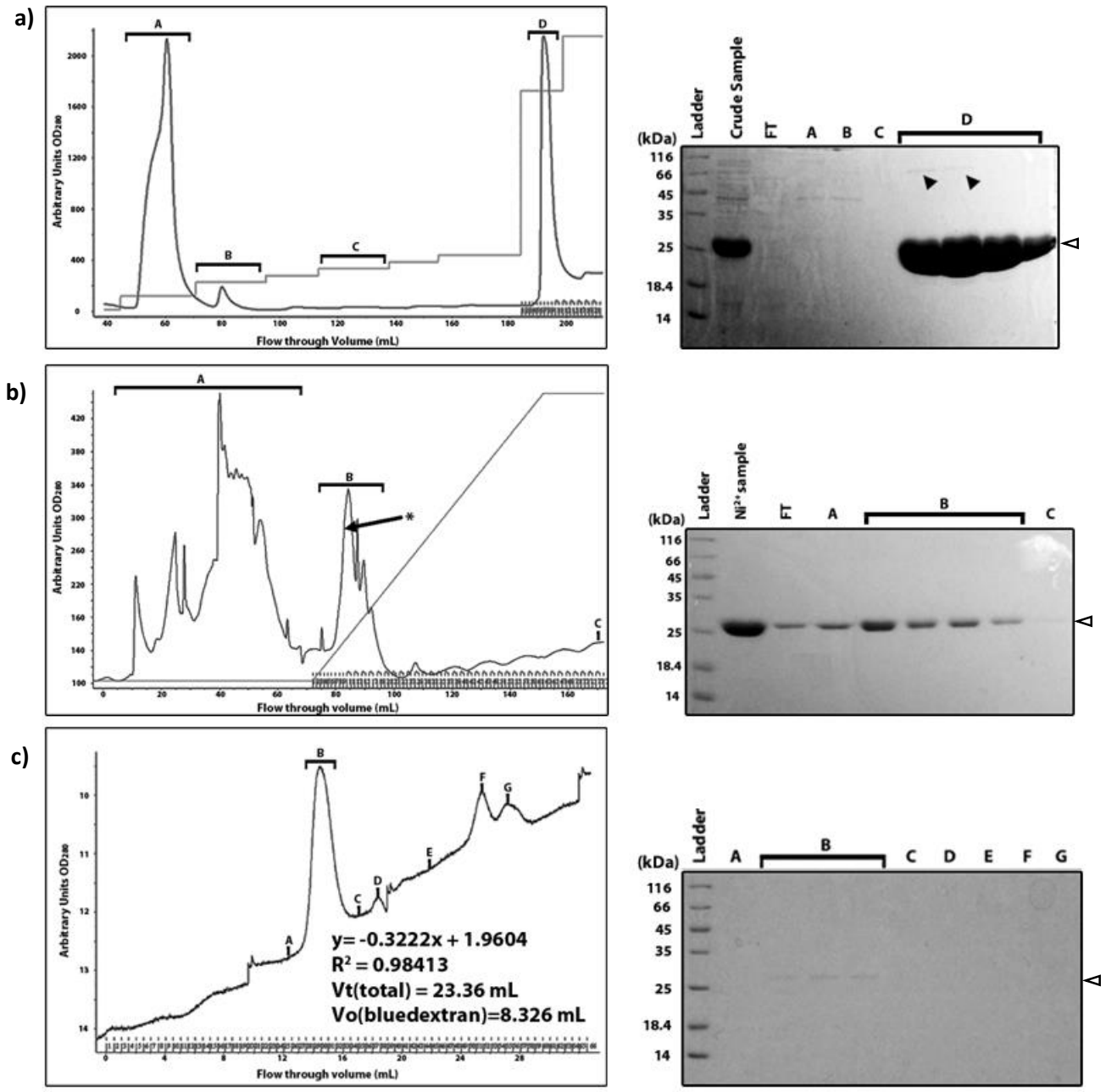

Figure 2.2. Purification of Lm-RNase III. a) *Ni^{2+} column purification:* The collected fractions (labeled A-D), were visualized by 15% SDS-PAGE. The untreated cell lysate is labeled as the crude sample. The flowthrough (FT) represents the fraction collected as the crude sample was loaded onto the Ni^{2+} column. The unfilled-arrow shows the expected size of RNase III. Protein contaminants are shown by solid arrows. b) *Mono Q column purification*: The fractions collected under the peaks A to C were loaded onto 15% SDS-PAGE. The Ni^{2+} sample on the gel represents the protein sample from Ni^{2+} purification and serves as a control to show the approximate size of Lm-RNase III. The FT represents the fraction immediately collected after loading the Ni^{2+} purified sample onto the Mono Q column. The bands seen at ~28 kDa correspond to Lm-RNase III. The asterisk arrow on the flow-elution graph indicates the fractions that were collected for further studies. c) *Superdex S200 sizing column purification*: The standard equation, listed in the figure, was used to approximate the molecular weight of the protein eluted under the peak B. The elution volume max was ~14.45 mL which equated to ~71 kDa (representing Lm-RNase III dimer).

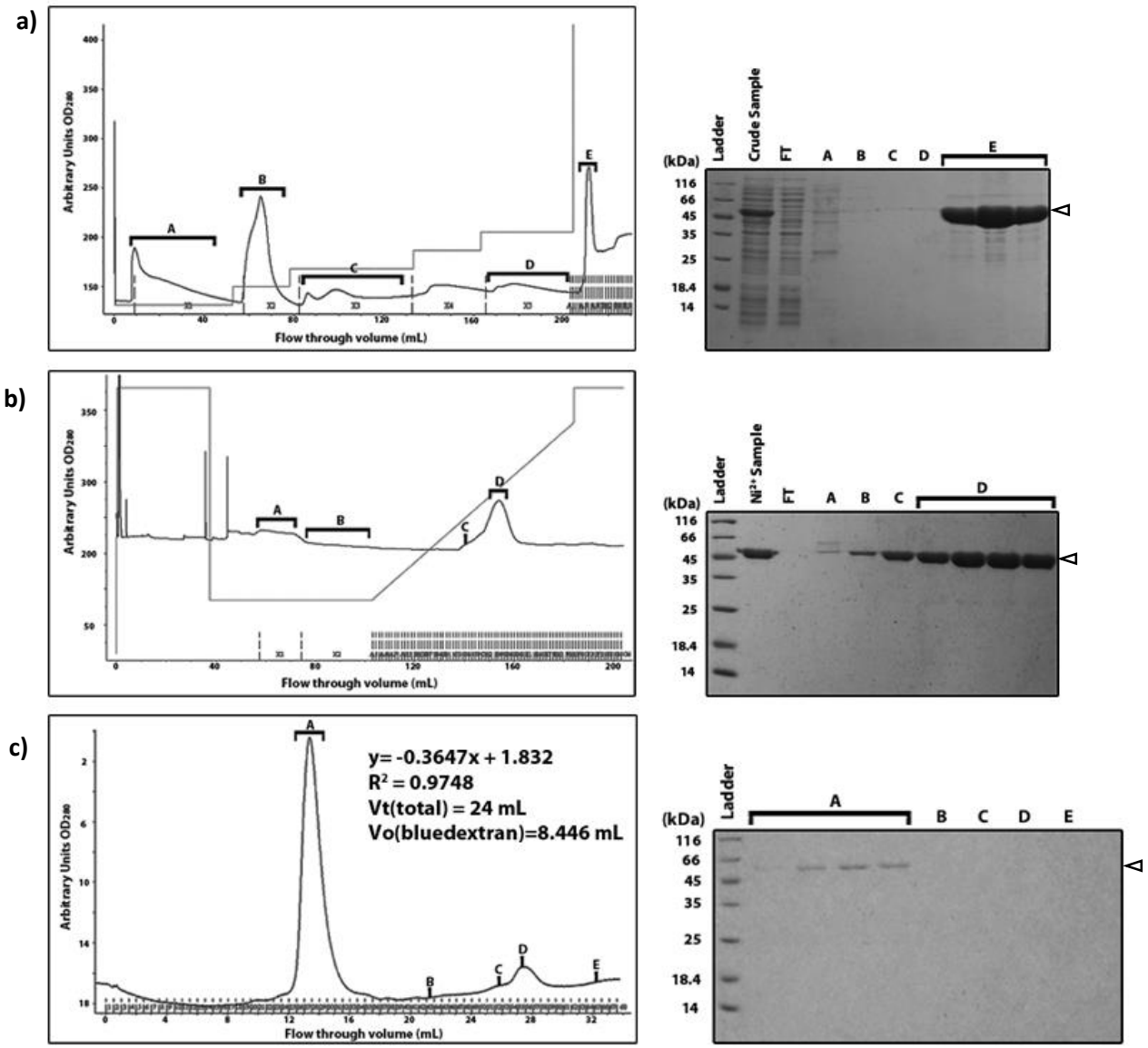

Figure 2.3. Purification of Lm-RNase G. a) *Ni^{2+} column purification:* The collected fractions (labeled A-E), were visualized by 15% SDS-PAGE. The untreated cell lysate is labeled as the crude sample. The flowthrough (FT) represents the fraction collected as the crude sample was loaded onto the Ni^{2+} column. The unfilled-arrow shows the expected size of RNase G. b) *Mono Q column purification*: The fractions collected under the peaks A to D were loaded onto 15% SDS-PAGE. The Ni^{2+} sample on the gel represents the protein sample from Ni^{2+} purification and serves as a control to show the approximate size of Lm-RNase G. The FT represents the fraction immediately collected after loading the Ni^{2+} purified sample onto the Mono Q column. The bands seen at ~53 kDa correspond to Lm-RNase G. c) *Superdex S200 sizing column purification*: The standard equation, listed in the figure, was used to approximate the molecular weight of the protein eluted under the peak A. The elution volume max was ~13.38 mL which equated to ~116 kDa (representing Lm-RNase G dimer).

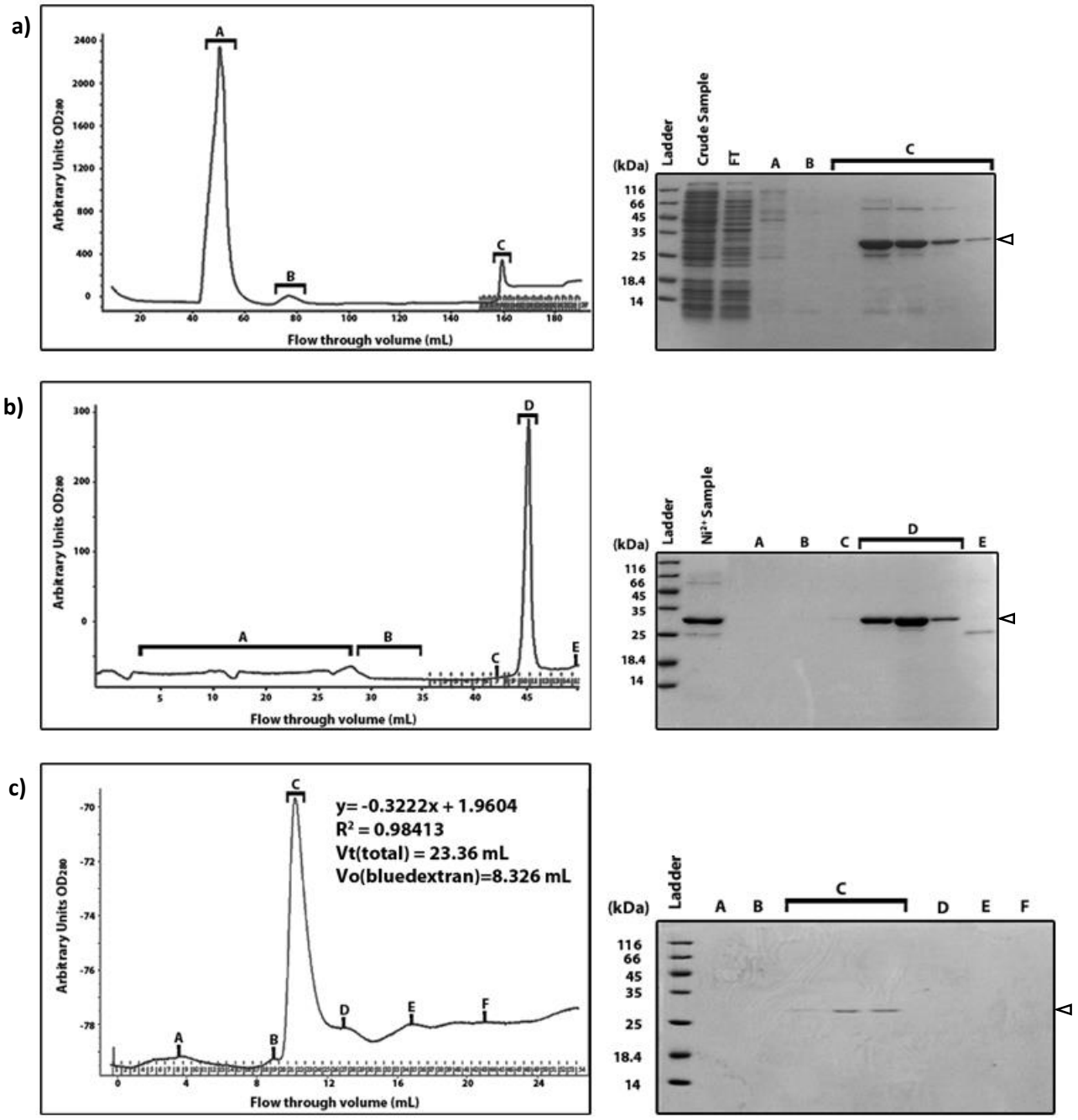

Figure 2.4. Purification of Lm-RNase HII. a) *Ni^{2+} column purification:* The collected fractions (labeled A-C), were visualized by 15% SDS-PAGE. The untreated cell lysate is labeled as the crude sample. The flowthrough (FT) represents the fraction collected as the crude sample was loaded onto the Ni^{2+} column. The unfilled-arrow shows the expected size of RNase HII. b) *Mono Q column purification*: The fractions collected under the peaks A to E were loaded onto 15% SDS-PAGE. The Ni^{2+} sample on the gel represents the protein sample from Ni^{2+} purification and serves as a control to show the approximate size of Lm-RNase HII. The FT represents the fraction immediately collected after loading the Ni^{2+} purified sample onto the Mono Q column. The bands seen at ~32 kDa correspond to Lm-RNase HII. c) *Superdex S200 sizing column purification*: The standard equation, listed in the figure, was used to approximate the molecular weight of the protein eluted under the peak C. The elution volume max was ~11.25 mL which equated to ~36 kDa (representing Lm-RNase HII monomer).

2.4 Synthesis and Purification of Oligonucleotides

All DNA or RNA used for cloning, assessing enzymatic reactions, and SELEX were purchased either from Integrated DNA Technologies (IDT) or Yale University Keck Facilities. All oligonucleotides were purified by 10% denaturing (8M Urea) polyacrylamide gel electrophoresis (dPAGE) before use. The DNA or RNA sequences used to assess enzymatic activity following protein purification are provided in the Table 2.2 and the sequences used for SELEX are listed in Figure 2.5.

Table 2.2

Enzyme	Sequences used to assess enzyme activity
RNase HII	5'AATAGAGAAAAAG**rArArArA**AAGATGGCAAAG (DNA-RNA chimera sequence) 5'CTTTGCCATCTTTTTTCTTTTTCTCTATT (complementary DNA strand)
RNase G	5' rGrGrGrArCrArGrUrArUrUrUrG (pBR13)
RNase III	5'GAATTC**TAATACGACTCACTATAG**GGAGAATAAACGTCATTCGCAAGAGTGGCGTTTAT (μR1.1 [5'+2] substrate) The underlined region shows the T7 RNA polymerase binding region. Primer 1: 5' GAATTCTAATACGACTCAC Primer2: 5' ATAAACGCCACTCTTGC

Some RNA sequences were made by *in vitro* transcription using 1 μg – 1 ng of PCR product or plasmid as template, 15-20 units (U) T7 RNA polymerase (Thermo Scientific), 1× T7 RNA polymerase buffer (Thermo Scientific), 5 mM ATP, CTP, GTP, 0.5 mM UTP (ribonucleotides purchased from BioBasics Canada Inc.), 10U Ribolock (Thermo Scientific), 50 μCi [α-^{32}P] UTP (Perkin Elmer), in a total volume of 50 μl or 100 μl. *In vitro* transcripts were purified by 10% dPAGE.

The λ N leader transcript substrate was made by first linearizing the pLKG002 plasmid containing the λ N leader gene fragment by using Bam HI restriction enzyme. The plasmid was

kindly gifted by Dr. David Bechhofer. Approximately 1 μg of linearized plasmid was used as template for *in vitro* transcription.

2.5 Assessing Enzyme Activity Following Protein Purification

DNA or RNA substrates were phosphorylated at the 5' end with 10 μCi [γ-^{32}P] dATP (Perkin Elmer) using 20 units of T4 polynucleotide kinase (PNK, Thermo Scientific), 1× PNK buffer A for 15 min at 37°C. The reactions setup is summarized in the Figure S4.1 in Chapter 4. The reaction buffer for RNase III and RNase G contained 30 mM Tris-HCl, pH 7.5, 160 mM NaCl, 1 mM DTT, 1 mM EDTA, 5% glycerol and that for RNase HII contained 15 mM Tris-HCl, pH 8.0, 50 mM NaCl, 1 mM DTT, 5% glycerol, 0.1 mM EDTA. The reactions for all three enzymes were initiated by adding $MgCl_2$ at a final concentration of 10 mM. The reaction mixtures were loaded onto a 10% dPAGE and DNA was visualized by phosphor-Imager using the Molecular Dynamics Typhoon, 9200.

2.6 Reverse-Transcriptase Polymerase Chain Reaction (RT-PCR)

The *L. monocytogenes* cells were grown to mid-log phase before RNA extraction. The total RNA was extracted following the guidelines provided by the Aurum Total RNA mini kit. Reverse transcription reaction was performed using 100U Maxima RT enzyme (Thermo Scientific), 20 ng of total RNA, 1 μM primer, 0.5 mM dNTPs, 1× reaction buffer (50 mM Tris-HCl pH 8.3, 75 mM KCl, 3 mM $MgCl_2$, 10 mM DTT) and 10U Ribolock with a total reaction

volume of 20 µl. The reaction was performed for 30 min at 50°C and quenched at 85°C for 5 min. 2 µl of the RT reaction was used as the template for the PCR reaction.

2.7 SELEX and Sequencing

Refer to Figure 2.5 for details on how SELEX was set up. The SELEX reaction was setup as described previously by Ali *et al.* (2011), Angew. Chem. Int. **50**, 3751-3754. The 1× selection buffer (SB) contained 50 mM HEPES, pH 7.5, 150 mM NaCl, 15 mM $MgCl_2$, and 0.01% Tween 20.

The round 15 DNA pool was amplified by PCR and cloned into a vector using the TA cloning method (Invitrogen). Cells containing plasmids with individual sequences were prepared according to the specification of Functional Biosciences Inc. for sequencing.

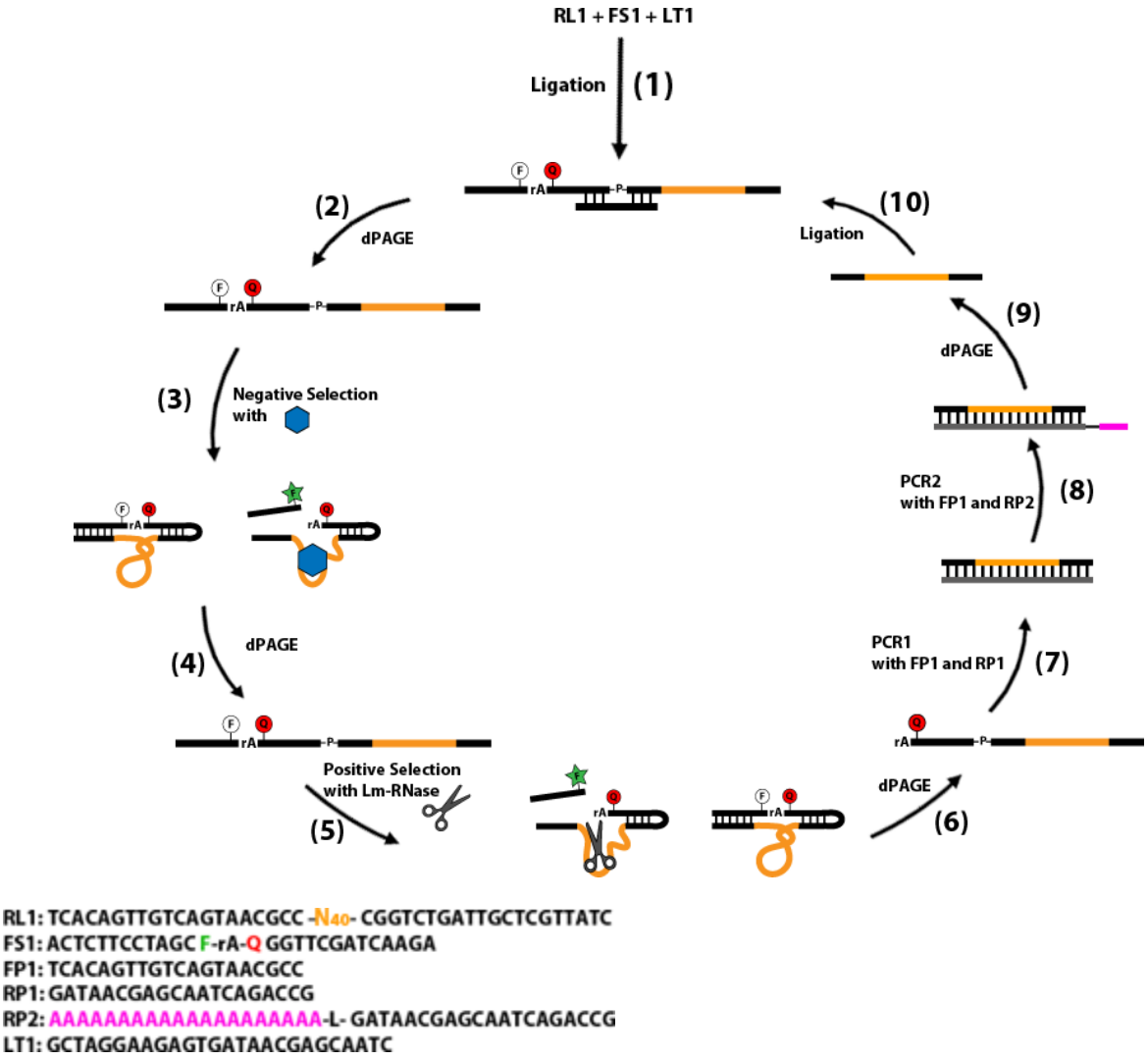

Figure 2.5. SELEX schematics for RFS. *Ligation of RL1 to FS1* (Step 1): The DNA library (RL1), composed of 40 randomized nucleotides (N_{40}) shown in orange, is ligated to the fluorescent substrates (FS1) using the ligation template (LT1). *Purification of Ligated RL1-FS1* (Step 2): The Ligated products are purified using 10% denaturing polyacrylamide gel (dPAGE). *Negative or Counter-selection* (Step 3): The ligated library is incubated with 1X selection buffer (SB) or solution containing non-specific targets. *Purification of uncleaved RL1-FS1* (Step 4): The sequences which are not cleaved in step 3 are purified using 10% dPAGE. *Positive selection of uncleaved RL1-FS1* (Step 5): The ligated library is incubated with the target of interest, *L. monocytogenes* endoribonuclease (Lm-RNase) in which some sequence are cleaved by the Lm-RNase. *Purification of cleaved products* (Step 6): The sequences which are cleaved by Lm-RNases in step 5 are purified using 10% dPAGE. *PCR1* (Step 7): The cleaved products are amplified using forward primer 1 (FP1) and reverse primer 1 (RP1). *PCR2* (Step 8): The product from PCR1 is used as the template DNA for PCR2. The reverse primer 2 (RP2) contains 20 adenines (A) at the 5' end separated by an 18 carbon spacer molecule (L); the DNA polymerase cannot amplify DNA sequences past the carbon spacer. *Purification of the sense strand* (Step 9): The sense strand of the PCR2 product codes for the sequence which interacts specifically with the RNase. The sense strands which are shorter than the antisense strands are separated by 10% dPAGE. *Ligation of RL1 to FS1* (Step 10): The enriched population of DNA sequences are re-ligated to the FS1. The enriched sequences are again subjected to positive selection (steps 5-10), multiple times until a unique sequences that are cleaved efficiently by the Lm-RNase are isolated. If the sequences cross-react with undesired RNases from different bacterial species, the enriched DNA pool can be subjected to counter-selection steps (steps 3 to 4), in an attempt to remove sequences that interact with the undesired target.

2.8 *In Vivo* Complementation Assay for RNase H Activity

E. coli MIC2067 cells were transformed with either an empty pBAD 30 vector, the pBAD 30 vector containing the wt or (ΔN) Lm-*rnhb* gene. Cells were spread on a Luria-Bertani (LB) medium plates containing 50 μg/mL ampicillin and grown at 30°C or 43°C.

2.9 Circular Dichroism (CD) Spectroscopy

The protein was placed in the buffer containing 20 mM Tris-HCl (pH 7.5), 50 mM NaCl, 5 mM DTT, 30% glycerol. The wavelength for obtaining the CD spectra was set from 260 nm to 197 nm on the Aviv model 410 CD spectrometer (Biomedical Inc). The reading was taken in a 0.1 mm-width glass vial at 25°C. Protein concentration was set from 0.1 to 0.5 mg/mL. The reading using buffer alone was used to correct the baseline. The following formula was used to convert the raw CD-signal data to mean residue ellipticity:

1) Ellipticity, [θ], in deg. · cm^2/dmol = (millidegrees X mean residue weight) / (path length in mm X protein concentration in mg/ml)

2) The mean residue weight of a protein is the molecular weight divided by the number of backbone amides (backbone amides= number of amino acids -1)

2.10 Assessing the *In Vitro* Activity of wt- and ΔN-Lm RNase HII

Substrates labeled with fluorescein at the 3' end (synthesized by IDT) (Chapter 3 Table 3.1) were used to assess the *in vitro* activity of wt- and ΔN-RNase HII. The RNA-DNA chimera sequences were mixed with the complementary antisense DNA sequences at a 1:2 mole ratio respectively, to form a heteroduplex. The buffer used for enzyme reaction contained 20 mM Tris-Cl pH 7.5, 50 mM NaCl, 50 mM DTT, 0.1 mM EDTA. The reactions were initiated by adding 10

mM $MgCl_2$ and were performed at 37°C for 30 min, unless otherwise stated. The enzyme and substrate concentrations varied with different experiments and are listed in the figure panels. Samples were loaded onto a 10% dPAGE and visualized the fluorescence emission at 526 nm (excitation was accomplished using a green laser of 532nm) using the Molecular Dynamics Typhoon 9200.

2.11 Enzyme Kinetics

The kinetic parameters for both the wt- and ΔN-RNase HII was determined using the R10D8/D18 heteroduplex substrate. The buffer used for enzyme reaction contained 20 mM Tris-Cl pH 7.5, 50 mM NaCl, 50 mM DTT, 0.1 mM EDTA. The reactions were initiated by adding 10 mM $MgCl_2$, with the total reaction volume set to 10 µl. The final enzyme concentration was set to 200 nM with varying substrate concentrations. The heteroduplex substrate was always kept at a 2:1 mole ratio of R10D8 to D18. The reactions were performed at 37°C at various time points ranging from 1 min to 2 h. All reactions were done in triplicates. Each reaction was quenched by the addition of 10 µl of 2× dPAGE urea loading dye and placed on ice. Samples were loaded onto 10% dPAGE and fluorescence was visualized using Molecular Dynamics Typhoon 9200. Cleavage was quantified using ImageQuant software and the data was plotted and fitted by non-linear regression curve using GraphPad Prism 4.

CHAPTER 3: Isolation and Characterization of RNase HII from *Listeria monocytogenes*

3.1 Abstract

Endoribonuclease (RNase) HII is an enzyme that plays a role in removing Okazaki fragments during DNA replication and misincorporated ribonucleotides within the genome. It has also been shown that RNase HII played a role in influencing the virulence of a foodborne pathogen, *Listeria monocytogenes* in an unknown manner. Our study is the first to purify and biochemically characterize *L. monocytogenes* (Lm) RNase HII. We confirmed that the *Lm4b* 01283 (a putative Lm RNase HII) codes for Lm RNase HII as it cleaves substrates mimicking Okazaki fragments and also remove a single ribonucleotide within a DNA duplex. The enzyme also demonstrated *in vivo* RNase H activity as it complements the temperature sensitive phenotype of *E. coli* MIC2067 (RNase H deficient strain). Furthermore, we also investigated the putative role the N-terminus played in substrate binding by deleting the first 57 amino acids (ΔN-Lm RNase HII). Both the wild type and N-terminus deleted enzyme preferred magnesium ions over manganese ions for catalysis. The kinetic parameters of wild type enzyme was measured to be k_{cat}= 0.24 ± 0.01 min^{-1}, K_m= 0.05 ± 0 .03 μM and for ΔN-Lm RNase HII k_{cat}= 0.09 ± 0.02 min^{-1} and K_m= 0.08 ± 0.01 μM. The deletion of the N-terminus increased the K_m value by ~2.5 fold suggesting that the N-terminus played a role in substrate binding. By testing the wt- and ΔN-Lm RNase HII activity at various concentrations of different divalent metal ions, we showed that the N-terminus also influenced catalytic rate. The N-terminus was predicted to fold

into three consecutive alpha-helices, which we called the α_3 motif, and is unique to the *Bacillus* and *Lactobacillus* organisms.

3.2 Introduction

Endoribonuclease HII (RNase HII) is an enzyme that cleaves ribonucleotides within a RNA/DNA heteroduplex and has been shown to play a role in DNA replication and repair.[1-3] Prokaryotic and eukaryotic RNase HII belong to a Type 2 RNase H family of enzymes that also includes RNase HIII. Type 1 RNase H family includes prokaryotic and eukaryotic RNase HI and the RNase H domain of reverse transcriptase.[1, 4] Bacterial species often contain a combination of two types of RNase H either HI/HII or HII/HIII and few contain the genes for all three RNase H.[4] The multiplicity of RNase H is not completely understood. Nonetheless, multiple copies of RNase H may act to protect the cells by overlapping functions since removal of a single RNase H does not result in cell death or significant cell growth defects. The removal of both RNase HI and RNase HII in *Escherichia coli* produces a temperature sensitive strain, whereas in *Bacillus subtilis*, the removal of RNase HII and RNase HIII results in cell death.[5, 6]

RNase HII contains a conserved DEDD (Asp-Glu-Asp-Asp) catalytic motif which coordinates two divalent metal ions near the RNA-DNA junction of Okazaki like substrates (RNA_n-DNA_n/DNA), and substrates with a single RNA (DNA_n-RNA_1-DNA_n/DNA) (Figure 3.1a).[5, 7-10] One metal ion is shown to position a water molecule that acts as a nucleophile to attack the scissile phosphate at the RNA-DNA junction (Figure 3.1b).[11-13] The second metal ion is coordinated to the oxygen atom of the scissile phosphate to assist the leaving group. In contrast,

RNase HI cannot recognize and cleave at the RNA-DNA junction and prefers only RNA/DNA heteroduplex substrates - this is also known as RNase H activity (Figure 3.1a)[7].

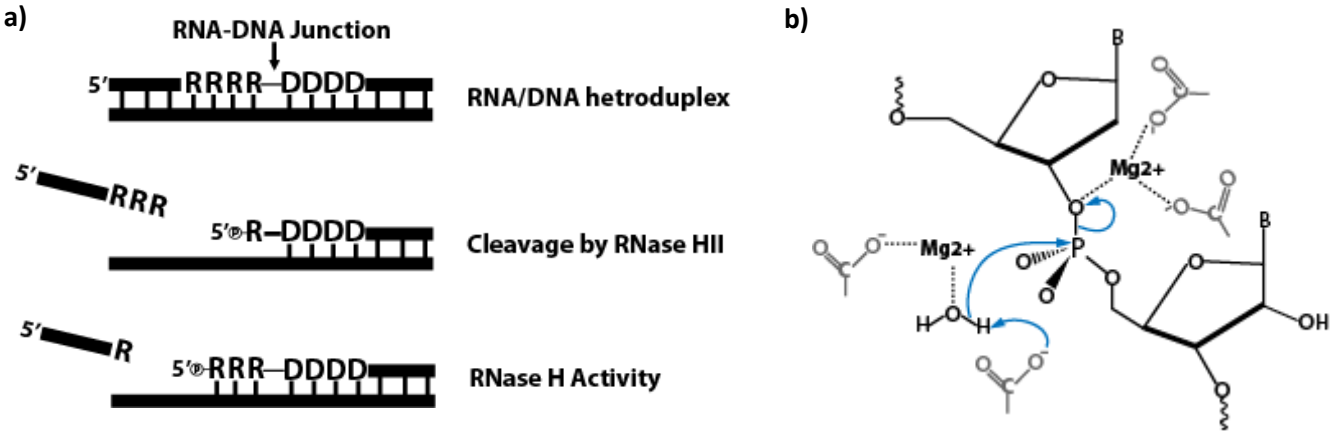

Figure 3.1. Substrate recognition by RNase HI and HII and their catalytic mechanism. a) The RNA-DNA junction is shown by the arrow. The ribonucleotides are labeled as uppercase R and the deoxyribonucleotides are labeled as uppercase D. RNase HII can recognize and cleave at the RNA-DNA junction leaving behind a single 5' phosphorylated (P) ribonucleotide. The RNase HI displays only RNase H activity since it cannot recognize RNA-DNA junction and cleaves only the RNA. b) Proposed reaction mechanism of RNase HII. The general base (carboxyl group, $-CO_2^-$) helps coordinate two magnesium ions (Mg^{2+}) and water molecule (H_2O). One of the magnesium ion help position the water that acts as a nucleophile to attack the scissile phosphate. The second magnesium ion is coordinated to the scissile phosphate oxygen to stabilize the charge of the leaving group.

The differences in substrate specificity may result in the different physiological roles for RNase H I, II and III. Recent work has shown that RNase HII plays an important role in removing ribonucleotides that are often misincorporated into the daughter strand during DNA replication.[3]

Some organisms consist of RNase HI or HIII that has an extended N-terminus. The most well characterized are the *B. stearothermophilus* (Bst) RNase HIII and the *Thermotoga maritima* RNase HI, and both have an N-terminus that play an important role in substrate binding.[14] However, the role of the RNase HII extended N-terminus has not been well characterized. A

single study showed that the N-terminus of Bst RNase HII, may play an important role in substrate binding and that removal of the N-terminus renders the enzyme inactive.[15] It is interesting that RNase HII with an extended N terminus can also be identified in pathogenic organisms such as *L. monocytogenes* but, it remains unknown whether this region plays a role in bacterial virulence.

Only recently it was shown that RNase HII could play a role in bacteria virulence in *L. monocytogenes*. Bigot *et al* showed that knocking out the *lmo1273* gene (a putative RNase HII) severely impaired the *in vivo* survival of the cells in mice.[16] We sought to purify and understand how this enzyme functions *in vitro* so that we can begin to shed some light into its physiological role particularly relating to virulence. Furthermore, we also truncated the Lm-RNase's HII extended N-terminus to further understand its role and potential link to virulence.

The results of our study show that Lm RNase HII most likely play an integral role in removing Okazaki fragments and misincorporated ribonucleotides during DNA replication. Our data also indicates that the N-terminus plays an important role for substrate binding, specificity and magnesium ion dependent activity.

3.3 Results

3.3.1 Phylogenetic Analysis of Lm RNase HII

The gene locus of *L. monocytogenes* 4b (strain CLIP80459) *Lm4b* 01283 was identified as Lm RNase HII through amino acid percent similarity. Lm RNase HII showed an amino acid percent similarity of 67.2% to *Bacillus subtilis* (Bs RNase HII), 45.8% to *E. coli* (Ec RNase HII),

33.3 % to *Thermococcus kodakaraensis* (Tk RNase HII), and 34.3% to *Archaeoglobus fulgidus* (Afu RNase HII). Structural alignment identified the conserved catalytic motif DEDD (Asp-77 Glu-78 Asp-169 Asp-186) which suggests that the catalytic mechanism of Lm RNase HII is similar to the other enzymes (Figure 3.2a).[11]The GRG motif was also conserved among all the RNase HII indicating a similar mechanism in recognizing the single ribonucleotide at the RNA-DNA junction of the substrate. Lm RNase HII contained an additional 70 amino acids at the N-terminus. Lm RNase HII amino acid sequence blast results are summarized in Figure 3.2b, and organisms with the extended N-terminus are identified in the order *Lactobacillales* and *Bacillales*. The N-terminus of Lm RNase HII was also compared with previously characterized extended N-terminus of *B. stearothermophilus* (Bst) RNase HIII which forms a TATA-box binding protein (TBP) like structure. The TBP structure of Bst RNase HIII is composed of a β-α-βββ-α-β structural motif and is involved in substrate binding.[14] Only a 29% amino acid similarity was shared between the first 70 amino acids of Lm RNase HII and Bs RNase HIII. The secondary structure prediction showed three consecutive alpha-helices in the extended N-terminus of Lm RNase HII and could not be matched with any identifiable motifs using online databank.

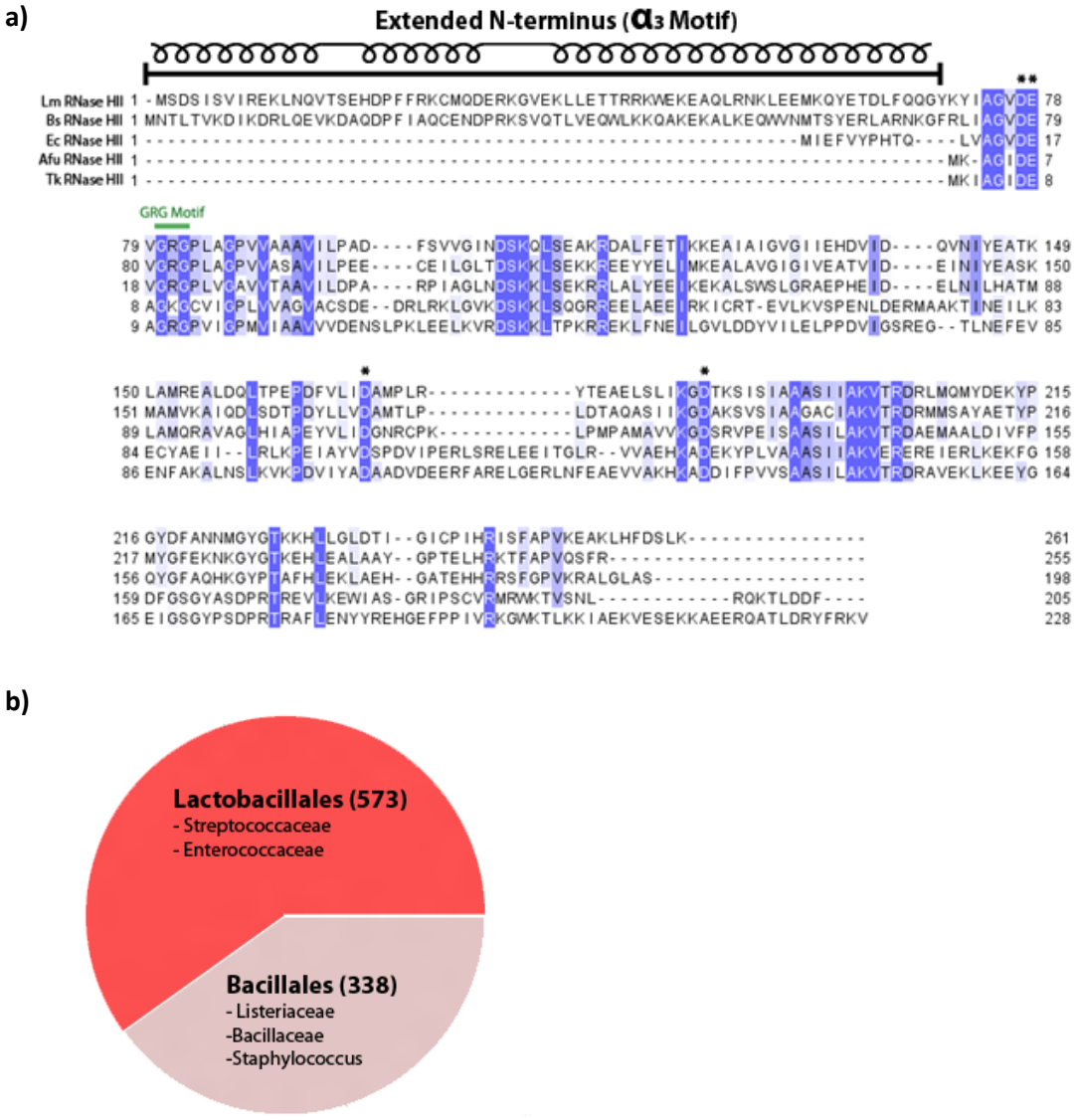

Figure 3.2. Sequence alignment and predicted structure of Lm RNase HII. a) The amino acid sequences of Lm RNase HII, *B. subtilis* (Bs) RNase HII, *E. coli* (Ec) RNase HII, *Archaeoglobus fulgidus* (Afu) RNase HII and (*Thermococcus kodakaraensis*) Tk RNase HII aligned using Clustal WS parameters provided by Jalview software. The conserved residues for catalysis are indicated by the asterisk. The three predicted α-helices of the extended N-terminus from Lm RNase HII are shown above the amino acid sequence. b) A chart showing the distribution of all the organisms with the extended N-terminus similar to Lm RNase HII. Blast results are obtained by online software UniProt.

3.3.2 Enzyme Properties of Wild Type and ΔN-LmRNase HII

The first 57 amino acids were deleted to isolate an N-terminus truncated enzyme (Lm-ΔN RNase HII) (Figure 3.3a). The far-UV circular dichroism (CD) spectra of both ΔN RNase HII and the wild-type (wt)-enzyme were similar, indicating no significant differences in the RNase H structure (Figure 3.3b). A sizing column was used to determine that the Lm RNase HII was predominantly a monomer in solution, which is consistent with previous observations of RNase HII from different organisms (Figure S3.1). The enzyme activity was assessed using the R10-D8 substrate which showed that both purified enzymes were functionally active, although the mutant displayed lower activity (Figure 3.4).

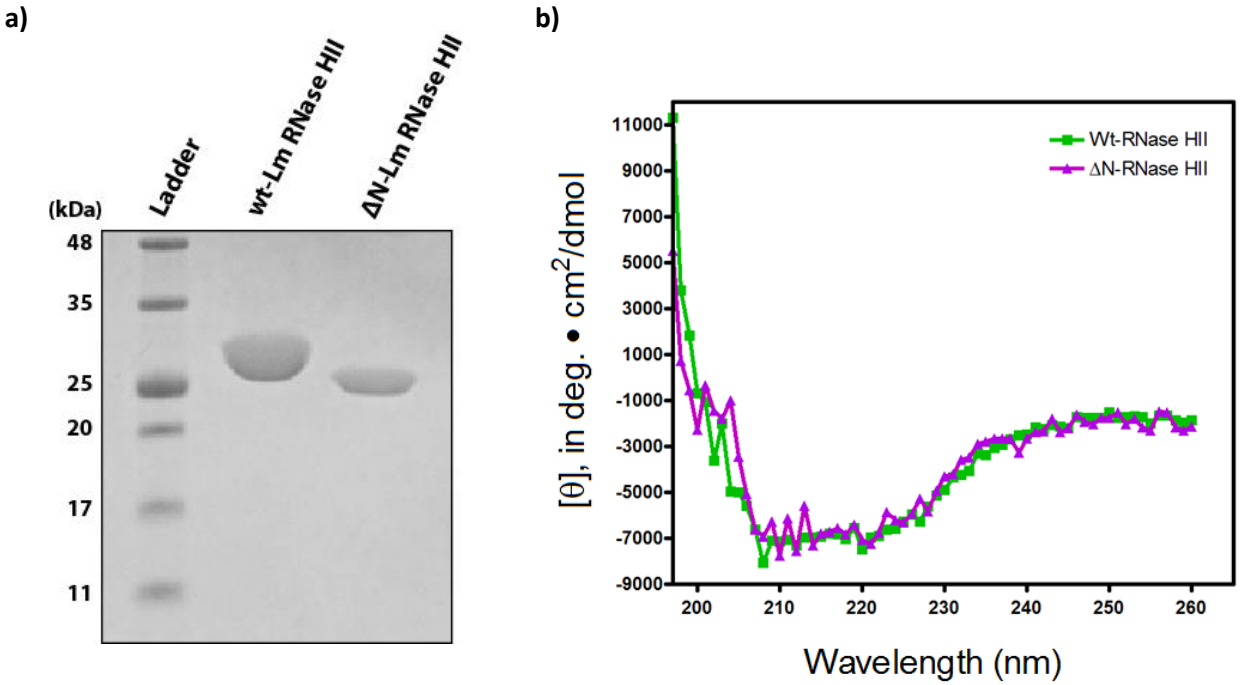

Figure 3.3. Protein purification and CD-spectra of wt- and ΔN-Lm RNase HII. a) Protein was purified as described in the material and method section. Samples were loaded on to 15% SDS-PAGE and stained with Coomassie Brilliant Blue. The molecular weight of the wt- and ΔN-Lm RNase HII is 32kDa and 24kDa, respectively. b) The far-UV circular dichroism spectra of both the wt-and ΔN-Lm RNase HII is shown.

The optimal conditions under which the wild type and the truncated Lm RNase HII functioned were determined using the R10-D8 substrate which mimics Okazaki fragments; all the substrates used for this study are summarized in Table 3.1. Both the wild type and truncated Lm-RNase HII were active in the presence of $MgCl_2$ and $MnCl_2$ (Figure 3.5a and b) although the enzyme was more active in the presence of $MgCl_2$. In presence of magnesium ions, the truncated enzyme showed ~4 fold decrease in activity compared to the wild type enzyme but, both functioned optimally in 10-50 mM $MgCl_2$. Concentrations of $MgCl_2$ greater the 50 mM begins to inhibit enzyme activity. The wild type enzyme functioned optimally in the presence of 0.1 mM $MnCl_2$ whereas the ΔN RNase HII showed greater activity in 1 mM $MnCl_2$.

Table 3.1. RNase HII substrates. Deoxyribonucleotides and ribonucleotides are shown in uppercase and lowercase respectively. All substrates except for D18 and the Anti-mut are fluorescently-labelled by Fluorescein amidite (FAM) at the 3' end. The bold letter indicate base tranverstions.

Substrate	Sequence
R18	gua cug cgg aga uga gcu (FAM)
R10-D8	gua cug cgg aGA TGA GCT (FAM)
D9-R1-D8	GTA CTG CGG aGA TGA GCT (FAM)
D10-R1-D7	GTA CTG CGG AgA TGA GCT (FAM)
D3-R1-D14	GTA cTG CGG AGA TGA GCT (FAM)
D14-R1-D3	GTA CTG CGG AGA TGa GCT (FAM)
Antisense D18	AGC TCA TCT CCG CAG TAC
Anti-mut 8C-A	AGC TCA T**A**T CCG CAG TAC
Anti-mut 9T-G	AGC TCA TC**G** CCG CAG TAC
Anti-mut 10C-A	AGC TCA TCT **A**CG CAG TAC

The optimal pH ranges for wild type and truncated enzymes were between 7.5-8.0 and 8.5-9.0, respectively (Figure 3.5c). The temperature range under which both enzymes achieved maximal activity was 37-42°C (Figure 3.5d).

The kinetic parameters were determined using the R10-D8 substrate under the condition of 37°C, 10 mM $MgCl_2$ and a physiological pH of 7.5. The results are summarized in Table 3.2. Wt-Lm RNase HII had a ~2.5 fold greater catalytic turnover rate compared to the truncated

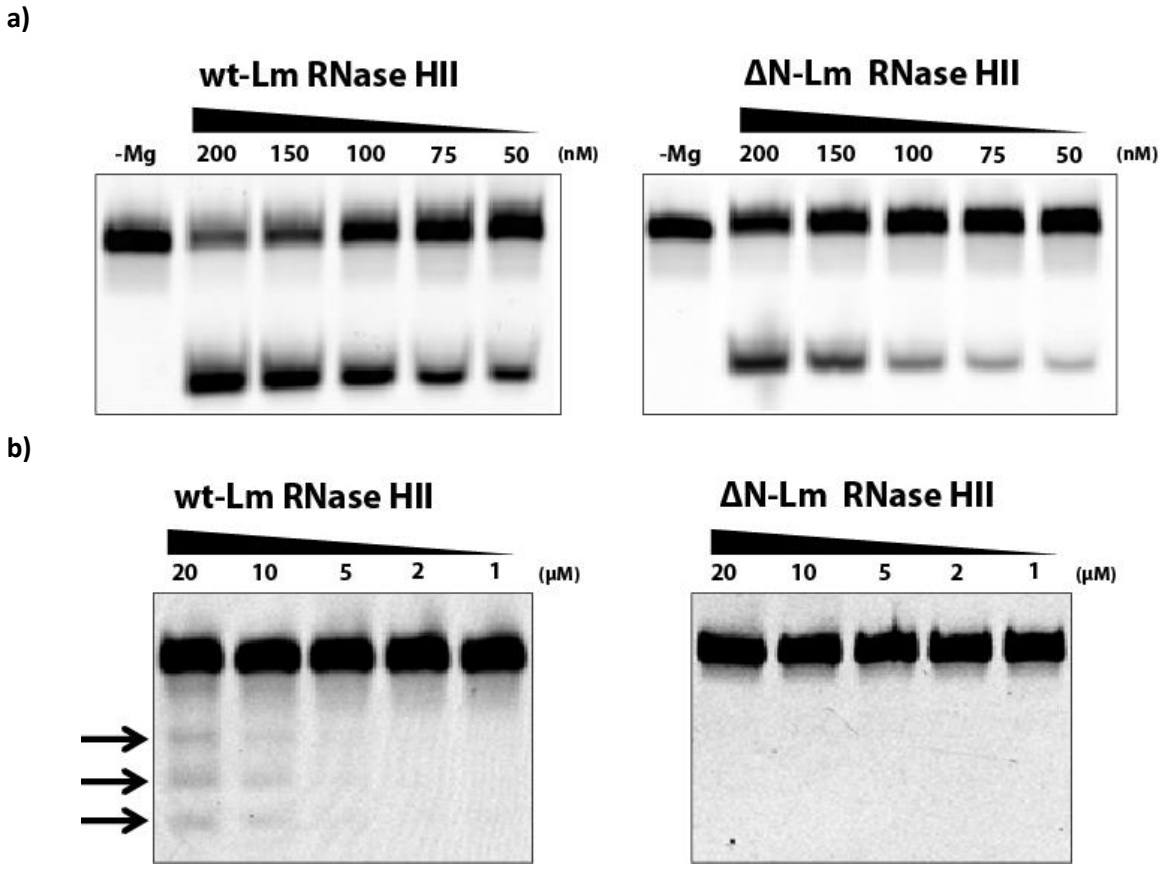

Figure 3.4. Assessing the *in vitro* activity of RNase HII. a) The R10-D8/D18 heteroduplex (400 nM final concentration) was mixed with increasing concentrations of wt- or ΔN-RNase HII. No cleavage is seen in the control sample lacking magnesium ions (-Mg). b) The *in vitro* RNase H activity was assessed by mixing the R18/D18 heteroduplex (400 nM final concentration) with increasing concentrations of wt- or ΔN-RNase HII. Arrows indicates the cleaved products produced due to RNase H activity.

enzyme. The K_m value for the ΔN-Lm RNase HII was ~1.6 fold greater than that of the wild type enzyme, which indicates a weaker affinity for the substrate.

3.3.3 *In Vivo* Complementation Assay to Test RNase H Activity

E. coli MIC2067 is an *rnha* and *rnhb* gene knockout strain that shows an RNase H temperature dependency.[5] The cells can grow normally at 30°C but, cannot grow at a temperature of 43°C unless complemented with a plasmid expressing Type 1 or Type 2 RNase H. Control cells carrying the empty pBAD30 vector were unable to grow at 43°C (Figure 4.6). In contrast, cells carrying pBAD30 containing the wt-Lm *rnhb* gene grew at 43°C, confirming that the Lm RNase HII exhibits *in vivo* RNase H activity. Cells complemented with the truncated Lm-*rnhb* gene also grew as well as the cells completed with the wild type enzyme at 43°C, indicating that the N-terminus does not disrupt the enzyme's *in vivo* RNase H activity.

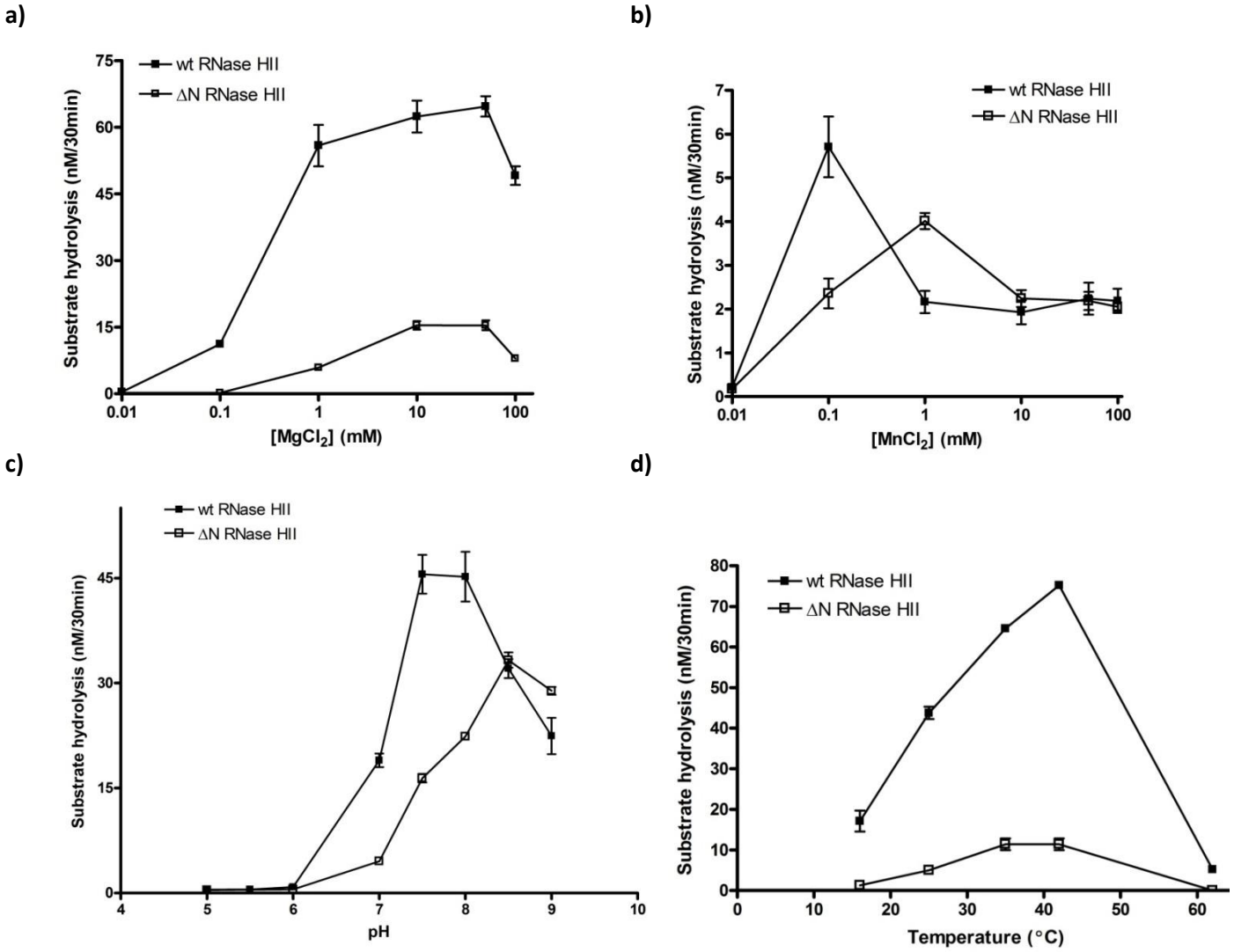

Figure 3.5. Testing the effects of metal ions, pH and temperature on Lm-RNase HII activity. The R10-D8/D18 heteroduplex (100 nM final concentration) was used for all the experiments with a final enzymes concentration of 50 nM. a) The $MgCl_2$ concentration was set to 0, 0.01, 1, 10, 50 or 100 mM. b) The experiment was setup in a similar manner to panel a. except $MnCl_2$ was used in the reaction. c) The reaction was performed under 10 mM $MgCl_2$, but with varying pHs adjusted using either 20 mM Tris buffer (used for high pH) or 20 mM MES buffer (used for low PHs). d) Temperature of the reaction was adjusted to 16, 25, 32, 42, 62°C and carried out in 10 mM $MgCl_2$. All reactions experiments were done in triplicates.

3.3.4 Lm RNase HII Cleaves RNA/DNA Heteroduplex Poorly

The activity of both the wt and ΔN-Lm RNase HII was assessed using the R18 substrate which formed a complete RNA/DNA heteroduplex. Cleavage of the substrate was only observed at a high concentration of wt-Lm RNase HII albeit poorly, indicating that the wild type enzyme does retain RNase H activity similar to RNase HI (Figure 3.4a). No cleavage was observed for the ΔN-Lm RNase HII (Figure 3.4b).

Table 3.2. Kinetic Parameters of RNase HII. The hydrolysis of R10-D8/D18 heteroduplex was used to determine the enzyme kinetics as described in material and methods.

Enzyme	k_{cat} (min^{-1})	K_m (μM)	k_{cat}/K_m
wt-Lm RNase HII	0.24 ± 0.01	0.05 ± 0.01	4.93 ± 0.01
ΔN-Lm RNase HII	0.09 ± 0.02	0.08 ± 0.01	1.24 ± 0.01
Bs RNase HII[2]	0.52	0.43	1.21
Afu RNase HII[8]	0.06	8.0	133.3
Pab RNase HII[8]	0.50	5.57	11.14

3.3.5 Comparison of wt and ΔN-Lm RNase HII Substrate Specificity

It was initially determined that Lm RNase HII performed hydrolysis at the 5' scissile phosphate of the RNA at the RNA-DNA junction leaving behind a ribonucleotide with a 5' monophosphate (Figure S3.2). This was in agreement with previous literature.[7-10] Furthermore, it was also established that the Lm RNase HII cannot cleave single stranded substrates containing RNA. The substrate must be in the form of a heteroduplex in order to observe enzyme activity

(Figure S3.3). Next, the activity of the enzyme was compared using different substrates (Figure 3.7). The wt-Lm RNase HII showed a slightly higher activity for substrates containing a single ribonucleotide (D9-R1-D8) over the substrate closely mimicking Okazaki fragments (R10-D8). In the case of ΔN-Lm RNase HII, the enzyme had a slightly higher activity for cleaving R10-D8 over D9-R1-D8. The position of the single ribonucleotide also affected the activity of the enzyme and it was observed that the enzyme preferred to cleave substrates containing a single ribonucleotide at the 5' end (D3-R1-D14) over the substrates with the ribonucleotide at the 3' end (D14-R1-D3). The D14-R1-D3 substrate hydrolysis was ~3.5 fold less than the hydrolysis of D3-R1-D14 in the presence of the wild type enzyme; however, substrate hydrolysis was reduced ~50 fold in the presence of the truncated enzyme.

3.3.6 RNase HII can Recognize Mismatched Ribonucleotide Substrates

We also investigated whether Lm RNase HII had the ability to recognize mismatched single ribonucleotide substrates. To accomplish this, the D9-R1-D8 was used as the substrate and a single nucleotide on the complementary DNA strand was altered to create a mismatch (Figure 3.8a). The bases were changed such that the mismatch occurred at the single ribonucleic acid, one nucleotide downstream (+1) and the other, one nucleotide upstream (-1). Both the wild type and the truncated enzymes hydrolysed all three different mismatched substrates although the truncated enzyme had far less activity (Figure 4.8b). The cleavage of the +1, 0 and -1 mismatch substrates compared to the control (no mismatch) was reduced ~2.2, 4.2 and 12 fold, respectively, in the presence of the wild type enzyme. The truncated enzyme also harboured a

similar trend in tolerating the mismatch at the +1 location most effectively and least effectively at the -1 location.

3.4 Discussion

3.4.1 *Listeria* Gene the *Lm4b 01283* Encodes for RNase HII

The predominance of RNase HII makes it the universal gene among organisms, especially in prokaryotes. Although the multiplicity of *rnh* genes is not entirely understood, it is believed that two or more RNase H plays a distinct role in the cells with some functional overlap.[1-4] Our work is the first to show that the *Lm4b* 01283 locus, which shares 67% amino acid similarity with Bs RNase HII (a characterized RNase HII), codes for an RNase HII. The enzyme can recognize and cleave at the RNA-DNA junction for both Okazaki-like substrates and substrates integrated with single ribonucleotides (Figure 3.7), thus highlighting its putative biological role in removing Okazaki fragments and the removal of misincorporated RNA during DNA replication.

3.4.2 Cell Complementation Assay to Test *In Vivo* RNase H Activity

Archaea and prokaryotic RNase HII also possess RNase H activity, the ability to cleave a stretch of RNA in a RNA/DNA heteroduplex, showing their overlapping function with RNase HI. RNase H activity is often detected by complementing a temperature sensitive phenotype of *E. coli* MIC2067 strain (RNase H knockout strain). The Lm RNase HII retained *in vivo* RNase H activity as it was able to complement *E. coli* MIC2067 (Figure 3.6). However, the *in vitro* RNase

H activity of Lm RNase HII was very weak when tested with R18 substrate (Figure 3.5). This suggests that additional cellular factors may be required to promote RNase H activity.

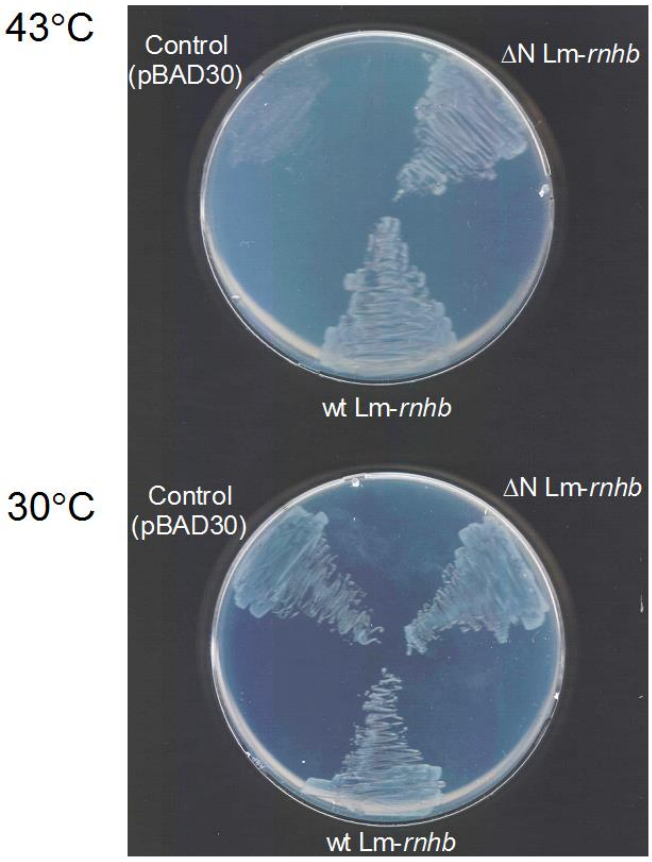

Figure 3.6. Effects of wt- and ΔN-Lm RNase HII on the temperature-sensitive growth of *E. coli* MIC2067. The *E. coli* strain MIC2067 was transformed with pBAD30 vector containing the wt Lm-*rnhb* or ΔN Lm-*rnhb* gene. The empty pBAD 30 vector served as a control. The *E. coli* MIC2067 cells grown normally at 30°C but cannot grow at 43°C. Cells complemented with functional RNase HII grow at higher temperature.

3.4.3 ΔN-Lm RNase HII is Active *In Vitro* and has *In Vivo* RNase H Activity

Previously, it has been shown that some *rnh* genes, such as the Bst RNase HIII, code for an extended N-terminus that play a role in substrate binding.[14] Crystal structures of Bst RNase HIII showed a highly conserved TBP domain at its N-terminus which consisted of a well-known structural motif β-α-ββββ-α-β.[17] The extended N-terminus, (amino acid 1-70) of Lm RNase HII

shows very little amino acid similarity (~29%) to that of Bs RNase HIII. The N-terminus was predicted to form a secondary structure of three consecutive alpha helices (α_3) (Figure 3.2a), and the sequence could not be matched with any known putative motifs. Phylogenetic analysis reveals that the α_3 motif is only present in organisms of the order *Lactobacillales* and *Bacillales*. Previous studies using *Bacillus stearothermophilus* (Bst) RNase HII (50% similarity to Lm RNase HII) showed that α_3 motif was important in substrate binding thus, the RNase HII N-terminus presents as a novel nucleic binding motif.[15] Furthermore, it was thought that the α_3 motif played a role in RNase HII activity as its removal rendered the enzyme inactive. We also tested the effects of truncating α_3 motif of Lm RNase HII by removing the first 57 amino acids. The removal of the N-terminus did not alter the enzyme's overall structure as indicated by the far UV CD spectrum (Figure 3.3b). We also found that truncating the N-terminus of Lm RNase HII did not entirely eliminate its activity. ΔN-Lm RNase HII cleaved substrates with RNA-DNA junction (Figure 3.4a). However, the RNase H activity was not observed even at high enzyme concentration of 20 μM (Figure 3.4b). This explains why previously it was thought that deleting the α_3 motif led to no enzymatic activity since only the *in vitro* RNase H activity was measured using RNA/DNA heteroduplex substrates.[15] Like the wild type enzyme, ΔN-Lm RNase HII retained *in vivo* RNase H activity as it was able to complement *E. coli* MIC2067 (Figure 3.6). This suggests that the α_3 motif does not play a significant role in promoting *in vivo* RNase H activity.

3.4.4 The pH Dependency of wt- and ΔN-Lm RNase HII

The conservation of the DEDD and the GRG motif indicates that the catalytic mechanism of Lm RNase HII is very similar to that of previously characterized Type 2 RNase H.[11, 13] Type 2 RNase H prefer alkaline conditions, between a pH range of 8-9, for optimal activity.[13] The preference for basic conditions may arise due to the requirement of ionisation of the four conserved DEDD carboxylate groups which helps with binding and positioning of metal ions correctly. The wt-Lm RNase HII prefers a basic pH range of 7.5-8 whereas the ΔN-Lm RNase HII prefers a pH range of 8.5-9 (Figure 3.5c). This suggests that the extended N-terminus may act as a common feature to allow the enzyme to function under less basic conditions which may serve advantageous to the organism's survival. Thus, it would be interesting to assess the pH dependency of RNase HII with α_3 motif from other organisms.

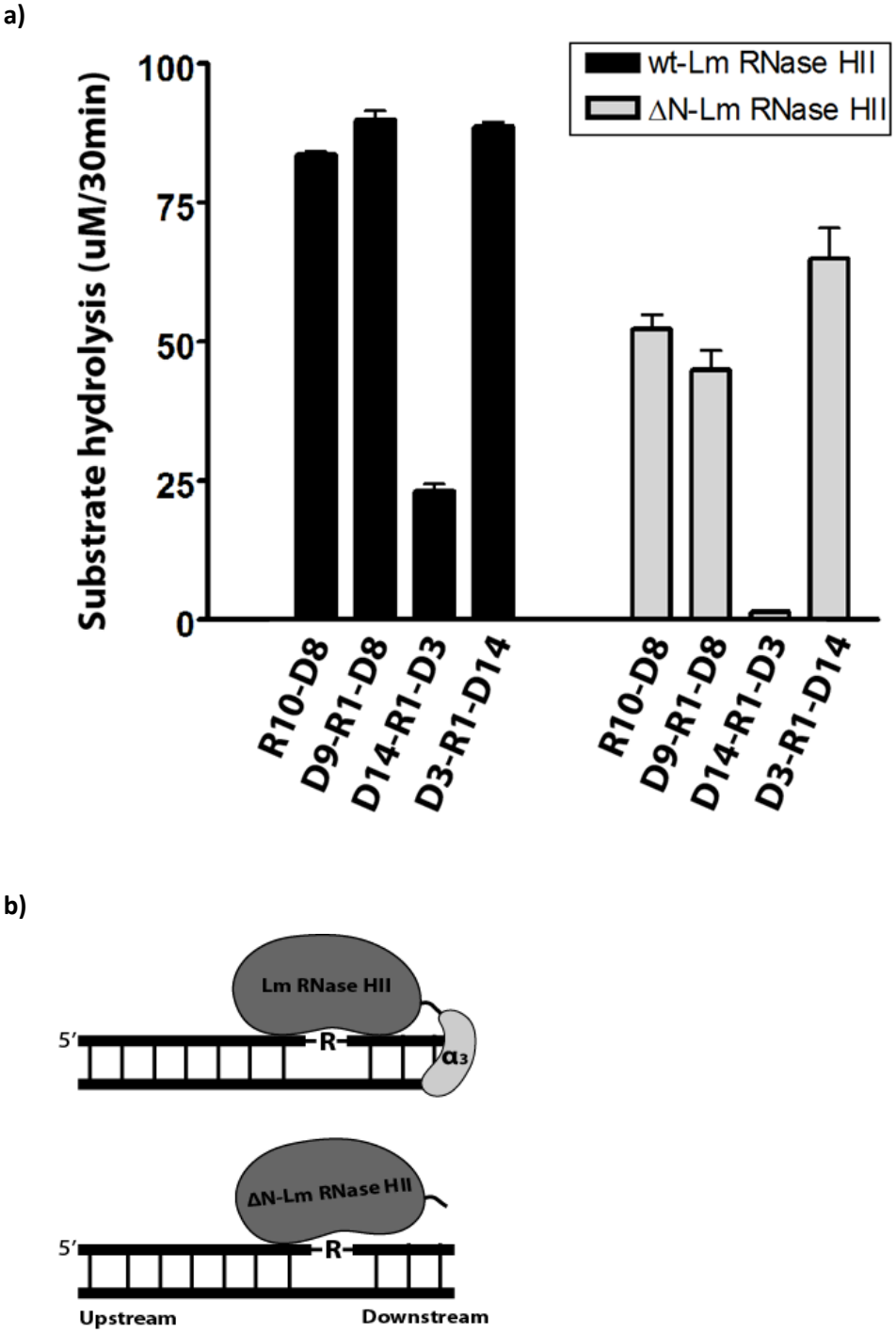

Figure 3.7. Comparing the amount of cleavage among different substrates using wt- and ΔN-Lm RNase HII. a) The substrates were kept at a final concentration of 100 nM and the enzymes at 50 nM. The reaction was performed at 37°C for 30 min in conditions listed in materials and methods. The reactions were done in triplicates and the data was quantified using ImageQuant in order to create the graph. b) A diagram showing the α_3 motif's involvement in substrate binding. It is predicted that this motif binds to the regions downstream of the RNA-DNA junction (depicted as -R-).

3.4.5 Metal Ion Dependency of wt- and ΔN-Lm RNase HII

Both the wt- and ΔN-Lm RNase HII prefer Mg^{2+} ions over Mn^{2+} ions as the optimal activity with Mg^{2+} being 10 fold greater and 4 fold greater over Mn^{2+} for wild type and truncated enzyme, respectively (Figure 3.5a and b). Interestingly, there is only a very slight decrease in the optimal activity between the wt and ΔN-Lm RNase HII when using Mn^{2+} ions. This suggests that removing the α_3 motif largely influences the Mg^{2+} dependent activity with minimal effects on Mn^{2+} dependent activity. The preference for Mg^{2+} ions has also been observed in *E. coli* and *Deinococcus radiodurans* RNase HII.[18, 19] However, the RNase H activity from *E. coli*, *D. radiodurans* and *A. fulgidus* RNase HII showed greater preference for Mn^{2+} while others like *T. kodakaraensis* RNase HII preferred Co^{2+}.[18, 20] We could not adequately test the preference for Mn^{2+} ions for RNase H activity by Lm RNase HII since the *in vitro* RNase H activity of Lm RNase HII was very weak. We also tested the preference of Lm-RNase HII for other divalent metal ions and saw that there was no activity with $CaCl_2$, $CuCl_2$, $NiCl_2$, and $CoCl_2$ (data not shown).

3.4.6 Enzyme Kinetic Analysis of wt- and ΔN-Lm RNase HII

Kinetic analysis using Okazaki-like substrates reveal that the enzyme turnover rate for the wild type (k_{cat}= 0.24 ± 0.01 min^{-1}) is about 2.5 fold greater than that of the truncated enzyme (k_{cat}= 0.09 ±0.02 min^{-1}) (Table 3.2). The reduced turnover rate can partially be ascribed to the weaker substrate affinity of ΔN-Lm RNase HII with a K_m values approximately 1.5 fold greater than the wild type enzyme. The weak substrate binding alone cannot account for the large decrease in the Mg^{2+} dependent activity. Thus, our data suggests that not only does the α_3 motif

help bind the substrate but, it also plays a subtle role in promoting substrate catalysis by potentially promoting ideal arrangement between the scissile phosphate group of the substrate and the Mg^{2+}ions at the active site. It would be interesting to see if any mutations of the basic residues which may be involved in substrate binding can alter enzyme activity to be similar to ΔN Lm-RNase HII.

Similar results have been reported using *Thermotoga maritima* (Tm) RNase HI, in which not only did the removal of the extended N-terminus reduced substrate binding but also significantly reduced Mg^{2+}dependent enzyme activity.[21] The N-terminus of (Tm) RNase HI displayed great similarity to hybrid binding domain (HBD), often present in eukaryotic Type 1 RNase H, which is often involved in double stranded RNA/DNA heteroduplex. Although there is very little sequence and structural similarities between the Type 1 RNase HBD and the Type 2 α_3 motif, they seem to possess similar functions in regards to substrate binding and influencing enzyme activity.

Table 3.2 also summarizes the catalytic efficiencies of previously characterized RNase HII. In general, thermophilic archaea RNase HII's catalytic efficiency is much greater (ranging from 11-133 $min^{-1}/\mu M$) compared to Lm RNase HII (4.93±0.01 $min^{-1}/\mu M$) and Bs RNase HII (1.2 $min^{-1}/\mu M$). Since the archaea enzymes are thermostable, the kinetic parameters are determined at higher temperatures, such as 60°C for *Pyrococcus abyssi* RNase HII, which allows for faster substrate binding and catalysis.[8] Lm RNase HII is not thermostable and could only maintain optimal activity between 37-42°C (Figure 3.5c). ΔN-Lm RNase HII enzyme also exhibited a

similar temperature dependency as the wild type, indicating that the α_3 motif does not contribute to thermostability.

3.4.7 Substrate Specificity Differ Between of wt- and ΔN-Lm RNase HII and Implication in Biological Role

Our data suggests that Lm RNase HII can play a dual role in the cell by removing the RNA primers at the Okazaki fragments and by assisting the removal of single ribonucleotides that are misincorporated into genomic DNA during replication. The wild type enzyme prefers substrates with a single ribonucleotide (D9-R1-D8) at the RNA-DNA junction slightly over substrates mimicking Okazaki fragments (R10-D8) (Figure 3.7a). However, the preference for the substrate was reversed when the N-terminus was deleted. This indicated that cells may tightly regulate substrate specificities through the interaction of the N-terminus and that other binding partners may be required to achieve these results.

3.4.8 The α_3 Motif Binds Substrate at Regions Downstream of Cleavage Site

We also found that the position of a single ribonucleotide at either the 5' end (D3-R1-D14) or the 3' end (D14-R1-D3) of the substrate influences the enzyme activity. The results showed that the wild type enzyme displayed 4 fold less activity when the single ribonucleotide was placed near the 3' end compared to its being closer to the 5' end (Figure 3.7a). In comparison, a 50 fold reduction was seen when the α_3 motif was deleted. This suggests that that the presence of only 3 base pairs or less downstream of the RNA-DNA junction is not sufficient for ideal enzyme-to-substrate contact. Also, a much larger decrease in the ΔN Lm-RNase HII

activity suggested that the α_3 motif may help bind the substrate mainly through interactions with nucleotides downstream of the RNA-DNA junction (Figure 3.7b). These results are similar to Tm RNase HI in which it was found that the HBD domain was largely binding to the downstream regions of the cleavage site.[21]

3.4.9 Lm RNase HII Can Recognize Mismatched Bases

We also tested the ability of Lm RNase HII in recognizing substrates with mismatch base paring that can occur naturally in cells due to erroneous priming by primase or during DNA synthesis by DNA polymerase.[22] More dramatic mismatches were created at the -1, 0, +1 position of D9-R1-D8 by transversion of the bases in the complementary DNA strand (Figure 3.8a). Mismatch at any one of the locations dramatically reduced substrate hydrolysis in Lm-RNase HII (Figure 3.8b). We predict that a mismatch disrupts the formation of the ideal helix geometry required by the enzyme for binding the substrate hence, the observation of reduced activity. Furthermore, the reduction of activity was not equal at the three positions. The greatest to smallest reductions in activity were observed in the order of -1, 0, +1. This is also consistent with observations made in another study looking at the effects of mismatch in *Chlamydia pneumonia* RNase HII.[23] It seems that base paring upstream of the RNA-DNA junction play a slightly greater role in substrate binding.

3.4.10 Lm RNase HII's Potential Role in *L. monocytogenes* Virulence

A recent study by Bigot *et al* investigated the role of the gene *lmo1273* which was involved in *L. monocytogenes* (EGD-e) virulence.[16] The gene was suggested to code for a putative RNase HII due to its high resemblance with other organisms. The study showed that knocking out *lmo1273* severely attenuated of virulence in mouse models as 50% of the lethal dose (LD_{50}) was a 100 fold higher for knockout cells compared to the wild type cells. However, it remains unclear how the removal of *lmo1273* effected virulence. In this study we have confirmed that *lmo1273* gene which shows a 99% similarity to *Lm4b* 01283 (from *L. monocytogenes* 4b strain) used in our study does indeed code for RNase HII and is likely involved in DNA replication and repair by removing Okazaki fragments, and single ribonucleotides misincorporated into the genome. It has already been shown that RNase HII plays an important role in maintaining the integrity of the genome in yeast, mammalian and *E. coli.*[24-26] The inability to maintain genomic integrity may have affected the *in vivo* survival of *L. monocytogenes* leading to reduced virulence. For example, studies have shown that removing RNase HI (involved in removing Okazaki fragments) from *Haemophilus influenza* led to a ~3 fold increase in the mutation rate of tetranucleotide repeats which affects phase transition process important for cells to adapt rapidly to fluctuations in the host environment.[27]

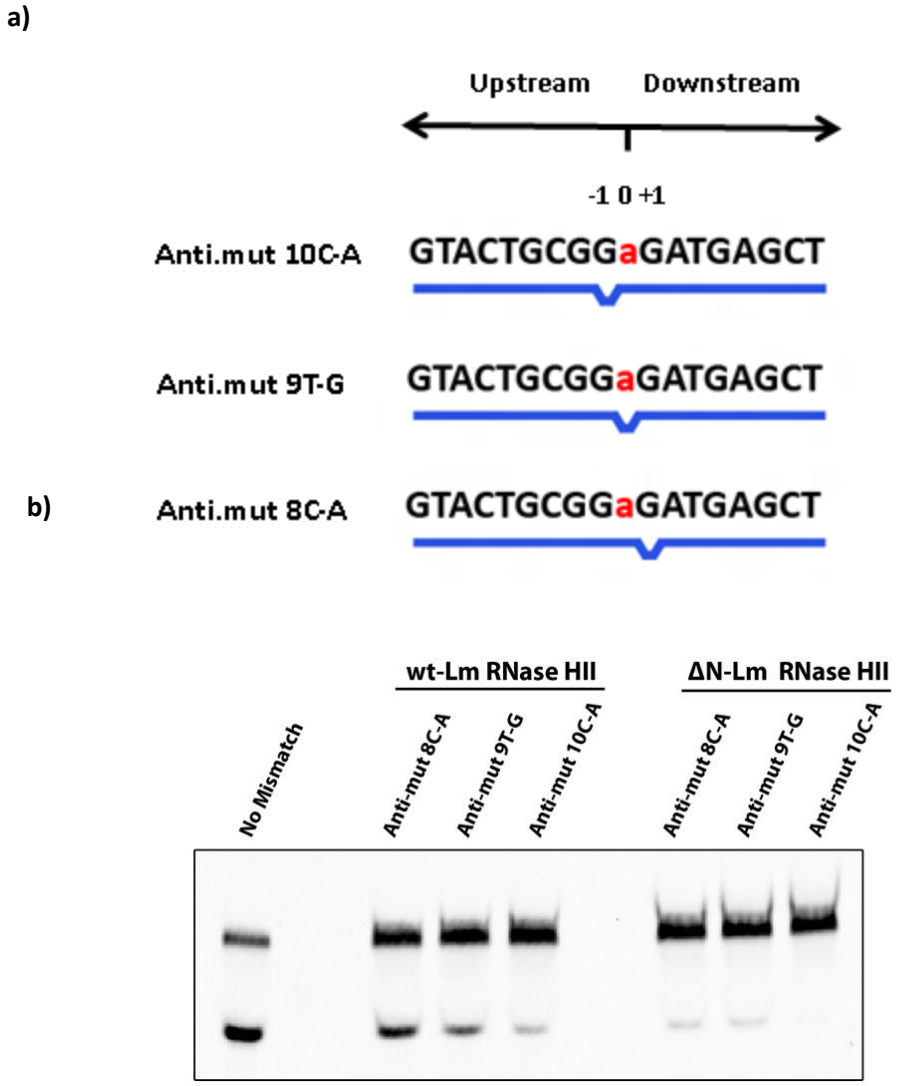

Figure 3.8. Effects of mismatch based on Lm RNase HII activity. a) The illustration shows D9-R1-D8 heteroduplexed with three different mutant antisense strands. The location the ribonucleotide is denoted 0 whereas the upstream and downstream bases are denoted by negative and positive numbers respectively. b) The dPAGE showing enzyme activity with different anti-mut antisense strands. A control reaction (No Mismatch) represents wild type enzyme activity with D18 antisense strand. The substrates were kept at a final concentration of 100 nM and the enzymes at 50 nM. The reaction was performed for 30 min at 37°C and the reaction conditions are mentioned in the material and methods section.

3.5 Conclusion

In our study we conducted *in vitro* analysis to confirm that *Lm4b* 01283 gene locus encodes for RNase HII. Our results showed that the enzyme likely plays a role in the removing Okazaki fragments and the misincorporated ribonucleotides which is important for maintaining genomic integrity. Furthermore, we showed that the extended N-terminus (or α3 motif) of Lm RNase HII is a new structural motif involved in substrate binding and influences Mg^{2+} dependent enzyme activity. Now that we have a greater understanding of RNase HII from pathogenic bacteria such as *L. monocytogenes*, we can now begin to understand how this enzyme influences virulence. Our next step will be to investigate the *in vivo* role of Lm RNase HII and specifically how it influences bacterial virulence.

3.6 References

1. Tadokoro, T., and Kanaya, S. Ribionuclease H: molecular diversities, substrate binding domins, and catalytic mechanism of the prokaryotic enzyme. *FEBS J.* **276**, 1482-1498 (2009).
2. Haruki, M., Tsunaka, Y., Morikawa, M. and Kanaya, S. Cleavage of DNA-RNA-DNA/DNA chimeric substrate containing a single ribonucleotide at the DNA-RNA junction with prokaryotic RNase HII. *FEBS lett.* **531**, 204-208 (2002).
3. Bubeck, D., Reujns, A.M., Graham, C.S., Astell, R.K., Jones, E.Y., and Jackson, P.A. PCNA directs type 2 RNase H activity on DNA replication and repair substrates. *Nucleic Acids Res.* **39**, 3652-3666 (2011).
4. Kochiwa, H., Tomita, M., and Kanai, A. Evolution of ribonuclease H gene in prokaryotes to avoid inheritance of redundant genes. *BMC Evol Biol.* (2007).
5. Itaya, M., Omori, A., Kanaya, S., Crouch, R. J., Tanaka, T., and Kondo, K. Isolation of RNase H genes that are essential for the growth of Bacillus subtilis 168. *J. Bacteriol.* **181**, 2118-2123 (1999).
6. Itaya, M., and Kondo, K. Molecular cloning of a ribonuclease H (RNase HI) gene from an extreme thermophile*Thermus thermophiles*HB8: a thermostable RNase H can functionally replace the *Escherichia coli* enzyme in vivo. *Nucleic Acids Res.* **19**, 4443-4449 (1991).

7. Ohtani, N., Tomita, M., and Itaya, M. Junction ribonuclease: a ribonuclease HII orthologue from *Thermus thermophiles* HB8 prefers the RNA-DNA junction to the RNA/DNA heteroduplex. *Biochem. J.* **412**, 517-526 (2008).
8. Laz, L.S., Goaziou L.A., and Henneke, G. Structure-specific nuclease activies of *pyrococcus abyssi* RNase HII. *J. Bacteriol.* **192**, 3689-3698 (2010).
9. Zang, Y.B., Ayalew, S., and Lacks, S.A. The *rnhB* gene encoding RNase HII of *Streptococcus pneumonia* and evidence of conserved motifs in eukaryotic genes. *J. Bacteriol.* **179**, 3828-3836 (1997).
10. Hou, J., Liu, Y., Lu, Z., Liu, X., and Liu, J. Biochemical characterization of RNase HII from *Aeropyrum pernix. Acta Biochim Biophys Sin* **44**, 339-346 (2012).
11. Muroya, A., Tsuchiya, D., Ishikawa, M., Haruki, M., Morikawa, M., Kanaya, S., and Morikawa, K. Catalytic center of an archaeal type 2 ribonuclease H as reveled by x-ray crystallographic and mutational analyses. *Protein Sci.* **10**, 707-714 (201).
12. Rychlik, P.M., Chon, H., Cerritelli, M.S., Klimek, P., Crouch, J.R., and Nowotny, M. Crystal structure of RNase H2 in complex with nucleic acid revel the mechanism of RNA-DNA junction recognition and cleavage. *Mol. Cell* **40**, 658-670 (2010).
13. Bastock, A.J., Webb, M., and Grasby, A.J. The pH-dependence of the *Escherichia coli* RNase HII-catalysed reaction suggests that an active site carboxylate group participates directly in catalysis. *J. Mol. Biol.* **368**, 421-433 (2007).
14. Chon, H., Matsumura, H., Kiga, Y., Takano, K., and Kanaya, S. Crystal structure and structure-based mutational analyses of RNase HIII from *Bacillus stearothermophilus*: A New Type 2 RNase H with TBP like substrate-binding domain at the N Terminus. *J. Mol. Biol.* **356**, 165-178 (2006).
15. Muroya, A., Nakano, R., Ohtani, N., Haruki, M., Morikawa, M., and Kanaya, S. Importance of an N-terminal extension in ribonuclease HII from *Bacillus stearothermophilus* for substrate binding. *J. Biosci. Bioeng.* **93**, 170-175 (2002).
16. Bigot, A., Raynaud, C., Dubail, I., Dupuis, M., Hossain, H., Hain, T., Chakraborty, T., and Charbit, A. *lmo*1273, a novel gene involved in *Listeria monocytogenes* virulence. *Microbiology* **155**, 891-902 (2009).
17. Kim, Y., Geiger, J. H., Hahn, S., and Sigler, P.B. Crystal structure of a yeast TBP/TATA-box complex. *Nature* **365**, 512-520 (1993).
18. Chai, Q., Qiu, J., Chapados, B.R., and Shen, B. *Archaeoglobus fulgidus* RNase HII in DNA replication: enzymological functional and activity regulation via metal cofactors. *Biochem. Biophys. Res. Commum.* **286**, 1073-1081 (2001).
19. Ohtani, N., Tomita, M., and Itaya, M. Junction ribonuclease activity specified in RNases HII/2. *FEBS J.* **275**, 5444-5455 (2008).
20. Haruki, M., Hayashi, K., Kochi, T., Muroya, A., Koga, Y., Morikawa, M., Imanaka, T., and Kanaya, S. Gene cloning and characterization of recombinant RNase HII from a hyperthermophilic archaeon. *J. Bacteriol.* **180**, 6207-6214 (1998).

21. Jongruja, N., You, D.J., Kanaya, E., Koga, Y., Takano, K., and Kanaya, S. The N-terminal hybrid binding domain of RNase HI from *Thermotoga maritima*is important for substrate binding and Mg2+-dependent activity. *FEBS J.* **277**, 4474-4489 (2010).
22. Rydberg, B., and Game, J. Excision of misincorporated ribonucleotides in DNA by RNase H (type 2) and FEN-1 in cell-free extracts. *Proc. Natl. Acad. Sci.* **99**, 16654-16659 (2002).
23. Hou, J., Liu, X., Pei, D., and Liu, J. RNase HII from *Chlamydia pneumonia* discriminates mismatches incorporation into DNA-rN-DNA/DNA duplexes. *Biochem. Biophys. Res. Commun.* **356**, 988-992 (2007).
24. McDonald, P.J., Vaisman, A., Kuban, W., Goodman, F.M., and Woodgate R. Mechanisms employed by *Escherichia coli* to prevent ribonucleotide incorporation into genomic DNA by Pol V. *PLoS Genet.* **8**, e1003030 (2012).
25. Chon, H., Sparks, J., Rychlik, M., Nowotny, M., Burgers, M.P., Crouch, J.R., and Cerritelli, M.S. RNase H2 roles in genome integrity revealed by unlinking its activities. *Nucleic Acids Res.* (2013).
26. Hiller, B., Achleitner, M., Glage, S., Naumann, R., Behrendt, R., and Roers, A. Mammalian RNase H2 removes ribonucleotides from DNA to maintain genome integrity. *J. EXP. Med.* **209**, 1419-1426 (2012).
27. D.Bayliss, C., Sweetman, A.W., and Moxon, E.R. Destabilization of tetranucleotide repeats in Haemophilus influenza mutants lacking RNaseHI or the Klenow domain of PolI. *Nucleic Acids Res.* **23**, 400-408 (2005).

3.7 Supplementary Figures

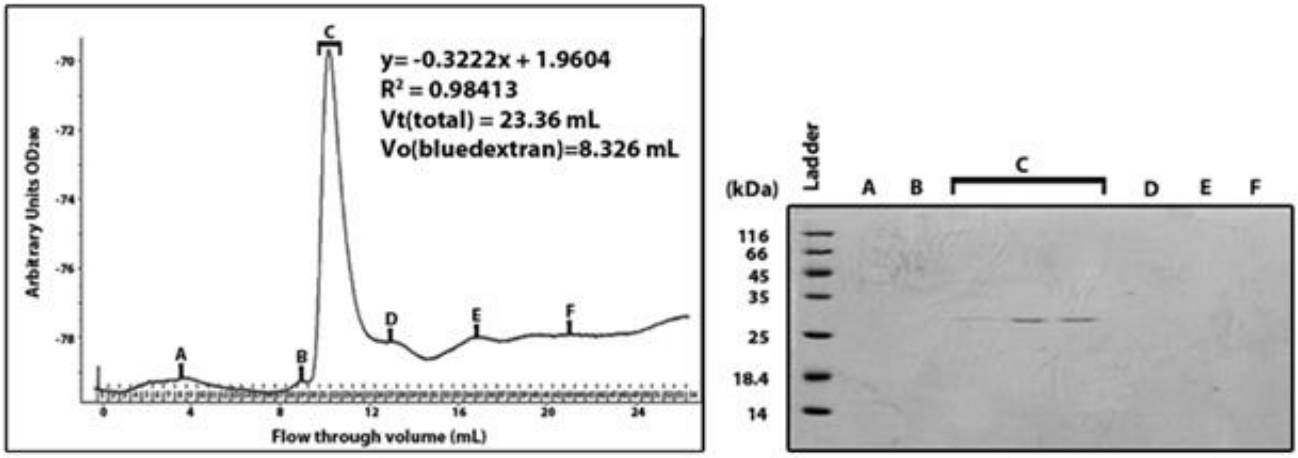

Figure S3.1: Superdex S200 size exclusion column purification of wt-Lm RNase HII. The flow elution graph is shown and the samples collected under the labeled peaks (A-F) were loaded onto a 15% SDS-PAGE and stained with Coomassie Brilliant Blue. The standard equation, listed in the figure, was used to approximate the molecular weight of the protein eluted under the peak C. The elution volume max was ~11.25 mL which equated to ~36 kDa, representing Lm-RNase HII monomer.

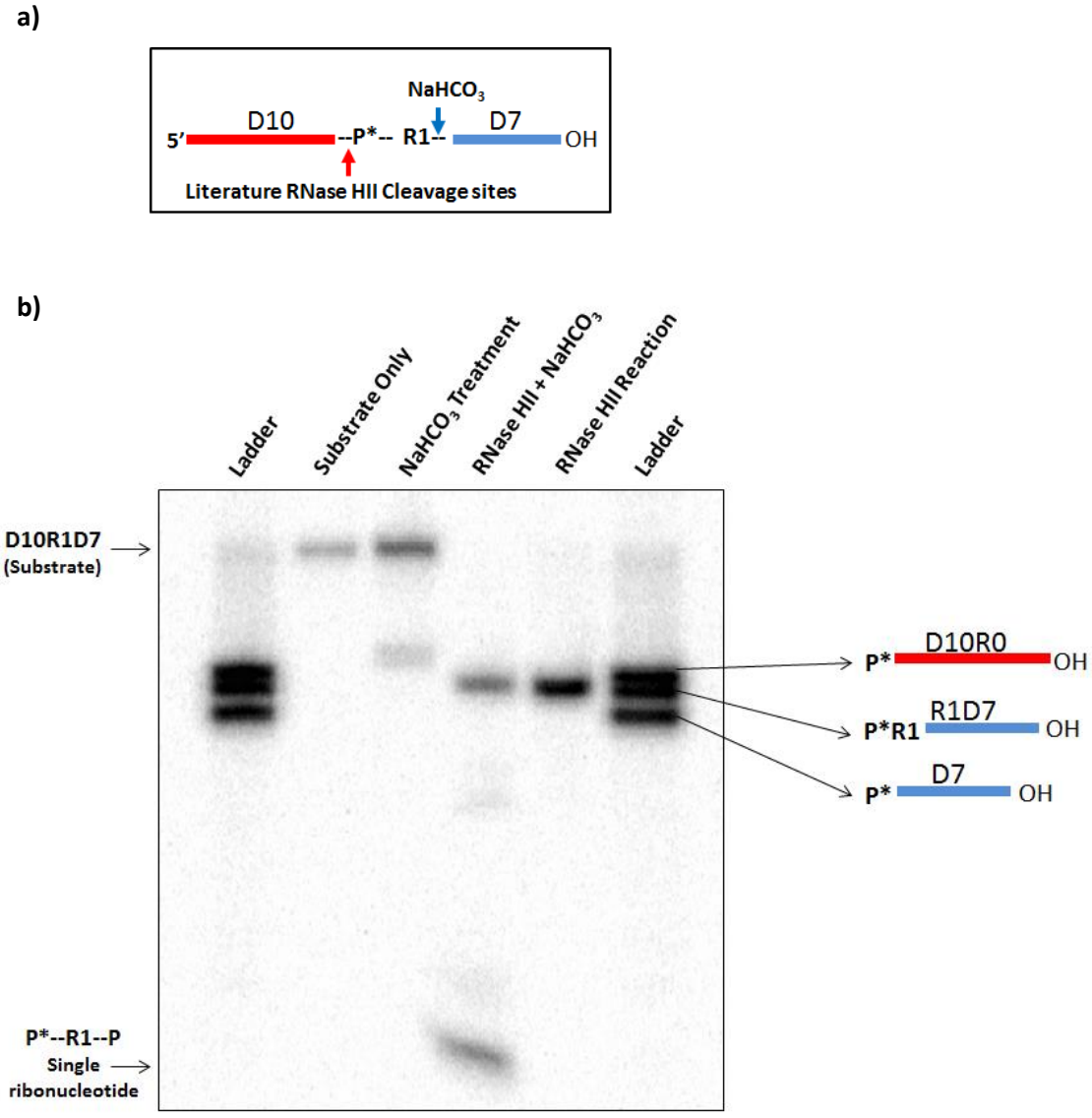

Figure S3.2. Assessing cleavage at the RNA-DNA junction by Lm RNase HII. a) The substrate D10R1D7 contained a ^{32}P at the 5' phosphodiester bond of the ribonucleotide (shown as P*). The cleavage site by RNase HII and under basic conditions using sodium bicarbonate ($NaHCO_3$) is indicated by the arrows. b) The different sized sequences used for the ladder is shown. The substrate only sample was not treated with Lm RNase HII or $NaHCO_3$. The RNase HII reaction was carried out by using 50 nM Lm RNase HII in 20 mM Tris-Cl pH 7.5, 50 mM NaCl, 50 mM DTT, 0.1 mM EDTA, 10 mM $MgCl_2$ for 30 min at 37°C. Half of the RNase HII reaction was separated and treated with 50 mM $NaHCO_3$ (pH 9.0) at 90°C for 30 min. The samples were loaded onto a 10% PAGE and visualized by phosphorimaging. Only the substrate treated with both RNase HII and $NaHCO_3$ produced a single P^{32} labeled ribonucleotide as shown. Thus, Lm RNase HII recognized RNA-DNA junction and cleaves at the 5' end of the ribonulceotide and leaving behind a 5' phosphate.

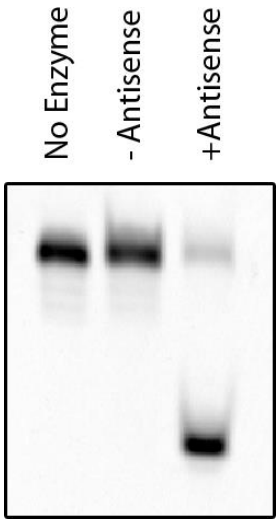

Figure S3.3. Lm RNase HII cannot cleave single stranded DNA-RNA chimera substrates. The R10-D8 substrate (100 nM final concentration) was mixed wt-Lm RNase HII (50 nM final concentration) either in the presence or absence of the antisense strand (D18). The reaction contained 20 mM Tris-Cl pH 7.5, 50 mM NaCl, 50 mM DTT, 0.1 mM EDTA, 10 mM $MgCl_2$ and was performed at 37°C for 30 min.

CHAPTER 4: Developing RNase-Cleaved Fluorescent Substrate (RFS) to Detect *Listeria monocytogenes*

4.1 Abstract

L. monocytogenes is a foodborne pathogen which can causes severe illness (listeriosis) in individuals with weakened immune systems. The fatality rate of individuals with listeriosis can reach up to 20%-30% thus, monitoring foods on a timely-bases for *L. monocytogenes* is necessary step to ensure the safety of public health. Current detection methods such as cell-plating analysis, enzyme-linked immunosorbant assay, or polymerase chain reaction fail to meet the demands for frequent-food screening since it can take 2-5 days to obtain results. In this study, we investigate the use of functional nucleic acid as a molecular tool to develop a sensitive and rapid biosensor to detect *L. monocytogenes*. We developed fluorescently labeled nucleic acid molecules that act as substrates for endoribonuclease (RNase) from *L. monocytogenes*. These substrates were termed RNase-cleaved fluorescent substrates (RFS) and were developed using a method called "Systematic Evolution of Ligands by Exponential Enrichment" (SELEX). We initially identified and purified three RNases (RNase III, G and HII) from *L. monocytogenes*. The RFS was first developed for RNase HII for which 15 rounds of SELEX were completed. All the sequence isolated at the end of round 15 contained CCATA nucleotides believed to be important for interacting with RNase HII. Six class of sequences termed C1 to C6 were most abundant in the round 15 sequence population and were further characterized in Chapter 5. When testing the ability of C1-C6 to detect native RNase HII in *L. monocytogenes* cell lysate, we found that only C4

was able to produce a signal after a 24 h incubation time. Thus, although we have developed a RFS which can detect purified RNase HII, further work is required to improve the detection of native levels of the enzyme in cell lysates. Furthermore, many challenges were encountered when developing RFSs for RNase III and G and the issues with SELEX are discusses within this chapter.

4.2 Introduction

The foodborne pathogen, *Listeria monocytogenes*, poses a public health concern across the globe as it has been responsible for multiple food contamination outbreaks over the past century.[1, 2] The pathogen is an intracellular, gram positive facultative anaerobe which can invade the body through the intestinal wall following consumption of contaminated food or drinks.[3] It is naturally found in soil, vegetation, waste water, insects, birds, animals, and fecal matter. It can grow at temperatures ranging from -7°C to 45°C, under high salt conditions and at a pH range of 4.0-9.5.[2, 4-6] Due to its robust nature, packaged food has become a common route of spread for the pathogen.[1] In 1992, contaminated pork tongue delicacies were consumed in France that led to a total of 279 cases from which 63 deaths and 22 abortions were reported.[1] A recent outbreak of *L. monocytogenes* in the United States was spread by the consumption of contaminated cantaloupes leading to over 125 infected individuals and at least 25 deaths.[7] Other *L. monocytogenes* outbreaks have led to massive recalls of food products, costing companies such as Maple Leaf Foods over $20 million as well as a loss of consumer trust.[8, 9] Furthermore, reports have estimated approximately 1600 cases annually related to *Listeria* infections resulting in 400 to 500 deaths.[10] The infection caused by *Listeria* is termed listeriosis, and can manifest as meningitis, an

inflammation of the protective covering of the spinal cord and brain and as endocarditis, a problem of the circulatory system.[11, 12] Listeriosis in healthy individuals is rare however, at-risk individuals can become severely ill with a fatality rate reaching as high as 20% to 30%, whereas, other food borne pathogens such as *S. typhimurium* and *E. coli* which have a fatality rate of only 1%.[2, 13] At-risk individuals include immuno-compromised patients (organ transplant patients, HIV positive individuals), infants, elderly and pregnant women.[2, 4, 10] Consequently, the government and health organizations like the World Health Organization (WHO) have put large efforts in studying listeriosis epidemiology and implementing good food hygiene practices to prevent future outbreaks.

Standards for the exact amount of *L. monocytogenes* that can be tolerated within processed food varies by country but the general standard set by the WHO (practiced within North America) is a zero tolerance within pasteurized food and a tolerance level of ≤100 cells/g or mL in all other foods.[2, 14] A higher level of contamination will require removal of the product from the market as it can pose serious harm to the consumer. Hence, the ability to detect *L. monocytogenes* in a quick and sensitive manner becomes important for the food industry as well as for health organizations. Furthermore, detection methods are required to monitor and assess *L. monocytogenes* in the environment as a way to trace outbreaks for epidemiological studies.

There are several methods to detect *L. monocytogenes* in food and environmental samples. The classical approved method uses chromogenic selective agar in conjugation with biochemical techniques and microscopy.[15, 16] This method can distinguish different *Listeria*

species and can determine the presence of *L. monocytogenes* with a success rate of 90% or greater.[1] However, this technique requires a high degree of training and can take anywhere from 3 to 5 days to produce results. Other techniques have been developed for rapid detection of *L. monocytogenes* such as PCR kits or enzyme-linked immunosorbant assay (ELISA). Although these rapid detection methods can provide species-specific detection of *Listeria* with detection limits of 10^1-10^4 CFU/mL, they possess their own caveats. The PCR and ELISA methods are expensive and require specialized equipment, training and proper handling and storage. Furthermore, it is common practice to implement a time consuming 24-hour enrichment step prior to detecting the pathogen. This step selectively allows the growth of *Listeria* and ensures that there are enough cells present for detection. Thus, despite the advancements in the methods to detect *L. monocytogenes*, there is still a need for an inexpensive, rapid and easy-to-use detection system. In this study, we propose the use of functional nucleic acid (FNA) molecules as a new approach to achieving such goals.

Functional nucleic acids have been widely studied and used for various applications ranging from studying biological systems, developing biosensors and as therapeutics. One class of FNAs, called aptamers, are highly specialized single-stranded deoxyribonucleic acid (DNA) or ribonucleic acid (RNA) molecules which have the ability to bind target molecules much like an antibody binds to its antigen.[17] Naturally occurring RNA-aptamers, called riboswitches, have been identified as part of gene control elements and are involved in regulating various metabolic genes.[18] Although various riboswitches have been identified such as those that bind to flavin

mononucleotide, S-adenosyl methionine, vitamin B_{12} and thiamin pyrophosphate, methods to artificially create aptamers have advanced over the past years. These aptamers have been developed to bind a wide range of targets such as amino acids, nucleotides, enzyme co-factors, blood coagulation factors, growth factor proteins, antibiotics, vitamins, viral proteins and whole cells. In a book chapter, Scott Silverman (2009) has summarized the most current FNAs and their dissociation constants (Kd).[19]

Aptamers are generated by a method called Systematic Evolution of Ligands by EXponential enrichment (SELEX) or *in vitro* selection. To obtain an aptamer, a pool of over 10^{15} DNA or RNA molecules each containing a randomized sequence region are subjected to selective pressures such that only sequences which are able to bind to the target analyte will be isolated.[17, 20] The isolated sequences are amplified with the use of PCR to generate a specialized population that again is subjected to the selective pressure. In order to narrow down and obtain sequences with the greatest ability to bind the target, more stringent selection conditions are introduced in successive rounds of selection. This includes either reducing the incubation time between the target and the DNA or RNA population, or reducing the concentration of the target. The cycles of selection are repeated multiple times until unique sequences are isolated which can bind the analyte with great affinity and high specificity. In order to improve specificity towards a target, a counter selection step can be introduced in an attempt to eliminate sequences that cross-react with non-specific targets. For this step, the enriched DNA or RNA pool is incubated with a non-

specific target and only the sequences which do not interact with the non-specific target are isolated.

In this study, FNAs that target various *L. monocytogenes* endoribonucleases (Lm-RNases)

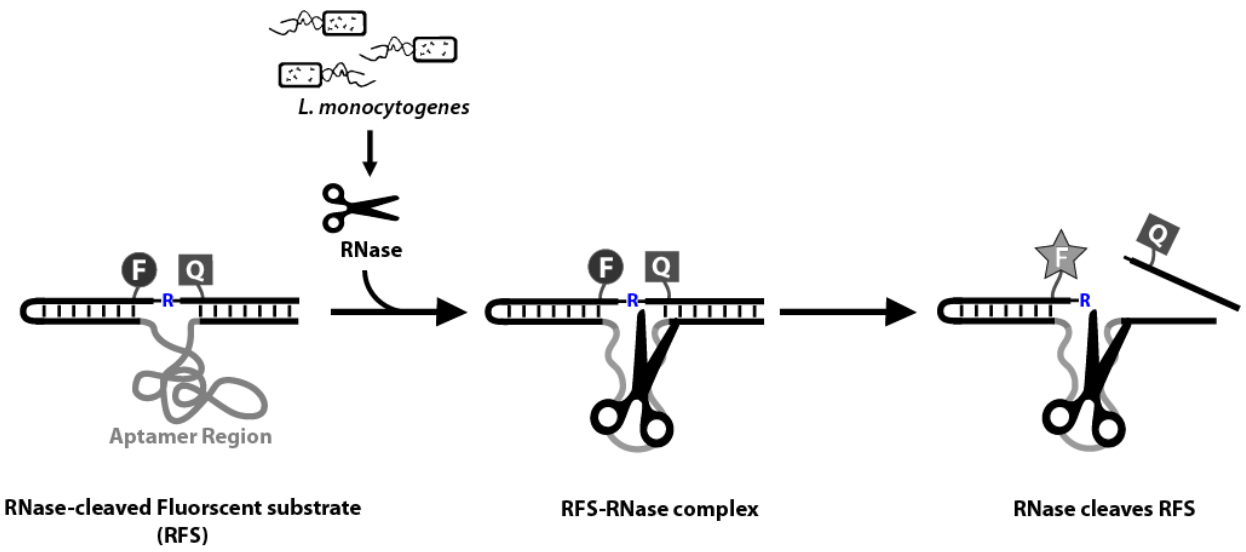

Figure 4.1. RNase-cleaved fluorescent substrate (RFS) used to detect *L. monocytogenes*. The RFS contains a DNA aptamer region which binds to a specific endoribonuclease from *L. monocytogenes*. The RFS sequence also contains a single ribonucleotide, (riboadenosine, labeled as R) which is situated between a fluorophore (F) and a quencher (Q)-modified deoxythymine. Initially there is minimal emission of fluorescence due to the close proximity of the fluorophore and the quencher. In the presence of *L. monocytogenes*, which produces RNases, a RFS-RNase complex can be formed. The RNase cleaves the single ribonucleotide which separates the quencher form the fluorophore thus enhancing fluorescence.

are generated using SELEX. However, these FNAs differ from traditional aptamers such that they undergo catalytic cleavage upon binding their respected target. These specialized DNA molecules are composed of two main components: 1) A DNA sequence behaving much like an aptamer by binding to the RNase; 2) A stretch of DNA flanking a single RNA moiety which acts as the substrate for the RNase. Furthermore, the RNA moiety is situated between a fluorophore and a quencher-modified deoxythymine, fluorescein (Emission max = 521 nm, green) and dabcyl

(Absorbance range = 400-550 nm), respectively (Figure 4.1). Since the RNase catalyzes the cleavage of single stranded or double stranded RNA molecules, the goal was to isolate highly specialized FNAs that would undergo cleavage at the single RNA moiety only upon binding to a particular Lm-RNase. Prior to cleavage, the close proximity of the quencher to the fluorescent molecule prevents fluorescence; however, upon cleavage, strong fluorescence would be present as the fluorescent molecule is separated from the quencher. These FNAs were termed RNase-cleaved fluorescent substrates (RFS) and the detailed SELEX strategy is illustrated in Figure 2.5 in Chapter 2.

We are exploiting the robust catalytic power of a natural protein enzyme to cleave artificially evolved functional nucleic acid molecules. Since natural RNases have relatively high turnover rates (catalytic efficiencies ranging 10^5 to 10^7 $M^{-1}s^{-1}$) we predicted that we could produce a highly sensitive detection method using the RFS.[21, 22] Furthermore, the RFS had the potential to be developed into a simple mix-and-read assay. For example, a contaminated food sample could be placed into a cell enrichment solution containing RFS probes. As the cells enumerate, fluorescence can be measured to indicate the presence of pathogen. Similar work done with a RNA-cleaving fluorescent DNAzyme (RFD) has shown that these simple mix-and-read assays can be developed into a sensitive and quantitative method to detect pathogens.[23] In the study, a single live *E. coli* cell was detected within eight to twelve hours of culture with minimum preparation steps. In our study, we investigated whether RFSs have the potential to detect *L.*

monocytogenes and provide significant advantages over the existing commercially available detection systems such as reduced detection time, simple to use and low cost.

4.3 Prospective Challenges of Developing RFS for Detecting *L. monocytogenes*

Most of the RNases have been well characterized in model organisms such as *E. coli* but essentially no characterization has been completed of the Lm-RNases. Thus, prior to developing RFS, the different endoribonuclease genes within the *L. monocytogenes* genome were identified with the aid of genomic analysis tools. For this study, Lm-RNase G, III, and HII were initially used to generate RFSs (see Table 4.1 below for more information on RNases).[24-31] Since these RNases play a vital role within most bacterial species, it was predicted that they were also expressed in *L. monocytogenes* which was later proved experimentally using reverse transcription polymerase chain reaction (RT-PCR).[32, 33] RNases are ubiquitous within various organisms thus, one of the potential challenges in this study will be the cross-reactivity of the RFS probes with different bacterial species. However, it was hypothesized that the differences within the primary amino acid sequences and the overall enzyme topologies would be sufficient to generate species-specific RFSs. In fact, it is already known that aptamers have the ability to distinguish between protein variants that are very similar.[19] For example, the aptamer developed for platelet-derived growth factor B chain (PDGF-B) has a 100 fold greater affinity than to PDGF-A; the variants share a 60% sequence similarity.[34] An aptamer (14F3'T) that binds to keratinocyte growth factor (KGF), a member of a larger family of fibroblast growth factors (FGFs), can discriminate against all other members by 10,000 fold.[35] An aptamer which binds to L-selectin shows specificity of

8,000-15,000 folds and 200-500 folds over P-selection and E-selection, respectively.[36, 37] Although cross-reactivity of RFS may not be entirely avoided, a high degree of specificity towards Lm-RNases can be used to discriminate against other bacterial RNases.

Table 4.1. List of endoribonucleases and their biological role.

Endoribonuclease	Substrate	Biological Function
Type 1 RNase H (RNase HI)	DNA/RNA heteroduplex	Removing Okazaki fragments during DNA replication
Type 2 RNase H (RNase HII)	DNA/RNA heteroduplex and DNA_n-RNA_n-DNA_n/DNA heteroduplex	Removing Okazaki fragments during DNA replication. Repairing genomic DNA by removing misincorporated ribonucleotides.
RNase E	Single stranded RNA and prefers to cleave in A/U rich region	Rate limiting step which initiates mRNA turnover via the formation of degradasome in gram negative bacteria. Involved in maturation of many RNA species within bacteria cells.
RNase G	Single stranded RNA and prefers to cleave in A/U rich region	A non-essential enzyme with very similar structure and function to RNase E but, does not form a degradasome complex. Involved in maturation of many RNA species within bacteria cells.
RNase III	Duplex RNA (shows preference to specific nucleotide regions within steam and loop of a hairpin structure)	Maturation of rRNA as well as mRNA.
RNase Z	Duplex RNA	Cleaves tRNA at 3' end in order for the addition of CCA nucleotides.
RNase T1 family	No specificity towards single stranded RNA sequence	Enzyme is secreted out of the cell to cleave extracellular RNA.
RNase T2 family	No specificity towards single stranded RNA sequence	Similar to T1 family in which it is secreted out of the cell to cleave extracellular RNA. (Functions optimally at lower pH of 4-5)
RNase P	5' end of the tRNA	A ribozyme in complex with protein cofactors to trim the 5' tRNA end for maturation.
RNase Y	Single stranded RNA	Rate limiting step which initiates mRNA turnover via the formation of degradasome in gram positive bacteria. Involved in maturation of many RNA species within bacteria cells.

In this study we attempted to generate three different RFS (each with a different fluorophore and quencher pair) targeting three different Lm-RNases. Thus, in the presence of the pathogen three simultaneous fluorescence signals would be generated each corresponding to a different RNase. The ratio between the different fluorescence signals will depend on 1) the strength of interaction between RFS and the RNase, and 2) the amount of RNase produced by the organism. Even if the RFS do cross-react with different organisms, the ratio-metric fluorescence profile would be different from that of *L. monocytogenes*. We predict that not only will the RFSs determine the presence of *L. monocytogenes*, the ratio-metric fluorescence profile can also help identify other bacterial organisms.

Overall, this study investigated the possibility of developing novel fluorescent nucleic acid probes used to detect *L. monocytogenes* (and potentially other bacterial organism) in packaged foods or environmental samples with high sensitivity, reduced detection time and low-cost.

4.4 Results and Discussion

4.4.1 Sequence Similarities between Lm-RNases to Other Bacterial Organisms

RNases from *L. monocytogenes* show percent sequence identity of less than 70% to other organisms (Table 4.2a). The percent similarity values reached as high as 87%; these values are expected to be larger than percent identity since the calculations also encompass amino acids which are chemically similar (Table 4.2b).

The percent identity and similarity between the different *Listeria* species is greater than 90%. This poses a challenge since only genus specific RFS may be isolated during the SELEX

process. Since all of the *Listeria* species are potentially pathogenic, the presence of any in packaged food or drinks is undesirable. Thus, making a rapid, simple to use detection system for the genus *Listeria* will also prove advantageous. It is feasible to make a species-specific RFS because although the RNases are essentially identical, their expression levels in different species may vary under different growth conditions. As mentioned earlier, ratio-metric fluorescence profile may help differentiate different *Listeria* species.

Table 4.2. Percent sequence identity of Lm-RNase to various bacterial organisms. a) The percent identity of Lm-RNases (protein sequence) was assessed by performing multiple global pairwise alignment using gene analysis tools provided by European Bioinformatics Institute (EBI) and National Center for Biotechnology Information (NCBI). Various bacterial organisms from the *Firmicutes* phylum were assessed and the highest percent identities in the various genus or class are listed. Sequences from three common pathogens from the *Proteobacteria* phylum were also aligned with Lm-RNases. Gram positive bacterium shows the lowest sequence identity to Lm-RNase. Bacterial organisms from the *Bacillus* genus show the greatest percent identity. Percent identity greater than 90% exists between the different species within the *Listeria* genus. (*)Note: RNase G lacks the C terminal domain often present in RNase E; the C terminal amino acid sequences of RNase E were not included during alignment. b) The organisms which scored the highest percent similarity are listed in this table. The organisms with RNases that scored the highest percent similarity and identity to *L. monocytogenes* RNases fall within the bacterial order *Bacillales*.

a)

		RNase III	RNase E/G*	RNase H II
Firmicutes (Gram +)	*Streptococcus* [a]	55%	----	----
	Lactobacillus [a]	57%	----	50%
	Bacillus [a]	65%	33%	60%
	Clostridia [b]	55%	33%	50%
	Listeria [a]	92-99%	92-99%	92-99%
Proteobacteria (Gram -)	*S.typhimurium*	40%	31%	50%
	E. coli	40%	31%	50%
	V. cholerae	38%	20%	36%

Taxonomy: [a] refers to genus and [b] refers to class,
(----) refers no significant sequence similarity found during sequence Blast

b)

Organism	RNase Type	Percent Similarity	Percent Identity
Geobacillus	RNase III	87%	66.1%
Streptococcus pseudoporcinus	RNase HII	81%	54 %
Bacillus megaterium	RNase HIII	85%	58%
Bacillus thuringiensis	RNase G	61%	31%

4.4.2 Reverse Transcription

Reverse-transcription (RT)-polymerase chain reaction was performed to assess whether or not the *L. monocytogenes* expressed the *rng* (RNase G), *rnc* (RNase III) and *rnhb* (RNase HII) genes (Figure 4.2). The size of the PCR products correlated well with the expected size of the *rng*, *rnhb*, and *rnc* mRNA transcripts, which were 1362 nucleotides (nt), 786 nt, and 690 nt, respectively. There were multiple RT-PCR products present for the *rng* gene and likely produced due to the primer annealing with sequences other that the *rng* mRNA transcript.

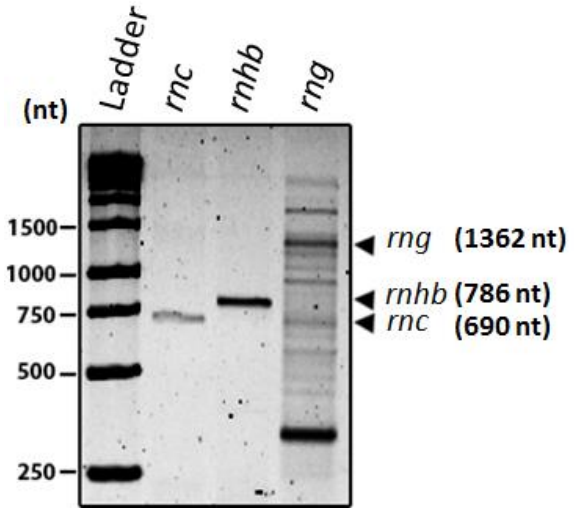

Figure 4.2. Reverse-transcription polymerase chain reaction. A 1% agarose gel showing the RT-PCR products for the *rnc*, *rnhb* and *rng* gene. The expected size of each PCR product (size in nucleotide, nt) is indicated.

4.4.3 Protein Expression, Purification and Activity

Three clones were created by transforming *E. coli BL21 (DE3)* with pET 15b vectors containing the genes for one of Lm-RNases G, III, and HII. The detailed protocol for solubility assays and protein purification are described in the materials and methods chapter.

Following purification, a single band of high intensity was visualized for the Lm-RNase III and HII samples, indicating that the samples were contaminant-free (Figure 4.3). However, the Lm-RNase G sample contained a high molecular weight band of ~ 116 kDa. Since this band is

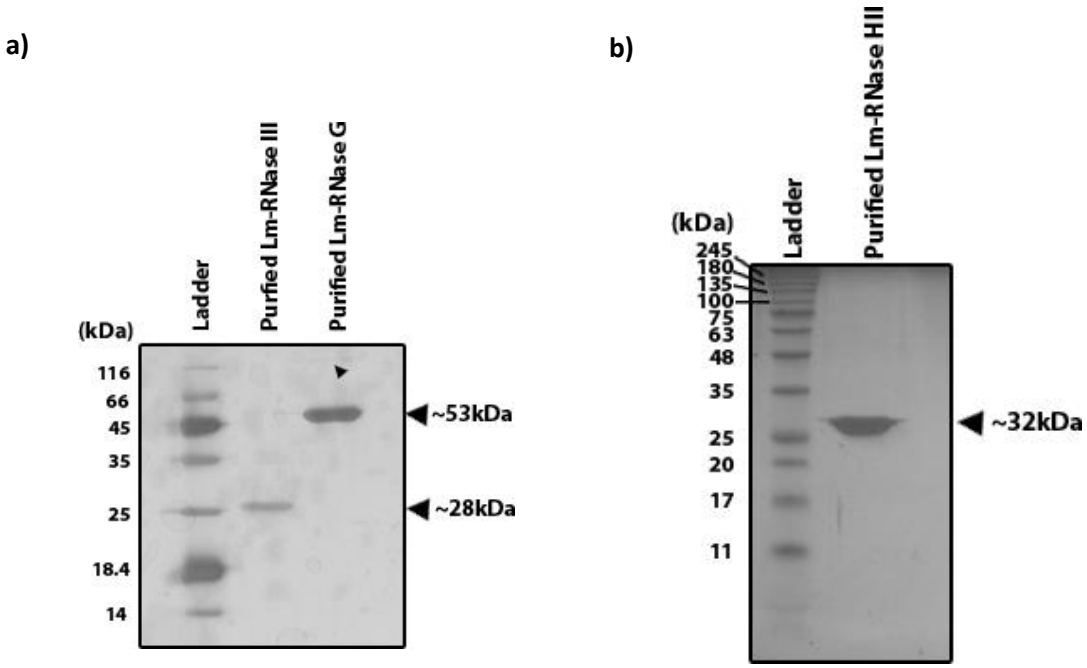

Figure 4.3. Silver Staining of Lm-RNase III, G and HII. a) Silver staining of Lm-RNase III and G. Approximatly 1 mg of protein was loaded on a 15% SDS-PAGE, and silver stained. The small arrow indicates the presence of a larger molecular weight protein within the Lm-RNase G sample. b) Silver staining of Lm-RNase HII: Approximately 1mg of the sample was loaded onto 15% SDS-PAGE and silver stained. A band of high intensity at ~32 kDa represents Lm-RNase HII.

approximately twice the size of the original 53 KDa band, it is likely the product of Lm-RNase G dimerization held together by disulfide bridges.

A Superdex (dextrose) size exclusion column was used to determine that the Lm-RNase III and G existed predominantly as a dimer *in vitro*, whereas Lm-RNase HII was a monomer (Chapter 2 Figure 2.2c, 2.3c, and 2.4c). These results are consistent with the multimeric states for the RNases identified in other organisms.[24, 38-40]

The purified Lm-RNase III failed to cleave a 5' ^{32}P radioisotope labeled RNA substrate called μR1.1 [5'+2] (a substrate previously used to study *E. coli* RNase III) in the presence of magnesium ions (Mg^{2+}), whereas the commercially available RNase III from *E. coli* cleaved μR1.1 [5'+2] as expected in the presence of the Mg^{2+} cofactor (Figure S4.1a).[41] Initially it was predicted that the enzyme aggregation was responsible for the lack of enzyme activity however, dynamic light scattering (DLS) analysis shows that the protein was soluble (data not shown). The study from which the μR1.1 [5'+2] substrate was adopted had the goal to identify a substrate with a minimal set of RNA sequence required for recognition by *E. coli* RNase III substrate hence, it is possible that the Lm-RNase III may not recognize or cleave μR1.1 [5'+2]. A natural substrate, *E. coli* 23S ribosomal RNA (rRNA), which is recognized by *E. coli* RNase III was adopted to test Lm-RNase III activity. However, the 23S substrate was not cleaved by the Lm-RNase III (data not shown). It is possible that *in vitro* conditions lack specific factors such as co-factors or other interacting proteins required by Lm-RNase III to recognize and cleave *E. coli* 23S rRNA substrate. Previous studies have elucidated that RNase III from *Bacillus subtilis* (*B. subtilis*), a

closely related bacterium to *Listeria*, was unable to cleave *E. coli* 23S rRNA *in vitro* but, its endogenous expression was able to complement *E. coli* RNase III mutants.[42, 43]

The N leader (viral) gene which can be recognized *in vitro* by *B. subtilis* RNase III was tested.[43] In *E. coli*, the λ N leader transcript is cleaved by RNase III to activate viral gene expression.[30] The plasmid which contained this gene downstream of a T7 RNA polymerase was linearized and transcribed to obtain the λ N leader RNA. The Lm-RNase III cleaved the transcript in presence of Mg^{2+} producing three bands of 150 nt, 131 nt, and 109 nt similarly to that of *E. coli* RNase III (Figure S4.1b). However, it is not clear why the substrate was cleaved to generate a band larger than 150 nt in the absence of Mg^{2+}. The control reactions, which contain only the λ N leader transcript, show no cleavage in presence or absence of Mg^{2+} thus, contamination by other ribonucleases or auto-cleavage of the transcript is unlikely. It is possible that Mg^{2+} ions are still tightly bound to the enzyme which led to enzyme activity.

The Lm-RNase G activity was tested using a short single stranded RNA substrate called pBR-13; this substrate had previously been used to study mycobacterial and *E. coli* RNase E/G kinetics.[31] Similar to previous reports with *E. coli* RNase E, the purified enzyme cleaved pBR-13 in the presence of Mg^{2+} (Figure S4.1c). This indicates that Lm-RNase G may play a similar physiological role as *E. coli* RNase E/G, such as ribosomal RNA processing (e.g 5S), tRNA maturation, and regulating messenger RNA turnover however, further investigations are required.[31, 32]

The Lm-RNase HII activity was assessed using a DNA (polydeoxythymine)-RNA (polyadenine) heteroduplex which has been previously used to study RNase HII activity. The activity assay revealed that the purified enzyme was functional and required Mg^{2+} as a cofactor (Figure S4.1d).[24]

4.5 Results and Discussion for Systematic Evolution of Ligands by Exponential Enrichment

4.5.1 RNase-Cleaved Fluorescent Substrate for Lm-RNase HII

A total of 15 positive rounds of *in vitro* selection were completed to isolate the RFS probe. The entire selection progress is summarized in Figure 4.4. The first round (R1) was initiated by incubating ~500 pmol of DNA library with a high concentration of enzyme (40 nM) for 30 min at room temperature. This resulted in only 2% cleavage (~10 pmol of product). All other selection rounds started with ~200 pmol of DNA library as this was the practical final yield obtained following the purification of PCR2. In round 2, the selective pressure was increased by reducing the enzyme concentration by 10-fold which resulted in a 7% cleavage (or ~10 pmol product). Even though a 7% cleavage seemed as a small quantity, this represented ~10^{12} DNA sequences carried over as products for the next round of selection. Thus, the stringency of selection from R3-5 was increased by decreasing the enzyme concentration to 400 pM and reaction time to 20 minutes.

Lowering the enzyme concentration also posed a risk of populating the DNA pool with self-cleaving sequences (or catalytic DNA). The activity of catalytic DNA is often promoted in

the presences of buffers containing divalent metal ions. Multiple motifs of catalytic DNA which cleave RNA in presence of various divalent metal ions have been independently isolated *via* SELEX.[44, 45] The dose of RNase HII was increased by 10-fold in R6 to assess whether the percent cleavage would also proportionally increase. An increase in the signal would indicate that cleavage was target dependent. If the percentage of cleavage remained the same, then the cleavage activity would largely be accounted by selfish catalytic DNAs. The R6 cleavage increased little less than 10-fold indicating that the DNA population consisted largely of target-dependent sequences over catalytic DNA sequences.

The reaction time for R7-10 was reduced to 15 minutes with the enzyme concentration set to 400 pM. No improvement in the catalytic activity was observed from R7 to R10 as the percent cleavage remained little less than 1%. If the DNA sequence diversity had reduced drastically over the many rounds of evolution, continuing successive rounds of selection would no longer isolate the strongest target-binding sequences. As a result, the DNA population at the end of R10 was sequenced (data not shown). Sequencing results showed that the DNA population still contained a very diverse set of sequences because they could not be collectively organized into large families based on sequence similarity. This scenario allowed for further increase in the stringency of selective pressure in later rounds.

The negative round (N1) served as a check point to ensure that DNA population did not contain selfish catalytic DNAs. N1 was performed by incubating the R10 population with buffer for 1 hour at room temperature. No cleavage was observed for N1, indicating that DNA

population was largely target-dependent. A very small percentage of cleavage by catalytic DNA may have occurred even though no visible cleavage was observed during N1. Fortunately, this small percentage of catalytic DNA sequences were eliminated from the population by gel separation.

Counter-selection (CS) is a process in which the DNA sequences that interact with agents other than the desired target are eliminated.[46] Biological samples often contain various nucleases such as DNases that degrade DNA strands non-specifically, posing problem for detection using DNA-based probes. Past work has demonstrated that the process of SELEX can often isolate target-specific sequences that can be resistant to non-specific nuclease degradation.[23] To address these issues, we employed a counter-selection step in which the DNA population after R11 was mixed with cell lysate obtained from *Bacillus subtillis*. To eliminate sequences which would be targeted for nonspecific degradation by nucleases or by other components in cells or excreted into the medium. The non-specific cleavage observed in counter-selection round (CS1) was large (~6%), indicating that many of the sequences present within the library were targeted by nucleases or other factors which helped promote RNA hydrolysis. Sequences that were resistant to cleavage in CS1 were isolated and subjected to a second counter-selective pressure (CS2) with similar conditions as CS1. The amount of non-specific cleavage seen in CS2 was less than 0.5%, indicating that the DNA library contained sequence that were more resistant to non-specific degradation. The sequences isolated after CS2 were subjected to a positive selection (R12) in order to assess if the DNA population could still respond to Lm-RNase HII. Although, counter-

selection steps provide an excellent strategy to eliminate undesired sequences, the caveat is that diversity of the DNA population can be drastically decreased due to removal of many sequences. Furthermore, there is a risk of losing key sequences that are important for performing the desired function. This would make it increasingly difficult to isolate desired sequences in later positive selection rounds. Thus, the enzyme concentration for R12 was increased to 4 nM to improve the

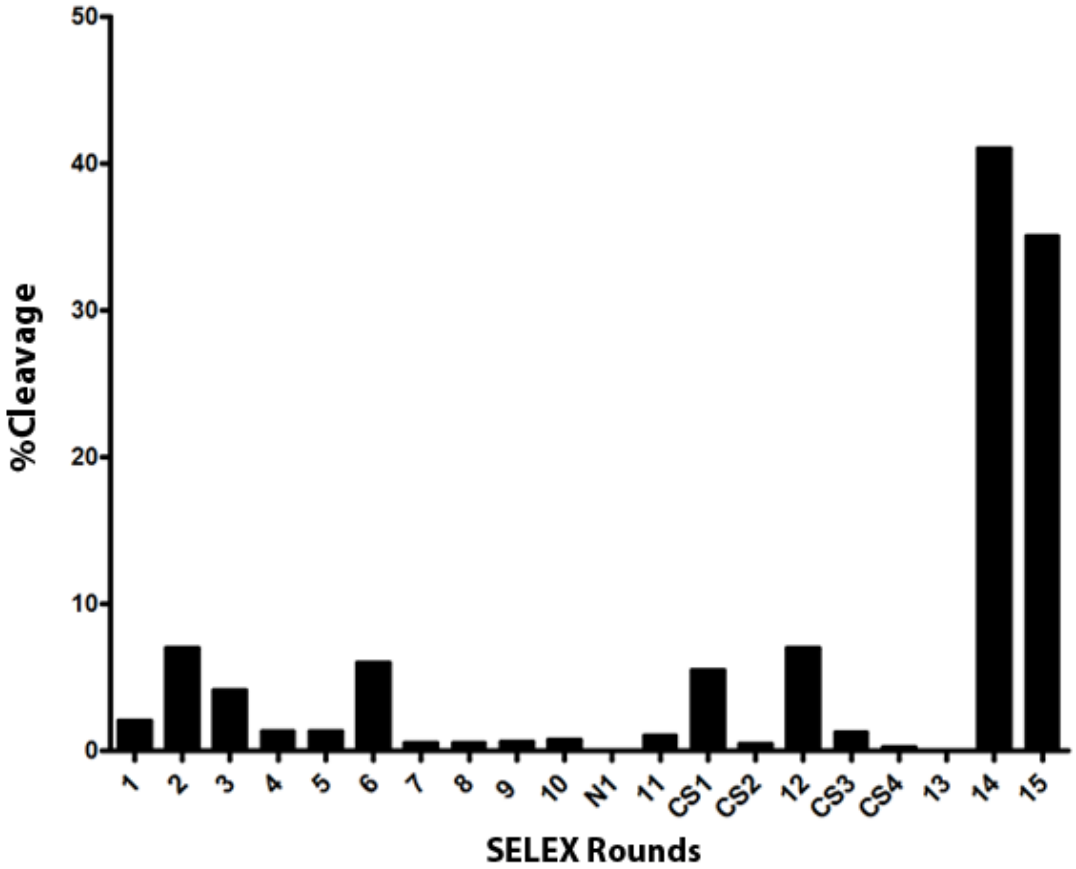

	1	2	3	4	5	6	7	8	9	10	N1	11	CS1	CS2	12	CS3	CS4	13	14	15
[Enzyme] (nM)	40	4	0.4	0.4	0.4	4	0.4	0.4	0.4	0.4	0	0.4	0	0	4	1	1	4	4	4
Time (min)	30	30	30	20	20	20	15	15	15	15	60	15	30	30	10	15	15	10	10	10

Figure 4.4. Progress of SELEX using RNase HII as the target. The percent cleavage of the DNA pool at each round of selection was graphed. The reaction time and the concentration of RNase HII used for each round of selection is listed in the table. In the negative (N) round, the DNA pool was incubated with the only SELEX buffer. Counter selection (CS) rounds 1 and 2 were incubated with cell lysate obtained from *B. subtilis*. CS3 and CS4 were incubated with a mixture of RNase HII purified from *C. difficile* and *S. typhimurium*.

chances of isolating RNase HII-dependent sequences. A cleavage of ~7% at R12 indicated that the DNA population were still target-dependent.

Two consecutive counter-selection steps (CS3 and CS4) were performed using a mixture of purified RNase HII from *C. difficile* (Cd) and *S. typhimurium* (St). This step was used to aid in the removal of sequences with affinity towards RNase HII from other pathogenic bacteria. A ~1.5% and less than 0.5% cleavage was seen for CS3 and CS4, respectively. The decrease in cleavage indicated that sequences at the end of CS4 were less likely to interact with Cd- and St-RNase HII.

No cleavage was observed at the end of R13 leading to the possibility that the counter-selective steps, CS3 and CS4, may have removed RNase HII binding sequences. This is likely since both the Cd- and St-RNase HII show close to 50% sequence similarity to Lm-RNase HII. However, this was not the case since the cleavage in R14 and R15 exceeded 35%. One possible explanation could be that at the end of CS4, multiple sequences that interact with RNase HII were eliminated with only a few sequences remaining within the population. Thus, no cleavage was observed in R13. Although not visible, the small set of sequences that were cleaved in R13 were amplified using PCR. This would repopulate the DNA population with sequences that strongly interacted with Lm-RNase HII therefore, observing the large percent cleavage in R14 and 15.

4.5.2 Sequencing of DNA population at the end of R15

The sequencing result for the DNA pool at the end of R15 is summarized in Figure 4.5. There are diverse DNA sequences which cannot be categorized into distinct families. Further positive selection rounds may assist in isolating more specialized class of sequences that have the strongest capability to bind Lm-RNase HII. These results also highlight that even with stringent counter-selective pressure, such as CS3 and CS4, the DNA pool can still have sequence diversity. Even though *in vitro* selection did not lead to the isolation of dominant sequences, the DNA pool did contain six classes that were more abundant. These classes, termed C1 to C6 based on sequence similarity, were not present at the end of R10 (data not shown), thus they only started to dominate the DNA pool over the last five rounds of positive selection. The analysis of C1 to C6 sequences are discussed in greater depth in Chapter 5.

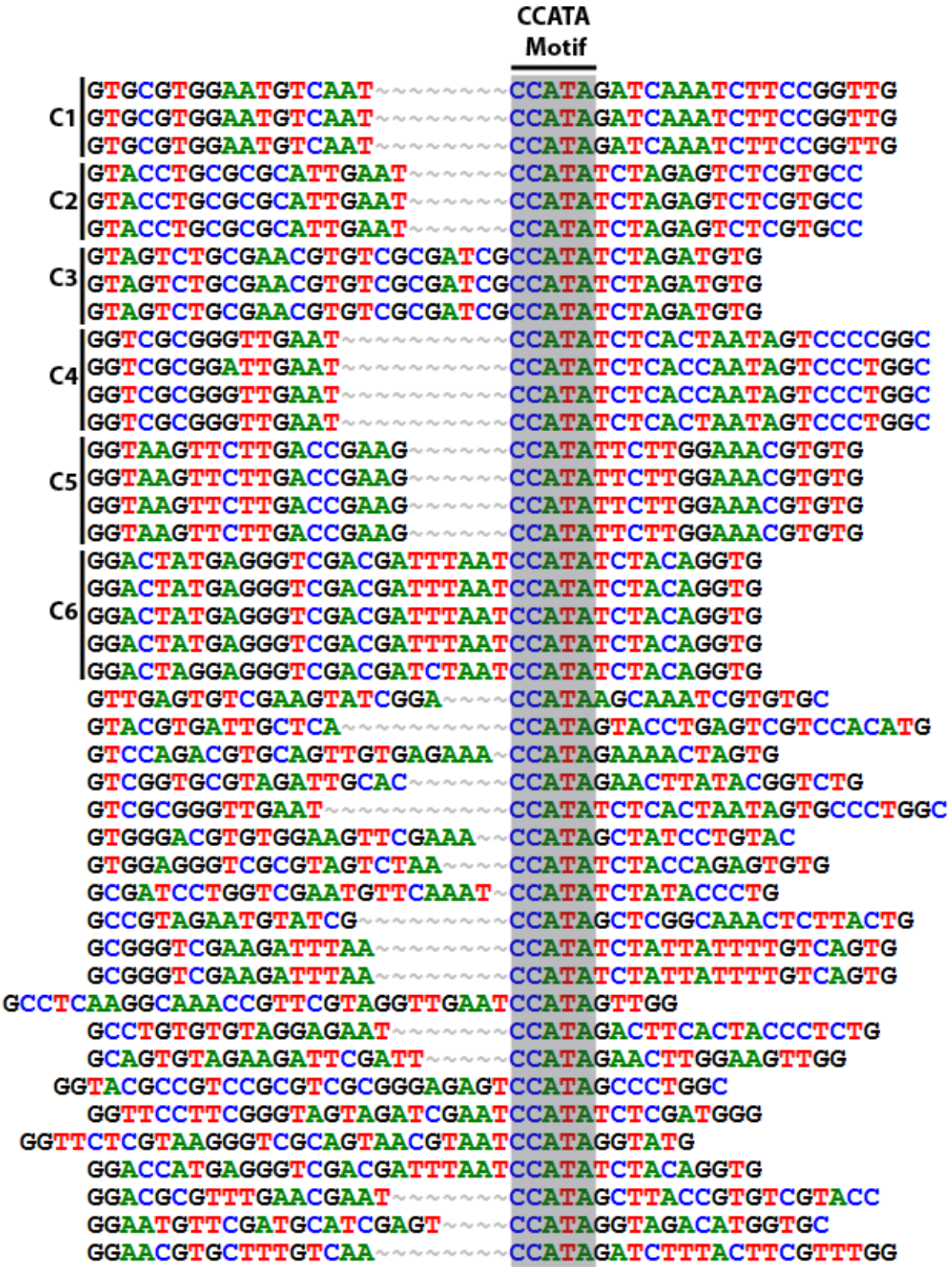
CCATA
Motif
C1
C2
C3
C4
C5
C6

Figure 4.5. Sequences present in the R15 DNA pool. Gaps (~) were inserted to align the CCATA nucleotides. The different sequence classes are labeled C1 to C6 based on their overall sequence similarity. The primer binding sequence was excluded from the alignment.

The motif CCATA was present in most sequences. This motif formed a five base pair duplex at the cleavage site containing the single ribonucleotide (Figure 4.6). A duplex structure is key for Lm-RNase HII to bind and perform catalysis thus, we repeatedly see the presence of the CCATA motif. The upstream and downstream regions of the CCATA motif for C1-C6 vary in their nucleotide sequence, length, and the number of Watson-Crick base paring. The variation in these regions play a role in influencing enzyme binding and catalysis. Further analysis of the sequences are discussed in Chapter 5.

Figure 4.6. CCATA nucleotides help form a duplex at the cleavage site. The CCATA sequence forms a duplex by paring with the region containing the single ribonucleotide (riboadenine, a). The location of the fluorophore (F) and a quencher (Q) is shown in the sequence.

4.5.3 Testing C1 to C6 RFS probes for detecting *L. monocytogenes* cells

We also tested whether C1-C6 probes could also detect *L. monocytogenes* cells. The cells were grown to mid-log phase (OD_{600} 0.7), pelleted and lysed using sonication. The cell lysate was used for the reaction and only C4 was cleaved (Figure 4.7). There are two distinct reaction products visible on the dPAGE by phosphorimaging. The higher molecular mass product was indicative of DNA cleavage by DNases within the cell lysate. Overlapping the phosphorimage with the fluorimage shows that this product retained the fluorophore thus, the cleavage did not occur at the single ribonucleotide but elsewhere. The lower molecular product was formed due to

RNA cleavage as indicated by the correct size correlating with that of the sodium hydroxide treated marker, and the band does not retain the fluorophore. It is still unclear whether RNA cleavage occurred due to the presence of RNase HII within the lysate or influenced by other factors.

Thus far, the results show that RFS, at least C4, may have the potential to detect *L.*

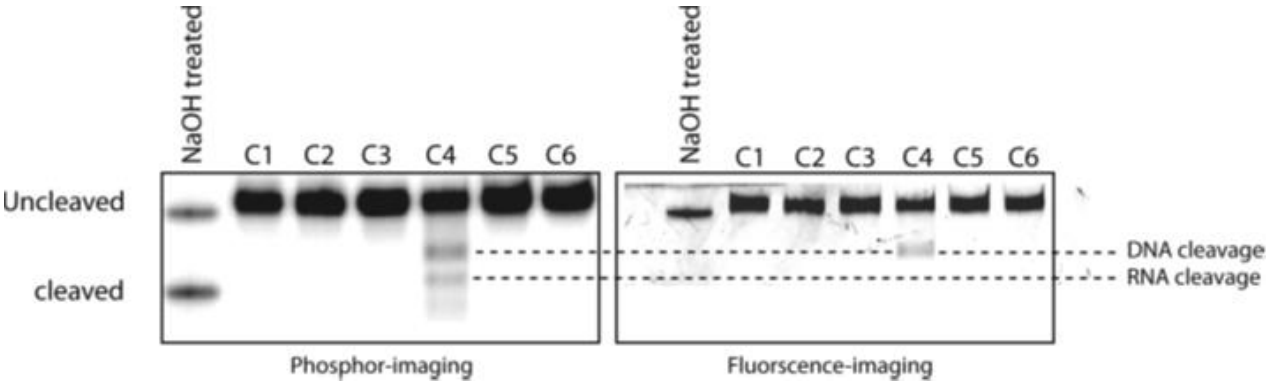

Figure 4.7. Testing if C1 to C6 cleavage using *L. monocytogenes* cell lysate. The *L. monocytogenes* cells were grown an OD_{600} of 0.7 and lysed using sonication (5 min). The lysate was directly added to a solution containing one of the sequences and the reaction took place for 24 hours. The cleavage was visualized on a dPAGE by phosphor-imaging and fluorescence-imaging. The marker sample contained alkaline treated (sodium hydroxide, NaOH) C1 sequence. The same cleaved bands within the phosphor-image and the fluorescent-image are indicated by the dotted line. The sequences that are cleaved at the RNA show no fluorescence, and those cleaved within the DNA show fluorescence. Only C4 sequence was cleaved in the presence of *Listeria* cell lysate.

monocytogenes however the sensitivity is quite low since a dense culture of cells (OD_{600} 0.7) and a reaction time of 24 h is required. It is possible is that the amount of target present within the cells is very low or that sonication may not be the ideal method for extracting cell lysate as it may damage the enzyme in the process. Other methods such lysozyme treatment, or high pressure cell disrupter need to be tested.

There are many factors that contribute to the lack of functionality of the RFS with cell lysates such as: 1) the amount of enzymes within cells is much lower than that of purified enzyme used during SELEX; 2) the enzyme may have altered binding affinity or catalytic rate compared to purified samples due to interaction with other cellular components; 3) other nucleases such as DNases can non-specifically cleave the DNA sequences. Thus, we recommend testing a slightly alternative method of SELEX when targeting enzymes such as RNases. SELEX should be done with medium more similar to the environment in which the target is naturally present such as using cell lysates. Of course, the caveat to this approach would be that some DNA sequences would evolve to bind to targets present within the cell lysates other than the desired target, but this could be minimized by doping cell extracts with purified target. An added benefit to this technique would be that not only would evolution isolate sequences that bind to the target (or the target complexed with other proteins), but also would eliminate sequences which would otherwise be inhibited by other cellular components *via* non-specific binding or degraded non-specifically by DNases. Further investigations are underway to see whether or not this strategy can improve the isolation of more sensitive, and specific RFS probe.

4.5.4 RNase-Cleaved Fluorescent Substrate for Lm-RNase G and Lm-RNase III

To develop a multi-probe analysis system for detecting *L. monocytogenes*, it was important that RFS targeting different Lm-RNases were isolated. An effort to isolate RFS for both Lm-RNase G and Lm-RNase III was done similarly to the selection strategy for RNase HII. However, despite having accomplished several round of selection (RNase III SELEX was repeated

twice), neither achieved desirable results (data not shown). The DNA populations could not be evolved to undergo cleavage by their respected target. Furthermore, we repeatedly encountered catalytic DNA sequences which were eliminated through negative selection steps. We believe that a single ribonucleotide present at the cleavage site may not be sufficient for the Lm-RNase G or III to perform catalysis. This is different from the case of RNase HII which has a natural ability to recognize and cleave single ribonucleotides present within DNA. Since our study is the first to look at the use of natural RNases for cleaving artificially evolved DNA-RNA hybrid sequences, the results show valuable insight into some of the limitations of this design. We learned that enzymes such as RNases G and III are very strict in binding and catalyzing ribonucleic acid sequences with specific structures. The former cleaves only single stranded RNA and the latter cleaves double-stranded RNA. Both enzymes require a stretch of ribonucleic acid where the 2' hydroxyl groups flanking the cleavage site aid in binding and catalysis. This may explain why our design for isolate RFS targeted by these enzymes was not successful. Our RFS sequence only contained a single ribonucleotide at the cleavage site, which may not be sufficient for catalysis by these enzymes. However, it is important to note that the number of selection rounds performed with these enzymes were limited (7 rounds RNase G, and 15 rounds RNase III). Due to the nature of the target, evolution of DNA sequences to be cleaved by the target enzymes may occur at a slower rate compared to that of RNase HII hence, more rounds of selection may be required. Thus, from our study, it is not yet conclusive whether our selection strategy failed at isolating the desired RFS for RNase G and III. Nonetheless, alternative RFS sequence design should be sought

out for analysis. We plan to test sequences with different stretch of RNA nucleotides at the cleavage site to determine if they can evolve *via* SELEX to be recognized and cleaved specifically by Lm-RNase G or III.

4.6 Conclusion

In our study, we investigated whether a new class of functional nucleic acid termed RNases-cleaved fluorescent substrates or RFS, could be developed for future downstream application for creating *L. monocytogenes* biosensors. We first identified and purified putative RNases (RNase G, III and HII) from *L. monocytogenes* and have briefly highlighted their cellular roles by *in vitro* analysis. We developed a RFS probe that targeted Lm-RNase HII and showed that it has the potential for bacterial cell detection. Furthermore, we showed that this probe could be exploited as a molecular tool for studying RNase HII activity from broad range of bacteria species and had distinct advantages over tradition methods for studying the enzyme (more on this in Chapter 5). Our study also demonstrated some of the limitation of SELEX and the importance of sequence design as we were unable to isolate RFS probes for RNase G and III using conventional sequence design. Overall, our study took the first step to look at the ability of SELEX to isolate sequences that can be targeted for cleavage by natural enzymes. Although we did not demonstrate the use of RFS as a bacteria biosensor, we highlighted key steps that are needed for developing such probes and challenges that need to be overcome for future studies.

4.7 References

1. Dever, P. F., Schaffner, W. D. & Slade J.P. Methods for the detection of foodborne *Listeria monocytogenes* in the U.S. *J. Food Safety* **13**, 263-292 (1933).
2. FAO, WHO & Codex committee. Proposed draft guidelines for the control of *Listeria monocytogenes*in foods, 1-37 (2003).
3. Gaillard, J., Berche, P., Frehel, C., Gouin, E., & Cossart, P. Entry of *L. monocytogenes* into cells is mediated by internalin, a repeat protein reminiscent of surface antigens from gram-positive cocci. *Cell* **65**, 1127-1141 (1991).
4. Doyle, M. E. Virulence characteristics of *Listeria monocytogenes. Food Research Institute Briefings* (2001).
5. Grorge, S. M., Lund, B. M. & Brocklehurst, T. F. The effect of pH and temperature on initiation of growth of *Listeria monocytogenes. Lett. Appl. Microbiol.* **6**, 153-156 (1988).
6. Sorrells, K. M. & Enigl, D. C. Effect of pH, acidulant, sodium chloride, and temperature on the growth of *Listeria monocytogenes. J. Food Safety* **11**, 31-37 (1990).
7. U.S. Food and Drug Administration (FDA) Environmental Assessment: Factors Potentially Contributing to the Contamination of Fresh Whole Cantaloupe Implicated in a Multi-State Outbreak of Listeriosis. http://www.fda.gov/Food/FoodSafety/FoodborneIllness/ucm276247.htm.
8. Government of Canada Report of the independent investigator into the 2008 listerosis outbreak.http://www.listeriosis-listeriose.investigation-enquete.gc.ca/index_e.php?s1=rpt&page=tab.
9. Greenberg, J., and Elliott, C. A cold cut crisis: Listeriosis, Maple Leaf foods, and the politics of apology. *Canadian J. Commun.* **34**, 189-204 (2009).
10. Ramaswamy, V., Cresence, V.M., Rejitha J.S., Lekshmi, M.U., Dharsana, K.S., Prasad, S.P., Vijila, H.M. *Listeria*-review of epidemiology and pathogenesis. *J Microbiol Immunol Infect.* **40**, 4-13 (2007).
11. Brouwer, M. C., Van de beek D., Heckenberg, S. G. B., Spanjaard L., & Gans, J. Community-acquired *Listeria monocytogenes* meningitis in adults. *Clin infect dis.* **43**, 1233-1238 (2006).
12. Hoeprich, P. D. & Chernoff, H. M. Subacute bacterial endocarditis due to *listeria monocytogenes. Am. J. Med.* **19**, 488-494 (1955).
13. Weinberger M., & Keller N. Recent trends in the epidemiology of non-typhoid Salmonella and antimicrobial resistance: the Israeli experience and worldwide review. *Curr. Opin. Infect. Dis.* **18**, 513-521 (2005).
14. WHO. Risk assessment of *Listeria monocytogenes*in ready-to-eat foods, MRA Series 4. **4**, 1-78 (2004).
15. Lovett, J. & Hitchins, A. D. in *Listeria isolation. Bacteriological analytical manual, Food and Drug administration (FDA)* (J. Assoc. Offic. Anal. Chem., Arlington, VA, 1988).

16. Lovett, J. Isolation and identification of *Listeria monocytogenes*in dairy products. *J. Assoc. Off. Anal. Chem.* **71**, 658-660 (1988).
17. Wilson, S. D. & Szostak W.J. *In vitro* selection of functional nucleic acids. *Annu. Rev. Biochem.* **68**, 611-647 (1999).
18. Garst, A.D., Edwards, A.L., and Batey, R.T. Riboswitches: Structure and Mechanisms. *Cold Spring Harb. Perspect. Biol.* 1-13 (2010).
19. Y. Lu and Y. Li. Functional Nucleic Acids for Sensing and Other Analytical Applications. 47-108 (Springer Press, NY, USA), 2009.
20. Schlosser, K., Gu, J., Lam, C. F. J. & Li, Y. In vitro selection of small RNA-cleaving deoxyribozymes that cleave pyrimidine-pyrimidine junctions. *Nucleic Acids Res.* **36**, 4768-4777 (2008).
21. Laz, L.S., Goaziou L.A., and Henneke, G. Structure-specific nuclease activities of *Pyrococcus abyssi* RNase HII. *J. Bacteriol.* **192**, 3689-3698 (2010).
22. Jiang, X., and Belasco, J.G. Catalytic activation of multimeric RNase E and RNase G by 5'-monophosphorylated RNA. *Proc. Natl. Acad. Sci.* **101**, 9211-9216 (2004).
23. Ali, M. M., Sergio D. A., Lazim H., & Li, Y. Fluorogenic DNAzyme Probes as Bacterial Indicators. *Angew Chem.* (2011).
24. Itaya, M. Isolation and characterization of a second RNase H (RNase HII) of *Escherichia coli* K-12 encoded by *rnhB* gene. *Proc. Natl. Acad. Sci.* **87**, 8587-8591 (1990).
25. Lai, B. L. & Voique, A., Kirsebom, A.L., Gopalan, V. Unexpected diversity of RNase P, an ancient tRNA processing enzyme: Challenges and prospects. *FEBS let.* **584**, 287-296 (2010).
26. Luhtala, N. & Parker, R. T2 family ribonucleases: ancient enzymes with diverse roles. *Cell* **35**, 253-259 (2010).
27. Kochiwa, H., Tomita, M. & Kanai, A. Evolution of ribonuclease H genes in prokaryotes to avoid inheritance of redundant genes. *BMC Evol Biol.* (2007).
28. Sierra-Gallay, I. L., Mathay, N., Pellegrini, O. & Condon, C. Structure of the ubiquitous 3' processing enzyme RNase Z bound to transfer RNA. *Nat. Struct. Mol. Biol.* **13**, 376-377 (2006).
29. Yoshida, H. in *Methods in Enzymology; The Ribonuclease T1 Family*, 28-41 (Academic Press, 2001).
30. Wilson, R.H., Yu, D., Peters K.H., Zhou, J.G., and Court, D.L. The global regulator RNase III modulates translation repression by the transcription elongation factor N. *EMBO J.* **21**, 4154-4161 (2002).
31. Callaghan, A.J., Marcaida, M.J., Stead, J.A., McDowall, K.J., Scott, W.G., and Luisi, B.F. Structure of *Escherichia coli* RNase E catalytic domain and implications for RNA turnover. *Nature* **437**, 1187-1191 (2005).
32. Codon, C. and Putzer, H. The phylogenetic distribution of bacterial ribonucleases. *Nucleic Acids Res.* 5339-5346 (2002).

33. Kaberdin, V. R. & Blasi, U. Translation initiation and the fate of bacterial mRNAs. *FEMS Microbiol. Rev.* **30**, 967-979 (2006).
34. Green, L.S., Jellinek, D., Ostman, A., Heldin C.H., and janjic, N. Inhibitory DNA ligands to platelet-derived growth factor B-chain. *Biochemistry* **35**, 14413-14424 (1996).
35. Pagratis, N.C., Bell, C., Chang, Y.F., Jennings, S., Fitzwater, T., Jellinek, D., and Dang, C. Potent 2'-amino-, and 2'-fluoro-2'-deoxyribonucleotide RNA inhibitors of keratinocyte growth factor. *Nat. Biotechnol.* **15**, 68-73 (1997).
36. Jenison, R.D., Jennings, S.D., Walker, D.W., Bargatze, R.F., Parma, D. Oligonucleotide inhibitors of P-selectin-dependent neutrophil-platelet adhesion.. 8, 265-279. *Antisense Nucleic Acid Drug Dev* **8**, 265-279 (1998).
37. O'Connell, D., Koenig, A., Jennings, S., Hicke, B., Han, H.L., Fitzwater, T., Chang, Y.F., Varki, N., Parma, D., Varki, A. Calcium-dependent oligonucleotide antagonists specific for L-selectin. *Proc. Natl. Acad. Sci.* **93**, 5883-5887 (1996).
38. Blaszczyk, J., Tropea, J.E., Bubunenko, M., Routzahn, K.M., Waugh D.S., Court, D.L., and Ji, X. Crystallographic and modeling studies of RNase III suggest a mechanism for double-stranded RNA cleavage. *Structure* **9**, 1225-1236 (2001).
39. Briant, D.J., Hankins, J.S., Cook, M.A., and Mackie, G.A. The quaternary structure of RNase G from *Escherichia coli*. *Mol. Microbiol.* **50**, 1381-1390 (2003).
40. Okada, J., Okamoto, T., Mukaiyama, A., Tadokoro, T., You, D.J., Chon, H., Koga, Y., Takano, K., and Kanaya, S. Evolution and thermodynamics of the slow unfolding of hyperstable monomeric proteins. *BMC Evol Biol.* **10**, 3-12 (2010).
41. Pretzev, A. V. & Nicholson, A. W. Characterization of RNA sequence determinants and antideterminants of processing reactivity for a minimal substrate of *Escherichia coli* ribonuclease III. *Nucleic Acids Res.* **34**, 3708-3721 (2006).
42. Panganiban, A. T., and H. R. Whiteley. Purification and properties of a new *Bacillus subtilis* RNA processing enzyme. *J. Biol. Chem.* **258**, 12487-12493 (1983).
43. Wang, W., and Bechhofer, D.H. *Bacillus subtilis* RNase III Gene: Cloning, Function of the Genein*Escherichia coli*, and Construction of *Bacillus subtilis* Strains with Altered *rnc* Loci. *J. Bacteriol.* **179**, 7379-7385 (1997).
44. Santoro, S.W., and Joyce, G.F. A general purpose RNA-cleaving DNA enzyme. *Proc. Natl. Acad. Sci.* **94**, 4262-4266 (1997).
45. Tram, K., Kanda, P., and Li, Y. Lighting up RNA-cleaving DNAzymes for biosensing. *J. Nucleic Acids* (2012).
46. Jayasena, S. D. Aptamers: an emerging class of molecules that rival antibodies in diagnostics. *Clin Chem*. **45**, 1628-1650 (1999).

4.8 Supplementary Figures

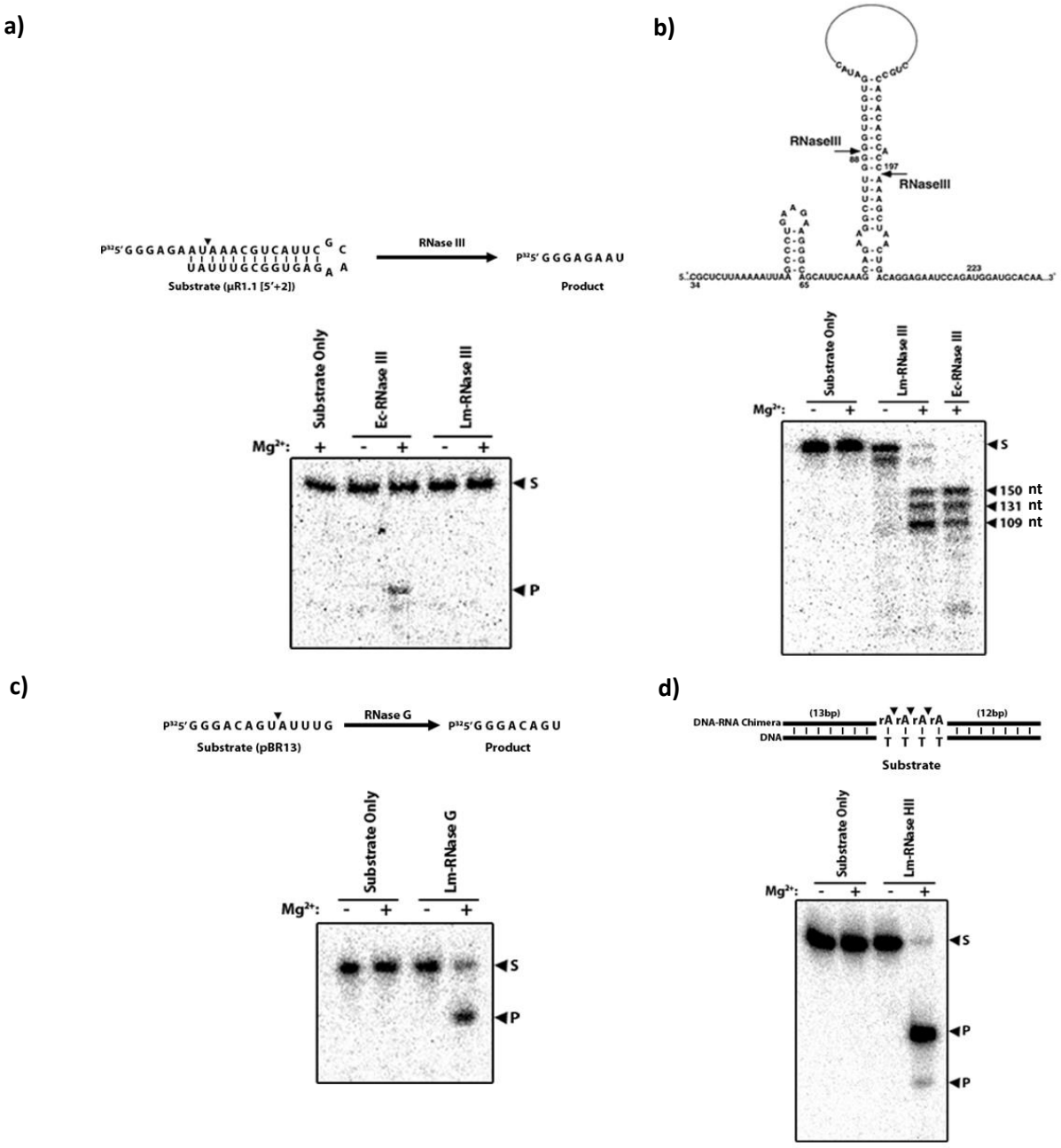

Figure S4.1. Assessment of enzyme activity. a) The 5' ^{32}P μR1.1 [5'+2] substrate (S) was incubated with either *E. coli* (Ec) or Lm-RNase III (300 nM), in the presence or absence of Mg^{2+} for 15 minutes. Cleavage product (P) is indicated by the arrow. b) The λ N leader transcript substrate (S) was incubated with either *E. coli* (Ec) or Lm-RNase III (300 nM) in the presence or absence of Mg^{2+}, for 15 minutes. The three primary products are visualized at 150 nucleotide (nt), 131 nt and 109 nt. c) The 5' ^{32}P pBR13 RNA substrate (S) was incubated with Lm-RNase G (300 nM), in the presence or absence of Mg^{2+} for 10 minutes. d) The DNA-RNA chimera substrate (S) contained four riboadenosine (rA) and the cleavage sites are indicated by the arrows. The DNA-RNA chimera sequence and the complementary DNA sequence were mixed in a 1:3 mole ratio, respectively. The substrate was incubated with Lm-RNase HII (300 nM), in the presence or absence of Mg^{2+} for 20 minutes.

CHAPTER 5: Development and Characterization of RNase-Cleaved Fluorescent Substrate (RFS) as a Tool to study RNase HII

5.1 Abstract

Endoribonuclease (RNase) H II plays an important role in the removal of Okazaki fragments during DNA replication and misincorporated ribonucleotides within the genome. Thus, it is important that we understand how the enzyme function. Developing a method which can measure enzyme activity in a simple and sensitive manner is essential in progressing our understanding of RNase HII. In this study, we developed a method to create an artificially evolved nucleic acid strand to act as a fluorescent substrate to measure enzyme activity. These substrates were termed RNase-cleaved fluorescent substrates (RFS) and were developed using a method called "Systematic Evolution of Ligands by Exponential Enrichment" (SELEX). We successfully isolated six sequence classes termed C1 to C6 that could measure RNase HII activity. The sensitivity of the RFS probes was found to be 0.1 picomolar (pM) and 1 pM using a gel based assay and fluorimeter, respectively. We also found that the DNA bulge two nucleotide upstream of the cleavage site played an important role in stimulating enzyme activity. The RFS probes that we isolated could also be used to study RNase HII from different organisms.

5.2 Introduction

Endoribonuclease (RNase) H is an enzyme which hydrolyzes RNA strands within a RNA/DNA heteroduplex.[1] It plays an important role in several cellular reactions such as DNA replication, DNA repair, and transcription.[1-4] This enzyme has been identified in many

organisms including archaea, prokaryotes, eukaryotes and even retrovirus and can be divided into two families based on amino acid sequence. The type 1 enzymes (RNase HI) play a key role in removing the Okazaki fragments during DNA replication.[1] The type 2 enzymes' (RNase HII) function overlaps with RNase HI and participates in DNA repair by removing misincorporated ribonucleotides.[5]

Since RNase H plays an important biological role, it is important that we understand how these enzymes function within the cells. Biochemical analysis and crystal structures of RNase HI and RNase HII have greatly increased our knowledge on how these enzymes recognize and catalyze their substrate.[6-9] However, gel electrophoresis, capillary electrophoresis, and HPLC have been the predominant means of studying enzyme activity and often require radioisotope-labeled DNA substrates.[8, 10-13] These methods often require high concentration of DNA (micromolar range), provide discontinuous enzyme kinetic analysis and are laborious. To address these issues, molecular beacon (MB) substrates were developed to conveniently study RNase H activity in real-time.[14, 15] However, even with the improvement of methods to study RNase H activity, we still do not understand the complete nature of how these enzyme recognizes substrates. Substrate design to study RNase H has mostly been limited to poly-rA/poly-dT heteroduplex. Testing the effects of various combination of nucleotide pairing and mispairing on enzyme activity is impractical using conventional methods of substrate design. Thus, a new method for designing substrates and testing RNase H activity is required. We took an alternative approach by using

Systematic Evolution of Ligands by Exponential Enrichment (SELEX) technique for creating substrates to study RNase H activity.

SELEX (or *in vitro* selection) is an *in vitro*, test-tube evolution method that begins with a large pool of randomized DNA or RNA sequences that were subjected to multiple rounds of selective pressure.[16, 17] Only the sequences that are capable of performing a desired function, such as binding to a specific target are isolated, amplified and subject to further rounds of evolution. This allows one to isolate a diverse set of sequences with the capability to bind the intended target tightly.

In this study, we devised a SELEX technique to isolate a set of fluorescently labeled RNA/DNA hybrid nucleic acid probes with optimal affinity for RNase HII. We called these sequences RNase-cleaved fluorescent substrates (RFS). The nature of this method allows for a convenient way to assess large possibilities of sequence pairing and mispairing important for enzyme binding. Thus, we were able to find new interactions between enzyme and substrates not previously addressed. We believe that our method's sensitivity to detect 1 pM of RNase HII is the lowest reported hence, it may prove to be advantageous when probing for low cellular levels of RNases HII.

5.3 Results and Discussion

5.3.1 Systematic Evolution of Ligands by Exponential Enrichment

RFS targeting RNase HII was isolated form a DNA pool containing 40 randomized nucleotide in 15 rounds of *in vitro* selection. More details on the selection design are discussed in Chapter 2.

The progress of selection depicting the evolution of the DNA pool over a few rounds of selection are summarized in Figure 5.1. Essentially no cleavage was observed by RNase HII using the initial Round 0 (R0) DNA population. However, by R3, close to 20% cleavage was observed indicating that the DNA population had quickly evolved to interact with Lm-RNase HII within the first 3 rounds of selection. From R3 to 15, the percentage cleaved increased only by 2 fold.

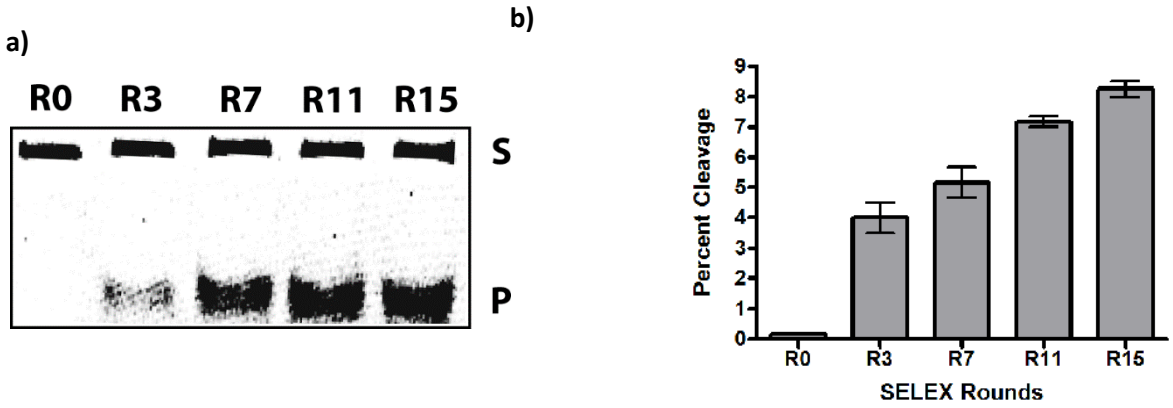

Figure 5.1. Progress of SELEX to develop RFS for RNase HII. a) Cleavage (P, product) of the full length DNA pool (S, substrate) from different rounds of selection on a 10% dPAGE. Approximately 2 pmol of DNA pool was incubate with 0.1 nM of Lm-RNase HII for 15 minutes. The DNA was visualized by measuring fluorescence b) The percent of cleavage visualized on 10% dPAGE was quantified using ImageQuant. The reactions were done in duplicates.

The slow evolution of the DNA pool in the later rounds indicated that large diversity of sequence still remained with the pool of DNA which can act as substrate for Lm-RNase HII. This idea was also supported by sequencing results obtained at the end of R15 (Figure 4.5 from Chapter 4) which shows the presence of a large diversity of sequences. To increase the stringency of selective pressure throughout R0-R15, the reaction time was reduced from 30 min to 10 min and varied the enzyme concentration from 4 nM to 0.4 nM (Chapter 4, Figure 4.4). The enzyme

concentration was maintained to ensure that the DNA pool was saturated with the desired target. This would also reduce the likelihood of isolating catalytic DNA sequences which are involved in cleaving RNA in the absence of target.

We next determined the sensitivity of the R15 DNA pool. Cleavage was observed at a concentration of 0.1 nM for a 5 minute reaction but, the enzyme concentration could be reduced further to 1 pM for a 30 minute reaction (Figure 5.2).

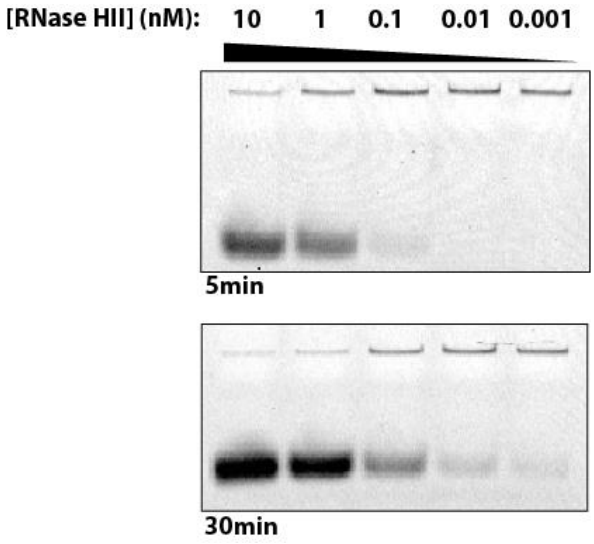

Figure 5.2. Testing for optimal SELEX condition at the end of R15. Approximately 0.5 pmol of R15 DNA pool was incubated with varying concentration of Lm-RNase HII at room temperature for 5 or 30 minutes. The DNA on dPAGE was visualized by measuring fluorescence.

5.3.2 Structure of Class 1 to 6 RFS sequences

Six distinct sequence classes (C1 to C6) were most frequent in the R15 pool (Chapter 4, Figure 4.5) and were further characterized. The secondary structures of C1 to C6 were approximated using M-fold. Structural analysis reveals that majority of the sequences folds into a duplex structure especially near the cleavage site containing the single ribonucleotide (Figure 5.3). The structure and sequences of the duplex near the cleavage site was very similar between the different classes of sequences, with five absolutely conserved nucleotides, CCATA. The tendency to isolate duplex structures stems from the fact that the natural affinity of RNase HII is

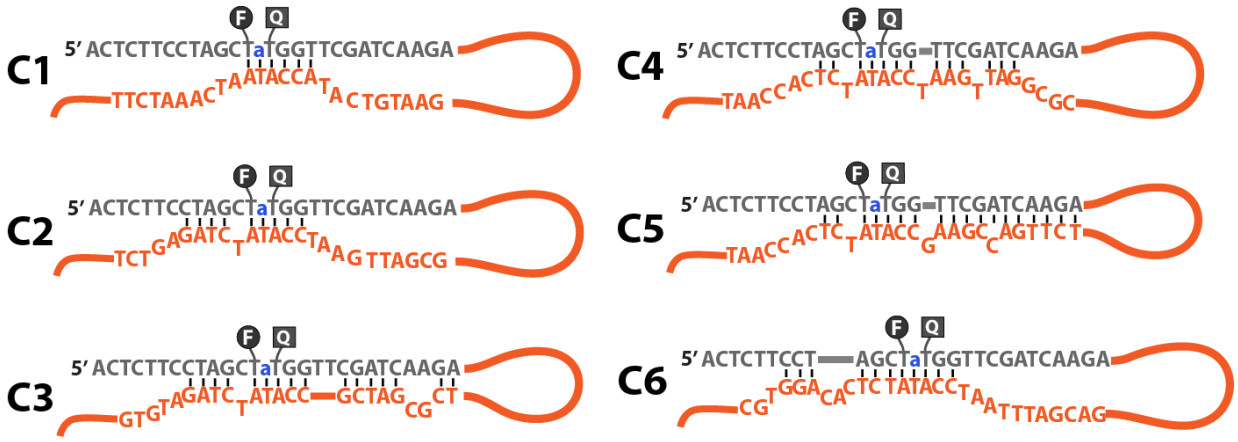

Figure 5.3. Highlighting key structural features of C1 to C6 sequences. M-fold was used to predict the secondary structure of C1 to C6. The key duplex regions near the cleavage site containing the single ribonucleotide (riboadenosine, a) is depicted above. The riboadenosine is situated between a fluorophore (F) and a quencher (Q)-modified deoxythymine, fluorescein (Emission max=521 nm) and dabcyl (Absorbance range=400-550 nm) respectively. All sequences contain the CCATA nucleotides within the core-duplex region near the cleavage site.

towards DNA/RNA heteroduplexes. Thus, throughout the course of the evolution, only the sequences able to form a suitable duplex structure were isolated. C3-5 contained a greater number of Watson-Crick base paring within the duplex structures compared to C1, 2 and 6. The

degree of variation within the duplex may account for the subtle differences in substrate affinity to the RNase HII.

5.3.3 Sensitivity of C1 to C6 Sequences

The cleavage activity of Lm-RNase HII using C1 to C6 was tested (Figure 5.4). All 6 classes are cleaved only in the presence of RNase HII and are not cleaved when mixed with only the reaction buffer. The percent cleavage between different classes of sequences was relatively similar with C3 displaying the greatest amount cleaved by 2-fold. Other regions within the sequences had less influence on the overall activity of the enzyme. This idea was supported by

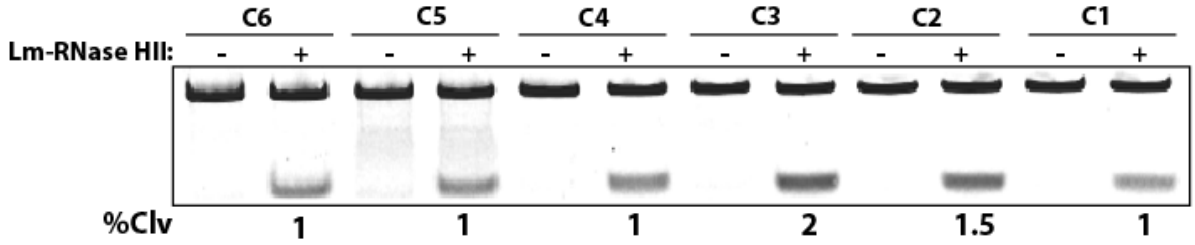

Figure 5.4. Assessing the cleavage of C1 to C6 with Lm-RNase HII. Approximately 2 pmol of DNA was incubated with or without 0.1 nM of Lm-RNase HII for 30 minutes. The DNA was visualized by measuring fluorescence and the percent cleavage (%Clv) was quantified using ImageQuant.

truncation analysis of the C3 sequence (Figure 5.5). Only minute differences in the percent cleavage between C3 and the truncated sequence C3a was observed. Even with the addition of extra nucleotides to make the duplex longer (C3b) the percent cleavage was not significantly altered. These results suggest that the duplex formed by the CCATA region is most important for influencing enzyme activity. This may also explain why such a diverse set of sequences were present at the end of R15. Sequences that contained the CCATA nucleotides had virtually an

equal opportunity of being cleaved by Lm-RNase HII, thus a diverse set of sequences were able to move onto the next rounds of selection.

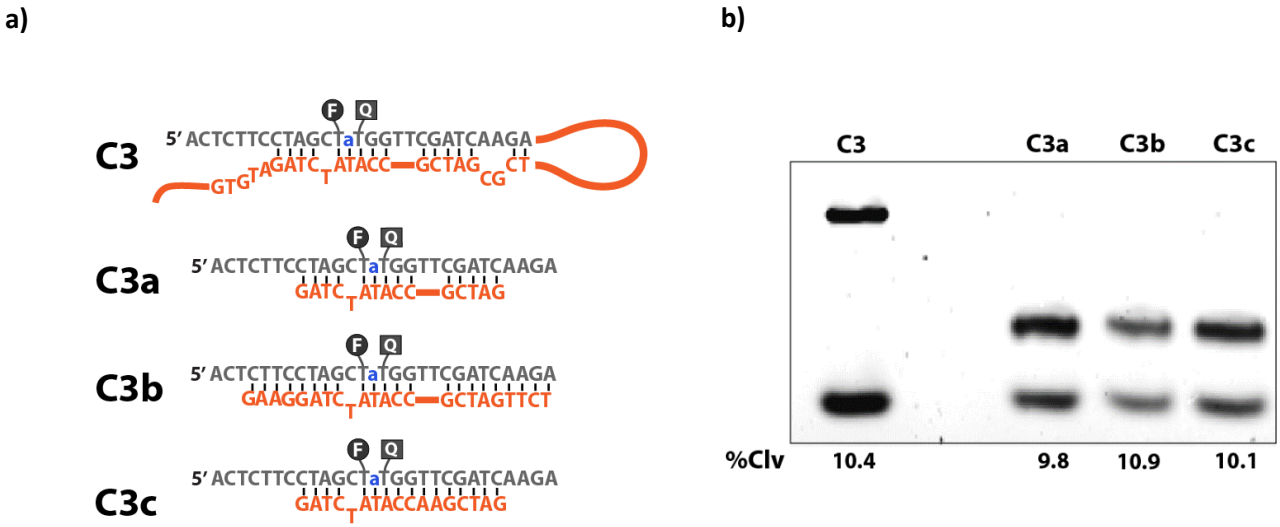

Figure 5.5. Comparing the amount of cleavage between different variants of C3 sequence. a) The different variations to the C3 probes are shown. C3a is the truncated form of C3 to only contain 15 nucleotides involved in the duplex formation near the cleavage site. C3b contains an additional set of nucleotides to make a longer duplex. C3c is similar to C3a with the exception of removing the thymine-thymine (TT) bulge by adding complementary nucleotides adenosine. b) Gel depicting the difference in cleavage between the altered C3 sequence variants. Approximately 2 pmol of DNA was incubated with 1 nM of Lm-RNase HII for 30 min. The DNA was visualized by measuring fluorescence and the percent cleavage (%Clv) was quantified using ImageQuant.

5.3.4 Detecting RNase HII with Gel-Based and Fluorometer Methods

We determined the sensitivity of C1-C6 by titrating it with different concentrations of Lm-RNase HII (Figure 5.6). For all six sequences, cleavage using 1 pM of Lm-RNase HII was clearly visible on the dPAGE after 30 min of reaction. Cleavage with 0.1 pM was also observed.

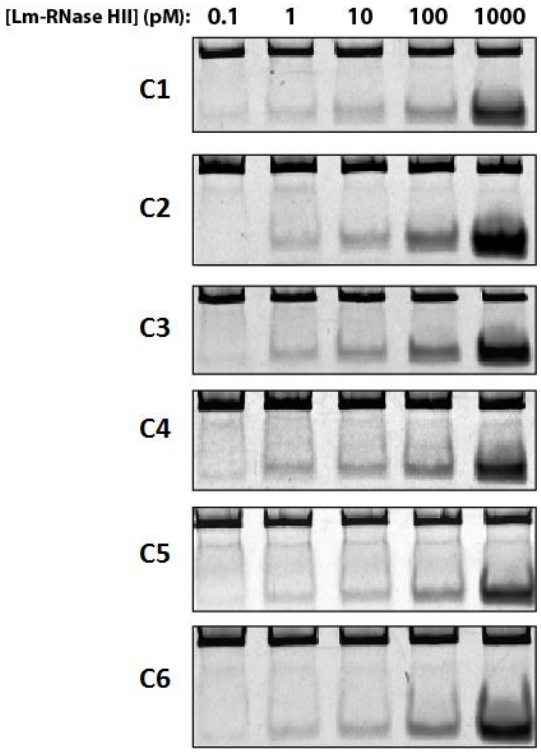

Figure 5.6. Assessing the sensitivity of C1 to C6 sequences. Approximately 2 pmol of DNA was incubated with varying concentrations of Lm-RNase HII for 30 minutes at room temperature. The cleavage was visualized by measuring fluorescence.

Since the RFS probes are developed for fluorescent analysis, we used C3 to test whether we could detect Lm-RNase HII with a fluorimeter with sensitivity similar to dPAGE. The fluorimeter based method had a sensitivity of 1 pM RNase HII (Figure 5.7). Unlike the gel based method, 0.1 pM enzyme signal was undistinguishable from the control (no enzyme) sample. Nonetheless, we demonstrated that the RFS probe can easily be used to detect low picomolar concentration Lm-RNase HII using a fluorometer.

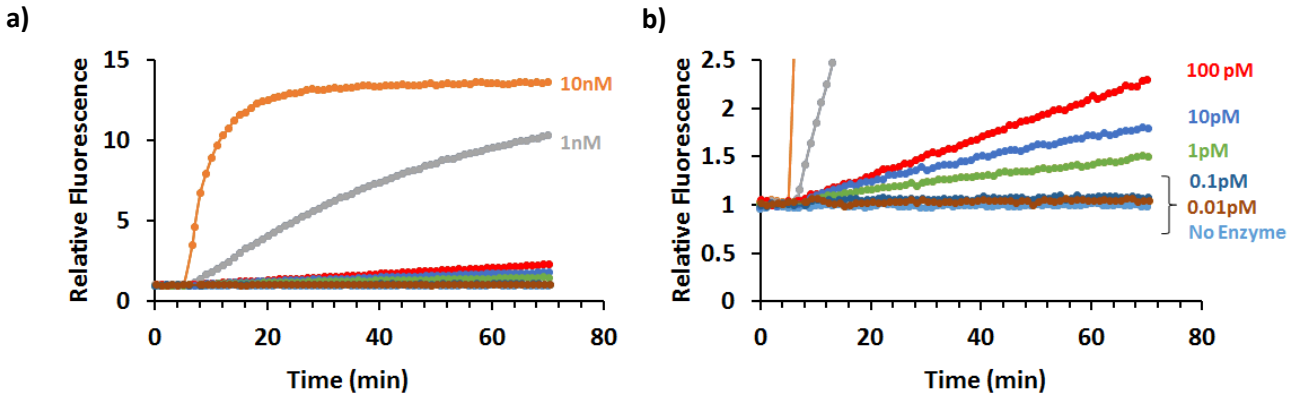

Figure 5.7. Detecting Lm-RNase HII using C3 sequence by a Fluorimeter. a) and b) represent the same set of data. Fluorescence generated over time due to the cleavage of the C3 probe by Lm-RNase HII was measured using the Cary Eclipse fluorescence spectrophotometer (Varian). Approximately 10 pmol of C3 was incubated with varying concentration of Lm-RNase HII for 65 minutes. The enzyme was added 5 minutes post the start of fluorescent measurements. The fluorescent measurements are based on relative fluorescence where the base line is set to an arbitrary unit of 1. The base line was determined by the control sample containing no enzyme.

5.3.5 Thymine Bulge within DNA Duplex Enhances C3 Cleavage

Another interesting structural motif observed was the presence of a bulge upstream or downstream of the cleavage site caused by nucleotide mismatch. Past literature has shown that RNase HII activity is reduced by mismatched base-pairing either upstream or downstream of the cleavage site.[10] Thus, it was interesting to see that the sequences isolated through in vitro selection had opted to preserve mismatched bases upstream or downstream of the cleavage site.

The thymine nucleotide bulge (T-bulge) within the C3c sequence (Figure 5.8a) was mutated to a guanine (C3d) to form a complete duplex. Initially we expected that removing the bulge would enhance catalytic activity of RNase HII but, to our surprise, opposite results were observed. By removing the T-bulge the activity of the enzyme was reduced by almost 2-fold. Figure 5.8b shows the cleavage activity of Lm-RNase HII using the C3c and C3d over the time course of 24 hours.

The C3 sequence also contains another bulge consisting of two consecutive thymine nucleotides (TT) which enhances the cleavage. The effects of removing the TT-bulge can be seen in Figure 5.5 which compares the percent cleavage between C3a and C3c (no TT-bulge) sequences. The amounts of cleavage seen for the two sequences are very similar indicating that the TT-bulge at this location does not significantly influence enzyme binding and activity.

The conventional method for understanding how mismatched bases influenced RNase HII activity was assessed by rationally designing substrates with strategically placed mismatched bases. Our results showed that SELEX is an excellent strategy for taking into account a large diversity of sequences and structural possibilities that can influence RNase HII activity. This has led to the identification new structural motifs which influence enzyme activity and has provided us with greater insight on understanding how RNase HII binds its substrate.

a)

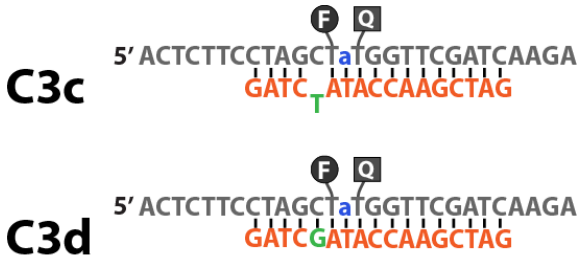

b)

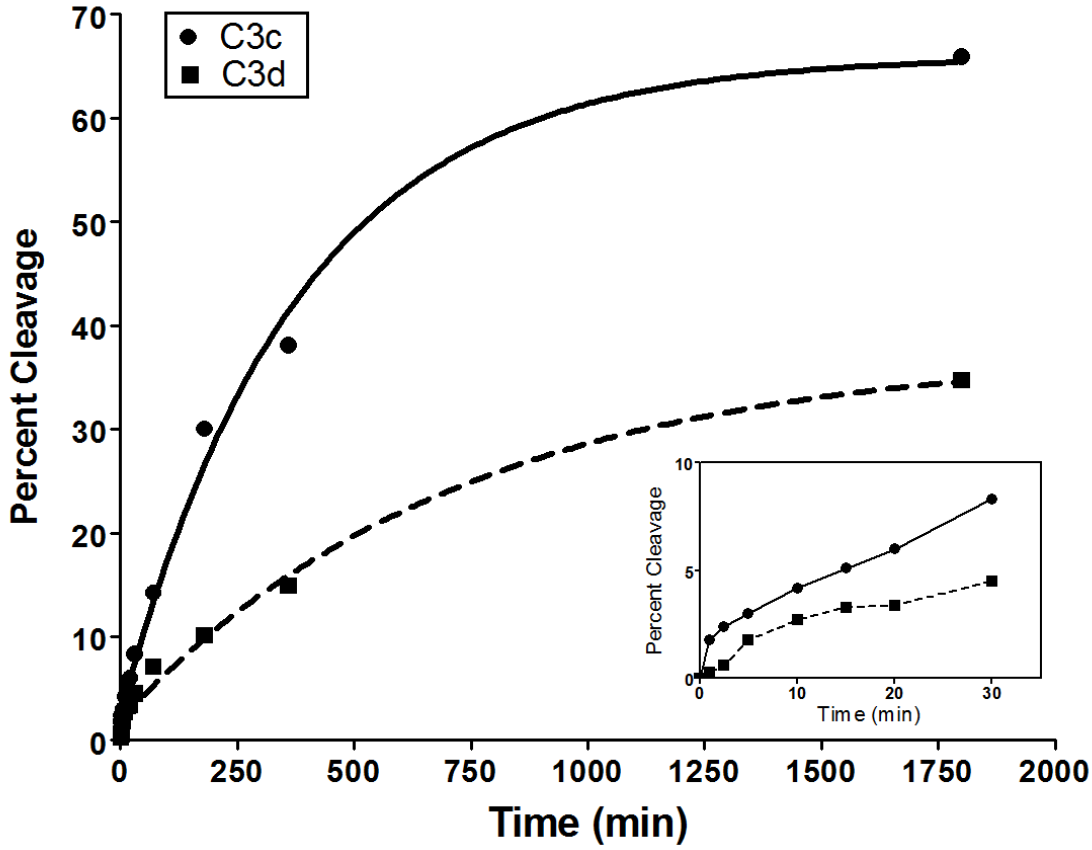

Figure 5.8. A single thymine (T) bulge enhances the cleavage of C3 sequence. a) The T bulge as shown in C3c was changed to a guanine to form a complete duplex. b) The graph shows a 24 hour reaction time course comparing the difference between the cleavage of C3c and C3d sequence. Approximately 3 pmol of DNA was incubated with 1 nM of enzyme. The cleavage was visualized by measuring fluorescence on 10% dPAGE and then graphed.

5.3.6 Class 1 to 6 RFS Specificity

The specificity of the different RFS classes was also tested using *Clostridium difficile* (Cd) and *Salmonella typhimurium* (St) RNase HII as non-specific targets. We found that despite the selection of the RFS probe using only the *Listeria* enzyme, C1-6 can also be used to test enzyme activity of RNase HII from other organisms (Figure 5.9). However, the amount of cleavage varies between the different RNase HIIs and may depend on both the differences in enzyme binding

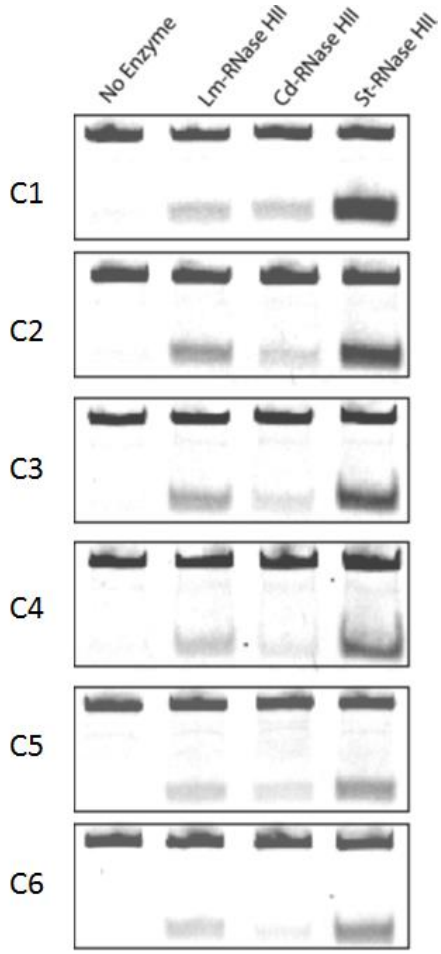

Figure 5.9. Specificity of C1 to C6 sequence. Approximately 2 pmol of DNA was incubated with 1 nM of RNase HII form either *L. monocytogenes* (Lm), *C. difficile* (Cd) and *S. typhimurium* (St) for 30 minutes.

affinity and the enzymatic turnover rate.

5.4 Conclusion

In this study we have shown that SELEX can be used to create efficient fluorescent substrates that can be used as a tool to study RNase HII. We had looked at six sequence classes isolated from SELEX in further details. All six probes were cleaved by RNase HII with C3 being cleaved most efficiently. We found that the regions forming the duplex near the single ribonucleotide were most important towards influencing RNase HII activity. Furthermore, we identified new nucleotide arrangements that influence RNase HII activity. We found that a single nucleotide mismatch (or DNA bulge) two nucleotide upstream of the cleavage site enhanced RNase HII activity. How this bulge enhances enzyme activity remains to be determined. The C1-C6 sequences could easily detect 1 pM of enzyme using a fluorimeter. We have also shown that these sequences can be used to study RNase HII from different organism.

5.5 References

1. Kochiwa, H., Tomita, M., and Kanai, A. Evolution of ribonuclease H gene in prokaryotes to avoid inheritance of redundant genes. *BMC Evol Biol.* (2007).
2. Tadokoro, T., and Kanaya, S. Ribionuclease H: molecular diversities, substrate binding domains, and catalytic mechanism of the prokaryotic enzyme. *FEBS J.* **276**, 1482-1498 (2009).
3. Haruki, M., Tsunaka, Y., Morikawa, M. and Kanaya, S. Cleavage of DNA-RNA-DNA/DNA chimeric substrate containing a single ribonucleotide at the DNA-RNA junction with prokaryotic RNase HII. *FEBS lett.* **531**, 204-208 (2002).
4. Bubeck, D., Reujns, A.M., Graham, C.S., Astell, R.K., Jones, E.Y., and Jackson, P.A. PCNA directs type 2 RNase H activity on DNA replication and repair substrates. *Nucleic Acids Res.* **39**, 3652-3666 (2011).

5. McDonald, P.J., Vaisman, A., Kuban, W., Goodman, F.M., and Woodgate R. Mechanisms employed by *Escherichia coli* to prevent ribonucleotide incorporation into genomic DNA by Pol V. *PLoS Genet.* **8**, e1003030 (2012).
6. Laz, L.S., Goaziou L.A., and Henneke, G. Structure-specific nuclease activies of *pyrococcus abyssi* RNase HII. *J. Bacteriol.* **192**, 3689-3698 (2010).
7. Zang, Y.B., Ayalew, S., and Lacks, S.A. The *rnhB* gene encoding RNase HII of Streptococcus pneumonia and evidence of conserved motifs in eukaryotic genes. *J. Bacteriol.* **179**, 3828-3836 (1997).
8. Hou, J., Liu, Y., Lu, Z., Liu, X., and Liu, J. Biochemical characterization of RNase HII from *Aeropyrum pernix. Acta Biochim Biophys Sin* **44**, 339-346 (2012).
9. Chon, H., Matsumura, H., Kiga, Y., Takano, K., and Kanaya, S. Crystal structure and structure-based mutational analyses of RNase HIII from *Bacillus stearothermophilus*: A New Type 2 RNase H with TBP like substrate-binding domain at the N Terminus. *J. Mol. Biol.* **356**, 165-178 (2006).
10. Hou, J., Liu, X., Pei, D., and Liu, J. RNase HII from *Chlamydia pneumonia* discriminates mismatches incorporation into DNA-rN-DNA/DNA duplexes. *Biochem. Biophys. Res. Commun.* **356**, 988-992 (2007).
11. Chai, Q., Qiu, J., Chapados, B.R., and Shen, B. *Archaeoglobus fulgidus* RNase HII in DNA replication: enzymological functional and activity regulation via metal cofactors. *Biochem. Biophys. Res. Commum.* **286**, 1073-1081 (2001).
12. Kanaya, E., and Kanaya, S. Kinetic analysis of *Escherichia coli* ribonuclease HI using oligomeric DNA/RNA substrates suggests an alternative mechanism for the interaction between the enzymeand the substrate. *Eur. J. Biochem.* **231**, 557-562 (1995).
13. Chan, K.C., Budihas, S.R., Le Grice, S.F., Parniak, M.A., Crouch, R.J., Gaidamakov, S.A., Isaaq, H.J., Wamiru, A., McMahon, J.B., and Beutler, J.A. A capillary electrophoretic assay for ribonuclease H acitvity. *Anal. Biochem.* **331**, 296-302 (2004).
14. Rizzo, J., Gifford, L.K., Gewirtz, A.M., and Lu, P. Chimeric RNA-DNA molecular beacon assay for ribonuclease H activity. *Mol. Cell. Probes.* **16**, 277-283 (2002).
15. Liu, B., Xiang, D., Long, Y., and Tong, C. Real time monitoring of junction ribonuclease activity of RNase H using chimeric molecular beacons. *Analyst* **138**, 3238-3245 (2013).
16. Mok, W. & Li, Y. Recent progress in nucleic acid aptamer-based biosensors and bioassays. *Sensors* **8**, 7050-7084 (2008).
17. Tuerk, C. & Gold, L. Systematic evolution of ligands by exponential enrichment: RNA ligands to bacteriophage T4 DNApolymerase. *Science* **249**, 505-510 (1990).